Binding of cytohesin 2 to the plasma membrane and its relationship with the EGFR

Dissertation zur Erlangung des Doktorgrades (Dr. rer.nat.)

der

Mathematisch-Naturwissenschaftlichen Fakultät

der

Rheinischen Friedrich-Wilhelms-Universität Bonn

Vorgelegt von

Nora Karnowski

aus

Hagen

Bonn, 2018

Angefertigt mit Genehmigung der Mathematisch-Naturwissenschaftlichen Fakultät der
Rheinischen Friedrich-Wilhelms-Universität Bonn

1. Gutachter: **Herr Prof. Dr. Michael Famulok**

2. Gutachter: **Herr Prof. Dr. Thorsten Lang**

Tag der Promotion: 26.10.2018

Erscheinungsjahr: 2018

Table of Contents

List of Abbreviations

A	Ampere
AMPAR	AMPA-like glutamate receptor
APC	Adenomatous polyposis coli
Arf	Adenosine ribosylation factor
Arl	Arf-like protein
ARNO	Arf nucleotide-binding site opener
ATP	Adenosine triphosphate
BAR	Bin-Amphiphysin-Rvs
BIG	Brefeldin A-inhibited GEF
B-Myb	Myb-related protein B
BRAG	Brefeldin-resistant Arf GEF
BSA	Bovine Serum Albumine
C	Concentration
Ca^{2+}	Calcium cation
CC	Coiled-coil
CCDC120	Coiled-coil domain containing protein 120
CCP	Clathrin-coated pits
CE	Cytoplasmic Extract
CEB	Cytoplasm extraction buffer
CFI	Cytoplasmic fluorescence intensity
CME	Clathrin mediated endocytosis
CNK1	Connector enhancer of KSR1
COP I/II	Coat protein complex subunit I/II
CoxII	Cytochrome c oxidase subunit II
CRTC	CREB-regulated transcriptional activator
DAG	Diacylglycerol
ddH_2O	Double-destilled water
DMSO	Dimethyl sulfoxid
DNA	Deoxyribonucleic acid
DNA-PK	DNA-dependent protein kinase
E.coli	Escherichia coli
EDTA	Ethylenediaminetetraacetic acid

LIST OF ABBREVIATIONS

EE	Early endosome
EFA6	Exchange factor for Arf6
EGF	Epidermal growth factor
EGFR	Epidermal growth factor receptor
ER	Endoplasmic reticulum
ESCRT	Endosomal sorting complex for transport
FACS	Fluorescence activated cell sorting
FBX8	F-box only protein 8
FWHM	Full width at half maximum
FYVE	Fab1-YOTB-Vac1-EEA1
GAP	GTPase activating protein
GBF	Golgi Brefeldin A-resistance factor
GDP	Guanosine diphosphate
GEF	Guanine nucleotide exchange factor
GFP	Green fluorescent protein
GPCR	G-protein coupled receptor
GRASP	GRP1-associated scaffolding protein
Grb2	Growth factor receptor-bound protein 2
GRP1	General receptor for 3-phosphoinositides
GTP	Guanosine triphosphate
Hek	Human embryonal kidney
HeLa	Henrietta Lacks
Ins(1,3,4,5)P	Inositol (1,3,4,5)-tetrakisphosphate
IP3	Inositoltriphosphate
JM	Juxtamembrane
kDa	Kilodalton
K-Ras	Kirsten rat sarcoma viral oncogene homolog
L	Length
LE	Late endosome
Lz	Leucine zipper
MAPK	Mitogen activated protein kinase
MARCKS	Myristoylated alanine-rich C-kinase substrate
ME	Membrane extract
MEB	Membrane extract buffer

mGLuR1a	Metabotropic glutamate receptor 1a
MMP	Matrix metalloproteases
MVB	Multivesicular bodies
NE	Nuclear extract
NEB	Nuclear extraction buffer
nEGFR	Nuclear EGFR
NFI	Nuclear fluorescence intensity
NLI	Nuclear localization index
NLS	Nuclear localization signal
nm	Nanometer
NPC	Nuclear Pore Complex
NSCLC	Non-small cell lung cancer
NuMa	Nuclear Mitotic Apparatus protein
PAGE	Polyacrylamide gel electrophoresis
PALM	Photoactivated Localization Microscopy
PBR	Polybasic region
PCC	Pearson correlation coefficient
PCNA	Proliferating cell nuclear antigen
PFA	Paraformaldehyde
PH	Pleckstrin homology
PI	Proteinase inhibitor
PI3K	Phosphatidylinositol-3-kinase
PIP	Phosphorylated phosphatidylinositol
PK	Pyruvate kinase
PKC	Protein kinase C
PLD	Phospholipase D
PLL	Poly-L lysine
PM	Plasma membrane
PML	Promyelocytic leukemia protein
PTK	Protein tyrosine kinase
PX	Phox homology
Rab	Ras-associated binding protein
ROI	Region of interest
ROS	Reactive oxygen species

RSD	Relative standard deviation
SBP	Streptavidine-binding peptide
SD	Standard deviation
SEM	Standard error of the mean
SRP	Signal recognition particle
SRPR	SRP-receptor
STED	Stimulated emission depletion
STORM	Stochastic optical reconstruction microscopy
TEV	Tobacco etch virus
TFR	Transferrin receptor
TGFα	Transforming growth factor alpha
TGN	Trans golgi network

List of Figures

List of Tables

0 Summary

Eukaryotic cells are compartmentalized by lipid membranes to achieve the spatial separation of biological processes and signaling pathways. Controlled trafficking of proteins between these compartments as well as the recruitment of proteins to the membranes themselves are crucial for trouble-free function of the cell.

Previous research has revealed several possibilities for interaction between proteins and membranes. For instance, anionic lipids attract positively charged protein domains by electrostatic force, so that phosphoinositides can specifically interact with certain protein domains.

This work focuses on the guanine nucleotide exchange factor ARNO, a multidomain protein that activates small GTPases like Arf6 and therefore is directly involved in the vesicle trafficking machinery of the cell.

In its autoinhibited form, ARNO is localized in the cytoplasm, whereas recruitment to the plasma membrane is a prerequisite for its activation of Arf.

In this context, previous research has been centered on the interaction of the PH-domain and the PBR-domain of ARNO with artificial membrane systems. To expand these findings in a system that accounts for the enormous complexity of the inner leaflet of the cellular plasma membrane, in this study, membrane sheets were employed. Systematically, the role of the different ARNO domains in binding to these sheets was analyzed.

It has been shown, that the different domains of ARNO aid to the interaction with the membrane in a cooperative manner. The PH-domain absolutely is required for association with the membrane, yet it is not sufficient for sequestration of ARNO in the membrane. Moreover, its interaction with the phosphoinositides can be altered drastically by the second messenger Ca^{2+}. Also, binding studies of the other ARNO domains conclusively showed, that the PBR-domain, the Sec7-domain as well as the coiled-coil domain participate in plasma membrane binding. Moreover, dimerization of ARNO also improves its binding ability, most probably by an increase of the local avidity.

The microscopic analyses showed, that membrane-bound ARNO proteins are organized in clusters which, partly, are associated closely with EGFR clusters

Overexpression of ARNO in HeLa cells results in a tendency towards increased activation of the EGFR after stimulation with EGF.

Both findings hint at a possible functional connection between ARNO and EGFR trafficking and phosphorylation, respectively that might be regulated by the second messenger calcium.

Upon activation, the EGFR can be translocated to the nucleus by retrograde endosomal trafficking. In regards of this specific trafficking event, no influence of ARNO overexpression or inhibition was found.

1 Introduction

1.1 The cell and its compartments

All biological cells are compartmentalized by membranes. This is a prerequisite for the separation of metabolic reactions and biochemical processes that might interfere with each other as well as for the reduction of signaling noise [1,2]. The origin of these compartments is subject to many speculations. Some of them, like mitochondria and plastids, most probably resulted from (endo-)symbiotic fusion of different cellular organisms. Others might be of autogenous origin, that is the development from preexisting intracellular structures as postulated for example for peroxisomes. However, it must be noted that for most organelles exogenous as well as autogenous origins have been proposed [3].

For instance, the spatial separation of transcriptional and translational processes is a trait found in eukaryotic cells. As the nuclear envelope, that is composed of two membranes, is basically continuous with the endoplasmic reticulum´s membrane, the nucleus most probably originated autogenously by coevolution of at least 27 cellular components [4].

As a consequence of cellular compartmentalization, many proteins regulate cellular processes depending on their subcellular localization [5].

1.2 Membrane trafficking

As the different compartments of the cell are diverse in protein and lipid composition, a flow of cargo-loaded membranous vesicles is crucial for the transport of macromolecules and the maintenance of homeostasis [6,7]. This complex and highly regulated stepwise process has been coined “membrane trafficking”. In its chain of events, the coat of the vesicle is assembled, the cargo molecules are recruited to the donor membrane by carrier proteins before the vesicle buds from the compartment and is transported along the cytoskeleton. Delivery of the cargo is accomplished by tethering the vesicle to the membrane of the compartment of destination first, then docking it to the membrane irreversibly and finally fusing the transport vesicle with the acceptor compartment resulting in the release of the cargo [8]. Thus, proteins can be sorted to the different organelles, specific intracellular membranes or secreted into the extracellular space.

Since the vesicles bud from the organelle membranes, they are delineated by a lipid bilayer [9]. Three evolutionarily related coat proteins (COPI, COPII and Clathrin) comprise the framework for these cargo-bearing vesicles. COPII directs its cargo from the ER to the Golgi apparatus while COPI is responsible for retrograde transport in the opposite direction and transfer of proteins between the different Golgi cisternae. Clathrin-coated pits (CCP) bud from the plasma membrane (PM) and the trans Golgi network (TGN) to fuse with endosomes and lysosomes [7]. However, it has to be noted that under biotic stress and during development, alternative secretory pathways can be employed by the cell [10].

An overview over this network is depicted in **Figure 1**.

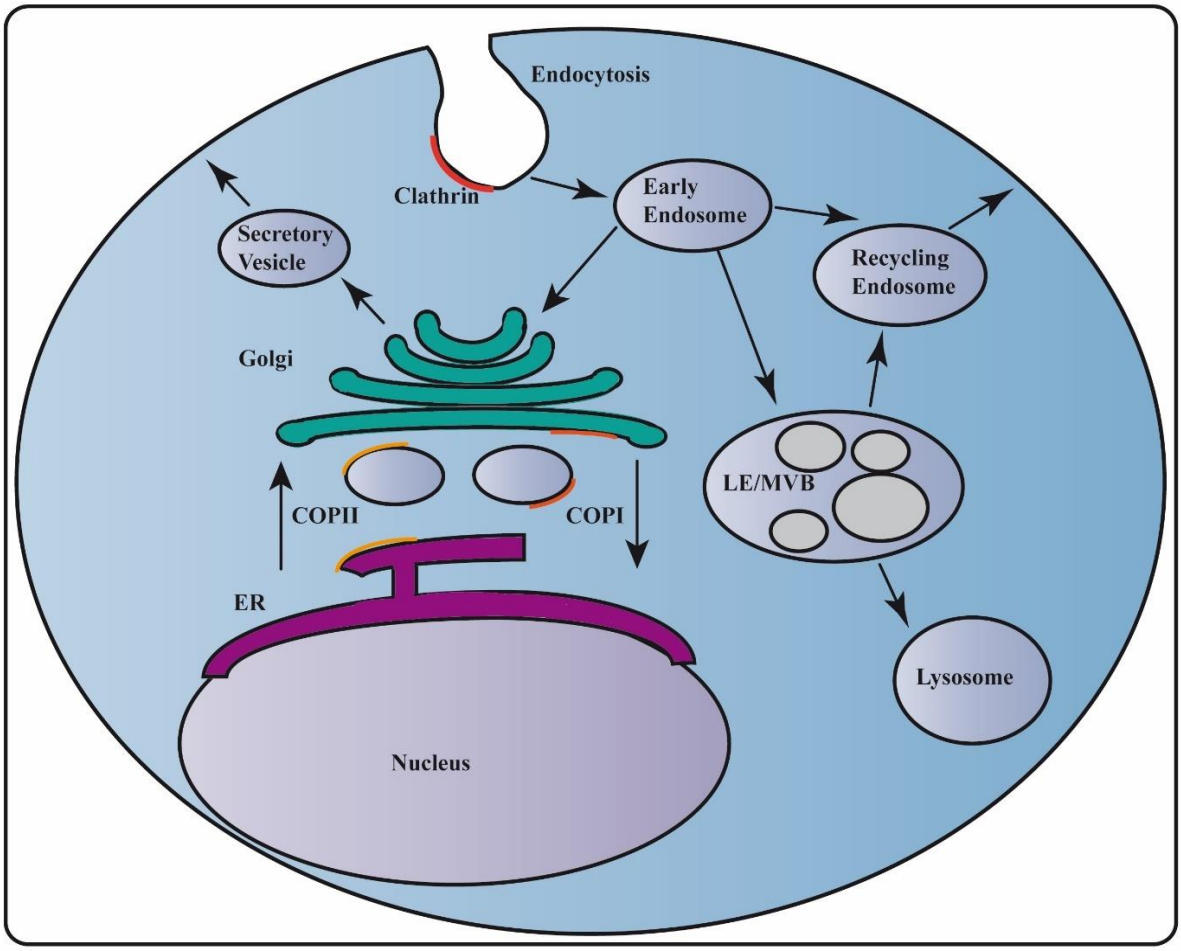

Figure 1: Targeted protein transport between different cellular organelles and the extracellular space. *Loaded cargo vesicles bud from the membranes and are directed to their destination depending, among other factors, on the specific coat proteins (COPI, COPII and Clathrin) that are embedded. ER = endoplasmic reticulum, LE = late endosome, MVB = multivesicular body. Figure inspired by [11].*

1.3 Small GTPases

Members of the Ras sarcoma (Ras) superfamily of small GTP hydrolases (GTPases) have been identified as major regulators of membrane trafficking as they are involved in almost all steps of this process. This superfamily is divided into five branches: Ras, Ras-like-proteins in brain (Rab), Ras-like-nuclear (Ran) proteins, Ras homologous (Rho) and ADP ribosylation factor (Arf) GTPases [12]. For membrane trafficking, mainly members of the Rab and Arf subfamilies are important. By recruitment of effector proteins, they control cargo selection, vesicle budding, the kinetic movement of the vesicles as well as participate to change the membrane identity [13]. Structurally, the members of the Ras superfamily are highly conserved, consisting of five α-helices and six β-sheets [14].

1.3.1 The GTPase cycle

As small GTPases function as nucleotide-dependent switches, they cycle between a GDP-bound "inactive" and a GTP-bound "active" conformation. Completion of this cycle is dependent on accessory proteins: guanine nucleotide exchange factors (GEFs) that facilitate release of GDP from and binding of GTP to the GTPase and GTPase activating proteins (GAPs) which stimulate the hydrolysis of bound GTP. Therefore, GEFs are commonly referred to as GTPase activators while GAPs are thought of as GTPase deactivators. This regulatory circle is schematically depicted in **Figure 2** [15].

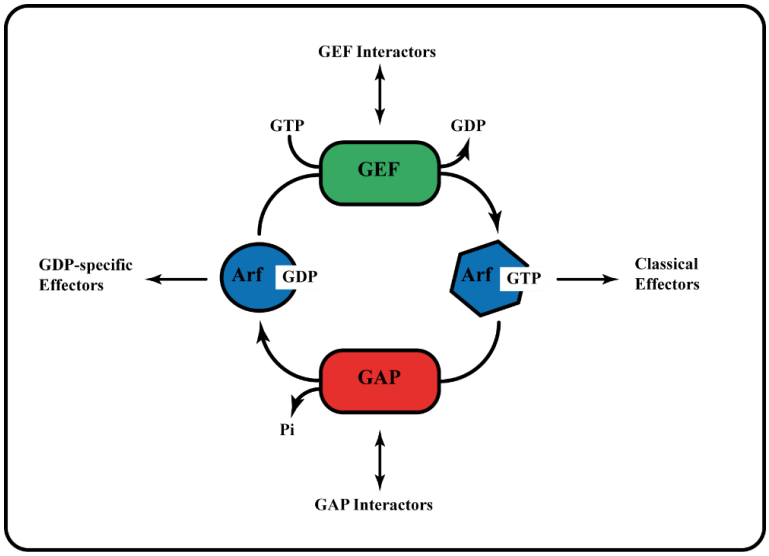

Figure 2: The GTPase cycle. *GTPases like Arf cycle alternate a GTP-bound and a GDP-bound form. Transition between the two states is mediated by Guanine nucleotide Exchange Factors (GEFs), like cytohesins, and GTPase Avtivating Proteins (GAPs). Adapted from* [16]

However, as already illustrated in **Figure 2**, the terms “active” and “inactive” GTPase are somewhat misleading as both nucleotide-bound conformations have been shown to interact with a plethora of effectors and thus regulate different signaling pathways in a spatio-temporal specific manner. For example, Koo *et. al.* were able to demonstrate that GDP-bound Arf6 binds to and therefore recruits Kalirin to the plasma membrane what subsequently enables the activation of Rac GTPases [17].

1.3.2 Arf GTPases and their role in membrane trafficking

There is evidence, that the ADP ribosylation factor (Arf) family of small GTPases is one of the decisive components in managing coat recruitment as well as curvature generation [18]. Arf proteins participate in vesicle formation by interacting with lipid-modifying enzymes and the direct recruitment of coat proteins [19,20]. In mammalian cells, this family is comprised of six members, namely Arf1-6, which are classified into three groups. Arf1-3 amount to Class I, though it is of note that Arf2 is absent in humans. Class II consists of Arf4 and 5 while Class III only contains Arf6. Class I and II Arfs predominantly localize to intracellular membranes of the Golgi and connected compartments as well as endosomes. Arf6, however, localizes to the plasma membrane upon activation [21].

Notably, for efficient activation of Arf GTPases the presence of membranes is required. Unlike other GTPases, Arfs have a myristoylated amphipathic N-terminus that is shielded by a helix in the GDP-bound form, leading to cytosolic localisation. However, probably an equilibrium of loosely membrane-associated protein exists. Displacement of the N-terminal helix by membranes leads to conformational rearrangements priming the GTPase for subsequent activation by GEFs [22].

1.3.3 The Sec7 family of guanine nucleotide exchange factors

Fifteen Arf GEFs are encoded in the human genome, a relatively substantial number of activating proteins in relation to the six existing Arf GTPases. This already hints at a delicate regulation and the importance of selective recruitment of the specific GEFs. These GEFs are, based on structure and domain organization similarities, organized in five families, namely (i) Golgi Brefeldin A-resistance factor 1/Brefeldin A-inhibited GEF (GBF/BIG), (ii) Arf nucleotide binding site opener (ARNO)/cytohesin, (iii)

exchange factor for Arf6 (EFA6), (iv) Brefeldin-resistant Arf GEF (BRAG) and (v) F-box only protein 8 (FBX8) [19]. They all share the highly conserved catalytically active Sec7-domain. Its structure was solved by X-ray diffraction 20 years ago and contains ten α-helices, numbered A-J, that form an irregular right-handed superhelical conformation resulting in cylinder with a length of 70 Å and a diameter of 20 Å at the N-terminus, increasing to 40 Å at its C-terminus. It is separated into two motifs by a solvent-exposed hydrophobic groove (**Figure 3**) [23].

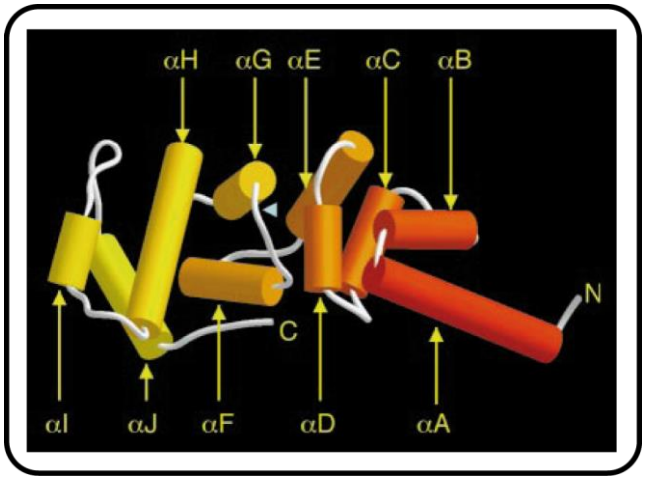

Figure 3: Crystal structure of the ARNO Sec7-domain. *The light blue arrowhead signifies the position of the Glu156, which is crucial for the catalytic function [23].*

Binding of Arf proteins to the Sec7-domain reduces the affinity of Arf for GDP for sterical as well as electrostatic reasons. The Sec7-domain perturbs the binding site for Mg^{2+} that coordinates the GDP´s β-phosphate thus facilitating release of the nucleotide. In addition, within the complex, the side chain of Sec7 Glu 156 is in the very close proximity of 3 Å to the β-phosphate resulting in profound steric as well as electrostatic repulsion [23]; [24].

A class of small molecules, coined Secins, is known to inhibit cytohesins *in vitro* as well as *in vivo* by specifically binding to its Sec7-domain. For instance, the compound Secin H3 binds the Sec7-domain of EFA6 30-fold weaker than to the cytohesin Sec7-domain [25].

1.3.3.1 Cytohesins

In the following, this work is focused on cytohesins as they are one of the most important groups of Arf regulators. Cytohesins belong to the so-called small, i.e. relatively low–molecular weight, Arf-GEFs.Their Sec7-domain is flanked N-terminally

by a coiled-coil-domain (CC) and C-terminally by a pleckstrin homology-domain (PH) to which a polybasic, positively charged region (PBR) is linked. A schematic illustration of the domain organization of cytohesin 2/ARNO is presented in **Figure 4 a**. In 2007, X-ray-crystallography revealed that a recombinantly expressed Sec7-PH fragment of Cytohesin 3 adopts an autoinhibited conformation. The C-terminal helix, together with the linker between Sec7- and PH-domain, acts as a pseudosubstrate by interaction with the α-G and α-H helices thus blocking the binding sites for Arf and the catalytically active glutamic finger. Since the structure of the Sec7- and PH-domain is highly conserved in the cytohesin family, this autoinhibitory mechanism is considered to be the same for ARNO. A ribbon representation of the crystal structure of autoinhibited cytohesin 3 is shown in **Figure 4 c** [26].

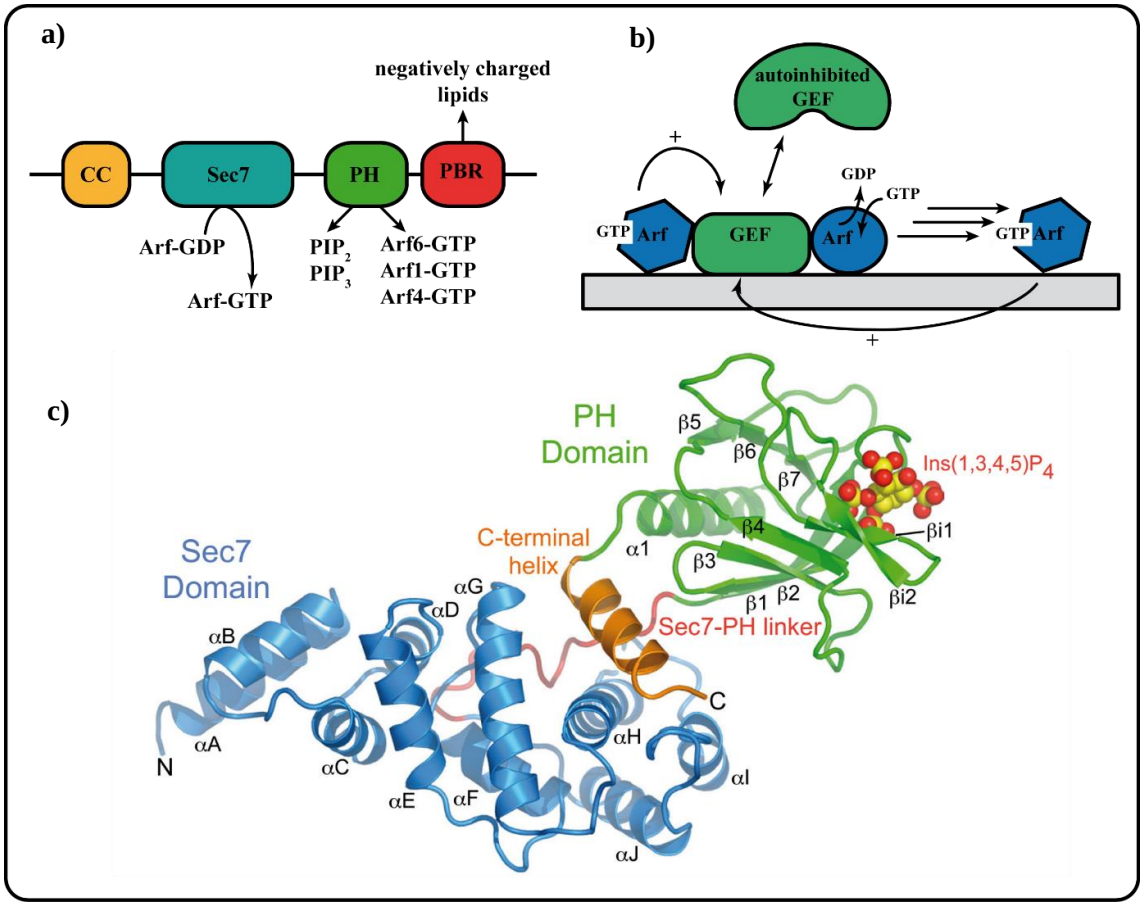

Figure 4: The structure of cytohesins. a) *Cytohesins are comprised of four major domains: A coiled-coil (CC) responsible for protein-protein-interactions, the catalytic Sec7-domain, the pleckstrin homology (PH) domain that interacts with lipids as well as proteins and a C-terminal polybasic region (PBR) known to interact with negatively charged lipids. Adapted from [27]. **b)** A model for the recruitment of GEFs and the release of autoinhibition by activated Arf-proteins resulting in a positive feedback loop. Adapted from [27]. **c)** Crystal structure based on the Sec7-PH fragment of cytohesin 3. Ins(1,3,4,5)P4 atoms are represented by yellow (carbon and phosphate) and red (oxygen) spheres. Adapted from [26].*

Interestingly, relief of this autoinhibition seems to be coupled to the binding to a membrane. As already presented in **Figure 4 a**, the PH- and PBR-domains of cytohesin has been shown to interact with phosphorylated, inositol containing phospholipids (PIPs) or negatively charged lipids like phosphatidylserine, respectively [28]. However, two different splice variants of cytohesins exist, resulting in PH-domains containing two or three glycines, respectively. This leads to differences in PIP binding affinity: While the affinity for PIP_2 is about the same, the 2G variant exhibits a ca 30-fold higher affinity for PIP_3, which does suggest a layer of regulation additional to random PH-PIP-interaction [29]. Indeed, several groups reported, that GEFs are recruited by GTP-bound Arf of Arf-like proteins (Arls) resulting in a positive feedback loop. *In vitro* as well as in transfected cells, it could be shown that the PH-domain of ARNO at the same time interacts with Arf-GTP and PIP which leads to conformational changes of the linker region and the C-terminal helix, relieving the autoinhibition and therefore enabling the activation of more GTPase molecules. Schematically, this signal amplification is depicted in **Figure 4 b** [30]; [31]; [27].

In spite of binding to PIP as well as membrane-bound Arf6, the ARNO PH-domain alone is not sufficient to mediate a persistent membrane association but needs at least the supporting interaction between the PBR-domain and phosphatidylserine [28]. Evidently, coordinated membrane recruitment of GEFs is crucial for controlled GTPase signaling. Nonetheless, in how far the other cytohesin domains participate in protein-membrane-interactions remains to be elucidated, even though one study suggests that the N-terminal coiled-coil-domain might impair binding of ARNO to membranes [32]. Clarification of the different ARNO domains´ contribution to membrane binding is one of the main objectives of this thesis.

Modification of cytohesins by phosphorylation appears to regulate the interaction between the cytohesin´s polybasic region and the plasma membrane. The Casanova group showed that phosphorylation of Serine 392 (S392) in the PBR reduces the interaction strength between ARNO and membranes both *in vitro* and *in vivo*, most probably due to the annihilation of positive charges [33].

1.3.4 Non-canonical functions of small GEFs

It is of note that, for some small GEFs, rather unexpected cellular functions independent from their ability to trigger nucleotide exchange have been described, also referred to as non-canonical functions. For example, poliovirus replication employs the Arf GEF GBF1 independently from its Sec7 activity [34].

Furthermore, the Bowerman group found that the N-terminus of the GEF EFA6 limits microtubule growth independently from Arf6 in the cortex of Caenorhabditis elegans (C. elegans) [35].

Cytohesin 2 has been proposed as an enhancer of EGFR signaling by direct interaction with the EGFR. It should be noted, that more recently this model has been challenged due to non-reproducibility of the *in vitro* binding mode of ARNO to EGFR [36]; [37]; [38,39].

1.4 Membrane recruitment of PH-domains via PIPs

Since the interaction between PIPs and the PH-domain of ARNO is known to be involved in the membrane recruitment of the protein, it is important to understand the role of PIPs in the plasma membrane.

Though low in abundance, about 1% in the plasma membrane, phosphorylated, inositol containing phospholipids (PIPs) regulate a plethora of biological functions by their interaction with proteins [40]. Among these are protein trafficking, membrane curvature, the regulation of ion channels, immune cell functions and chemotaxis. As depicted in **Figure 5 a**, even though the inositol moiety contains five hydroxyl groups that theoretically could be phosphorylated, in nature only those at position -3, -4 and -5 have been found to be modified by kinases such as the phosphoinositide-3-kinase (PI3K), resulting in a family of seven different PIPs [41].

Selectivity of the involvement in such an impressive number of signaling pathways is controlled by spatial and temporal distribution of the different PIPs. For example, $PI(4,5)P_2$ and $PI(3,4,5)P_3$ are most abundant in the plasma membrane while PI(3)P is detected in early endosomes and $PI(3,5)P_2$ can be found in early endosomes, late endosomes and lysosomes. This specific distribution of PIPs provides the means for recruiting PIP-binding proteins specifically to the respective subcellular localization [40].

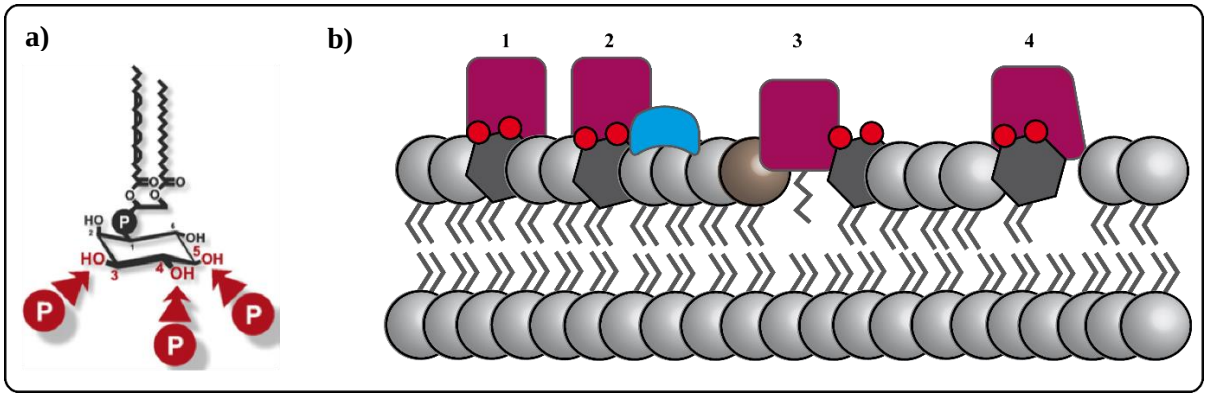

Figure 5: The structure of phosphatidyl inositol and its interactions with proteins. a) *Structure of phosphatidyl inositol. The hydroxyl residues that can be phosphorylated in mammalian cell are indicated in red.* ***b)*** *Illustration of the four major ways in which PIPs interact with proteins. 1: High affinity interaction between PIP and protein. 2: Coincidence interaction, here in combination with another protein-protein interaction. 3: Electrostatic interaction between the protein and the anionic lipid head groups. 4: Allosteric conformational change of the protein upon binding to PIP. Adapted from [42].*

Generally, PIPs interact with proteins and thus modulate their function in the respective signaling pathways in four different ways **(Figure 5 b)**.

1) Some proteins, like the general receptor protein 1 (GRP1) bind with high affinity to specific PIPs, for example $PI(4,5)P_2$ and are thus transiently relocalized to the plasma membrane upon activation of the phosphoinositide-3-kinase (PI3K) [43].
2) In other cases, the affinity for PIPs is too low to be sufficient for stable membrane association of the protein. The term "coincidence-detection" was coined to describe a cooperative increase of avidity by the PIP-protein-binding in addition to other molecular interactions. For example, sorting nexins employ the interaction of its PX-domain with PIPs in combination with membrane-curvature-sensing by BAR domains to direct cargos differentially in the endosomal pathway [44].
3) More trivially, some proteins, like K-Ras, interact with the plasma membrane by simple electrostatic interaction between the anionic lipid head groups with cationic, polybasic protein domains [45].
4) Finally, in addition to simple membrane recruitment, for some proteins, e.g. the Arf GEF Brag2, the interaction with PIPs leads to an allosteric activation and therefore plays a direct role in modulation of signaling pathways [46].

Since 2005, McLaughlin and colleagues suggested that eukaryotic cells use the regulation of its intracellular Ca^{2+} concentrations to control the level of accessible PIP_2 [47].

The ability to recruit proteins could consequently lead to protein clustering. For example, several proteins, such as for example Syntaxin 1A and myristoylated alanine-rich C-kinase substrate (MARCKS), have been shown to be clustered along with PIP_2 thus forming microdomains in the plasma membrane [48].

1.5 The role of PIPs in protein clustering

Advanced microscopy has revealed that membrane proteins are not evenly distributed but organized in islands of high protein density [49]. These protein islands are segregated by the cytoskeletal proteins actin and spectrin and depend on cholesterin [50]. This demonstrates, that membrane protein distribution is governed by protein-protein as well as protein-lipid interactions.

Within these protein rich regions in the plasma membrane, the proteins form nanoscale domains or clusters with a typical size of around 100 nm. Formation of these clusters is driven by forces which depend on the individual protein sequence, like the van der Waals force, electrostatic interactions and hydrogen bonding, as well as on membrane mediated interactions such as curvature or depletion mediated forces [51].

On top of that, charged lipids like PIPs can themselves form microdomains, promote protein clustering and influence protein function. For example, PIP_3 is required for maintenance of AMPA-type glutamate receptor (AMPARs) clusters in the postsynaptic membrane. Downregulation of PIP_3 synthesis leads to increased mobility of AMPARs and synaptic dysfunction [52].

Especially PIP_2 plays a functional role in many protein clusters and microdomains, such as in Ca^{2+}-dependent mesoscale domains with syntaxin 1a, a SNARE protein which is crucial for controlled exocytosis or the cell adhesion molecule CD44 clusters [53,54].

1.6 PIP_2 in EGFR signaling

The epidermal growth factor receptor (EGFR) is a member of the receptor tyrosine kinase (RTK) superfamily and involved in transmembrane signaling resulting in cellular growth and replication. Hence, misregulation of the EGFR has been observed in many types of cancer [55].

The 170 kDa glycoprotein is subdivided into a ligand-binding extracellular domain, a helical transmembrane domain, a positively charged, basic juxtamembrane domain, the catalytically active kinase core and a structurally flexible C-terminal tail [56].

Activation of the EGFR requires binding of one of its seven peptide ligands, to its extracellular domain inducing conformational changes of the whole receptor which leads to formation of asymmetric homodimers with another EGFR molecule or heterodimers with other members of the family [57]. In these dimers, the so-called donor kinase phosphorylates the receiver kinase initiating to receptor activation and phosphorylation of the C-terminal tail leading to downstream signaling (**Figure 6**) [58].

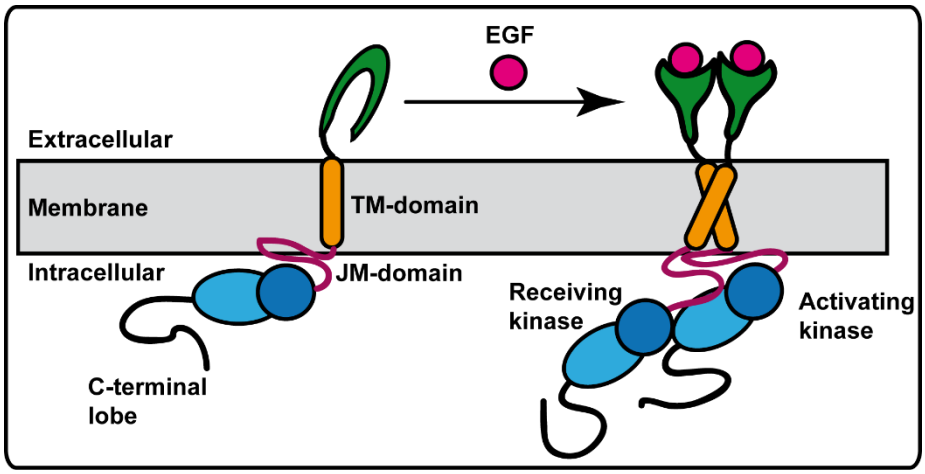

Figure 6: EGFR activation. *Binding of EGF induces a conformational change and receptor dimerization. The receiving kinase is then phosphorylated by the activating kinase leading to receptor activation. Figure inspired by [58].*

Since the intracellular part of the EGFR is highly active in solution, some studies suggest that the JM-domain´s ability to interact with the membrane is crucial for the receptor´s autoinhibition in the absence of ligand. They hypothesize, that one of the conformational changes that is required for the asymmetric dimer formation is the general extraction of the juxtamembrane domain from the plasma membrane [47,59].

On the other hand, other groups focused on the aspect that the JM-domain´s cationic residues´ sequestering of PIP_2 is actually aiding the stabilization of the active dimer [60–62].

However, despite the controversy with respect to the exact nature of these interactions, their existence and regulatory importance is generally accepted.

1.7 The different subcellular fates of the EGFR

Binding of ligand to the EGFR sets off a plethora of intricately balanced signaling cascades and cellular mechanisms. One of them is the accelerated internalization of stimulated EGFR molecules.

Generally speaking, a protein´s destination is mainly controlled by signaling peptides within their sequence, so-called localization signals, that are recognized by cargo receptors so that they are packed into the appropriate vesicles [11].

Hence, subsequent subcellular localization is governed by four major factors [63]:

1) Which kind of localization signal is present in the protein sequence and how many of them are there?
2) How strong is each of the localization signals?
3) What´s the concentration of the protein?
4) What´s the concentration and activity of the localization signal receptors?

Post-translational modification of proteins provides an additional layer of control and has the advantage that it often is reversible and faster than the control of the protein expression.

A prominent example for a post-translational modification involved in subcellular protein trafficking is the phosphorylation of the cargo protein nearby or in its localization signal. This can influence the protein´s binding affinity for its cargo receptor and therefore alter its transport, e.g. into or out of the nucleus [64].

Some of the factors participating in the internalization and the destination of the EGFRs depend on the type of extracellular ligand, its concentration and the duration of the stimulus [65].

This is of special interest since downregulation and trafficking of the EGFR is, given its involvement in multiple types of cancer and other diseases, of clinical relevance. A schematic overview of the different subcellular trafficking pathways of the EGFR is presented in **Figure 7**.

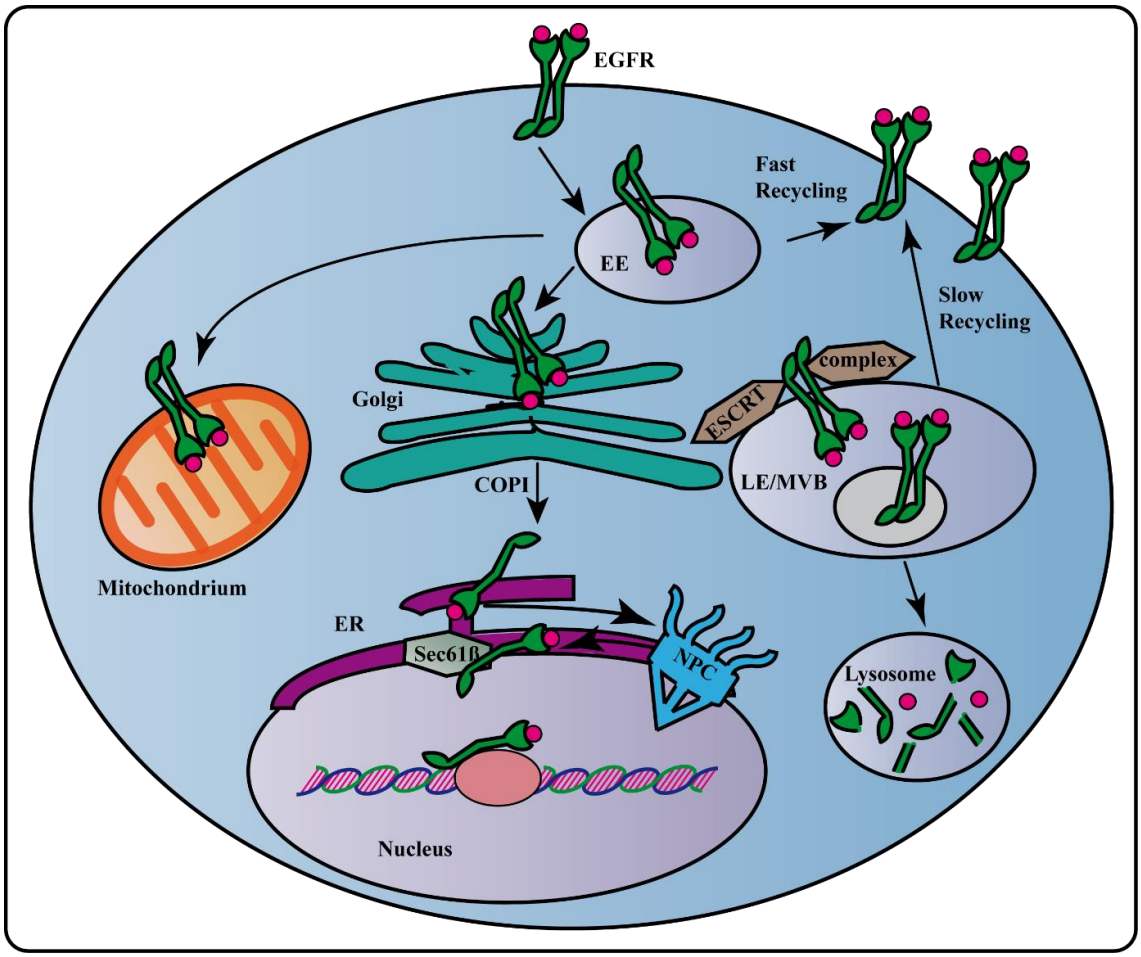

Figure 7: Illustration of EGFR trafficking in human cells. *After ligand activation or other stimuli like irradiation, the EGFR molecules are internalized into early endosomes (EE) in the cell. From these, the EGFR can either be recycled back to the plasma membrane, translocated to the mitochondria or undergo retrograde Golgi transport to the nucleus (NPC = nuclear pore complex). Maturation of the early endosomes to late endosomes and eventually lysosomes leads to degradation of the EGFR molecules.*

1.7.1 Degradation and Recycling of the EGFR

At physiologically low concentrations of EGF, the majority of EGFR dimers are quickly internalized by clathrin mediated endocytosis (CME). Interestingly, the enrichment of PIP_2 in the plasmamembrane adjacent to the receptor is essential for vesicle formation [66]. The clathrin coated pits (CCP) fuse with a tubovesicular compartment known as the early endosome. Its lumen has a mildly acidic pH so that neither the EGFR dimers nor the EGFR-EGF-complex dissociate substantially, thus maintaining kinase activity. Other ligands, as Tumor Growth Factor alpha (TGFα), however, do dissociate from the receptor under these conditions. [67].

From these early endosomes, most of the EGFR molecules are recycled back to the plasma membrane directly. Others are processed into the lysosomal pathway for

degradation. In this fate decision, the ubiquitination pattern of the EGFR´s lysine residues plays a crucial role [68]. Early endosomes containing ubiquitinated EGFR complexes that can interact with sorting proteins like Endosomal Sorting Complex Required for Transport (ESCRT) mature to multivesicular bodies. From these, a slower recycling to the plasma membrane can occur. More common, however, is the fusion with lysosomes and subsequent degradation [66,67].

1.7.2 Nuclear EGFR

Active transport of proteins into the nucleus is a well-known mechanism for the transcriptional activation of certain target genes.

For example, the CREB-regulated transcriptional activator (CRTC1), has been shown to couple synaptic stimulation in neurons to transcriptional activation [69]. In unstimulated cells, phosphorylated CRTC1 is bound to the 14-3-3 protein and therefore localized cytoplasmatically. Depolarization of the neuronal cell leads to an increase of the intracellular Ca^{2+} level and subsequent activation of the Calcineurin phosphatase [70]. Consequently, CRTC1 is dephosphorylated, dissociates from the 14-3-3 protein and is translocated from the cytoplasm in spine and dendrites of the neuron to its nucleus. There, CRTC1 acts as a transcription factor influencing, among other things, dendrite morphology and contextual memory [71].

More than 25 years ago, the presence of nuclear EGFR (nEGFR) in adrenocortical carcinomas has first been reported [72]. Since then, accumulating data report the translocation of the EGFR to the nucleus after its endocytosis. There, it regulates the transcription of a plethora of oncogenes by interaction with different transcription factors. Apparently, Importin β interacts with the EGFR´s tripartite, basic nuclear localization signal (NLS) which is located in its juxtamembrane domain. Subsequently, COPI-mediates the retrograde transport through the Golgi to the ER [73]. Next, the EGFR is shuttled through the nuclear pore complex (NPC) and is released into the nucleoplasm in a Sec61β-dependent way [74].

Nuclear EGFR has been detected in a multitude of tumors and cell lines and is correlated with poor overall survival, tumor size as well as resistance to chemo- and radiotherapy [75]. This is due to its interaction with transcriptional regulators resulting in the upregulation of protooncogenes such as Cyclin D1 or B-Myb [76,77]. Other interaction

partners of the nEGFR include members of the DNA repair machinery like DNA-PK or PCNA [78,79].

An overview of the proteins the nEGFR is interacting with in the nucleus and the regulated genes is shown in **Table 1**.

Table 1:Interaction partners and biological consequences of nuclear EGFR

Interaction partner	Regulated Gene	Effect	Source
	c-fos		80
LMP1, TIF2	Cyclin D1	Proliferation ↑, Genetic instability ↑, Gefitinib resistance ↑	81 76
STAT3	iNOS	Inflammation ↑, Tumor progression ↑, Metastasis ↑	82
E2F1	B-Myb	Proliferation ↑	77
STAT3	STAT1	Inflammation ↑	83
STAT5	Aurora A	Chromosome instability ↑	84
c-Src, STAT3	c-myc		85
	Prostaglandine-endoperoxide synthase 2, COX 2		86
	HIF1A	Angiogenesis ↑	87
	TWIST1		88
	BCRP	Drug resistance ↑	89
	Ki-76	Inflammatory response ↑	90
RNA helicase A			91
MUC1		Chromatin-bound EGFR ↑	92
PCNA		Cell proliferation ↑, DNA repair ↑	79
DNA-PK		Repair of DNA ds breaks ↑	93 94 78
P53, MDC1		Formation of DNA repair foci ↑	95
PRKDC		Repair of DNA ds breaks ↑	96
PNPase		Radioresistance ↑	97
PMLIV		Transcriptional activity of nEGFR ↓, Tumor progression ↓	98

The role of nEGFR in healthy cells and the delicate regulation thereof is not fully understood, yet. However, the Promyleocytic Leukemia Protein (PML) Isoform IV decreases the transcriptional activity by direct interaction with and inhibition of the nEGFR [98]. In how far nEGFR might play a role e.g. in protecting the cells from damage by natural UV-irradiation remains speculative and is subject to future investigation.

2 Aims of this study

The purpose of this work is to gain a deeper understanding of the way the guanine nucleotide exchange factor cytohesin 2/ARNO interacts with plasma membrane components. Specifically, two main emphases are elucidated:

1) ARNO is an activator of Arf GTPases and therefore involved in the intricately regulated vesicle trafficking machinery. In its inactive form, it is located in the cytoplasm, while activation of Arf requires binding of ARNO to the plasma membrane. Therefore, understanding the interaction between ARNO and the plasma membrane is important for comprehension of how intracellular vesicle trafficking is orchestrated. In this study, the question which domains of ARNO contribute to plasma membrane binding and how this binding can be modulated is addressed.

2) During the last years, a functional relationship between ARNO and the EGFR has been discussed controversially. Since dysregulation of the EGFR is a trait found in many diseases such as cancer, unraveling every aspect of its function in detail is highly relevant for possible therapeutic approaches. This work examines the spatial relationship between ARNO and EGFR clusters in the plasma membrane, the impact of the overexpression of ARNO on the activity of the EGFR and its influence on the nuclear translocation of the EGFR.

3 Materials and Methods

3.1 Materials

3.1.1 Equipment

Table 2: List of Equipment

Equipment	Manufacturer
Analytical Balance	Sartorius, BP 211D
Blotting Chamber, wet	BioRad
Centrifuges	Beckmann; Eppendorf
Electrophoresis apparatus	BioRad
FPLC, ÄKTA Prima	GE Healthcare Life Science
French Press FA-032	Thermo Scientific
Heating block	Bachofer
Incubator (bacteria) Innova 4430	Eppendorf
Incubator (mammalian cells)	Binder
Infinite M1000 Pro plate reader	Tecan
Microwave	Bosch
Nanoquant Infinite M200	Tecan
Odyssey Imager	Li-COR
Overhead-tumbler	Grant-Bio
Peristaltic pump	Mettler Toledo
pH-Meter	Mettler Toledo
Pipette-boy	Brand GmbH & Co
Pipettes	Eppendorf
Protino Ni-NTA columns 5 ml	Macherey Nagel
Sterile Hood (mammalian cell culture)	Heraeus
Superdex 200 HR 10/30 column	GE Healthcare Life Science
Tecan M1000 Pro Infinite	Tecan
UV/Vis Spectrophotometer	Thermo Spectronic
Vortex Zx3	Velp Scientifica
Water bath	GFL
Water purification system	TKA-Lab

Table 3: Fluorescence microscope IX81 (Olympus, Tokyo, Japan)

Equipment	Specifications	Company
Objective	60x 1,49 NA Apochromat oil immersion	Olympus, Germany
Lamp	150W Xenon	Olympus, Germany
Filter sets	F36-500 DAPI HC F36-525 EGFP HC F46-009 Cy5 ET F36-503 TRITC HC	AHF Analysentechnik AG, Tübingen, Germany
Detector	EMCCD camera ImagEM C9100-13	Hamamutso Photonics, Japan
Software	Xcellence rt 1.2	Olympus, Germany

Table 4: STED microscope easy-3D (Abberrior, Göttingen, Germany)

Equipment	Specifications	Company
Objective	UPlanSApo 100x/NA 1.4 oil immersion	Olympus, Hamburg, Germany
Lamp	Pulsed 488 nm excitation laser Pulsed 640 nm excitation laser Pulsed 775 nm STED laser	Abberior Instruments Abberior Instruments MPBC, Montreal, Canada
Filter sets	500-520 nm filter set 650-720 nm filter set	Abberrior Instruments
Detector	Single photon counting modules	Excelitas, Waltham, MA
Software	Imspector version 0.10 & higher	Abberior Instruments

Table 5: Confocal microscope Eclipse Ti (Nikon, Düsseldorf, Germany)

Equipment	Specifications	Company
Objective	CFI Plan Fluor 40X Oil, NA 1.3 CFI Plan Apo Lambda 20X, NA 0.75	Nikon
Lamp	Intensilight 488 nm argon ion laser 562 nm saphire laser 640 nm two-diodes laser	Nikon Melles Griot, Bensheim Coherent, Dieburg, Germany Melles Griot

Filter sets	525/50 595/40	Nikon
Dichroic mirrors	DAPI/Cy5 dual MHE 46660	Nikon
Detector	Four Photomultipliertubes	Nikon
Software	NIS Elements C	Nikon

Table 6: Automated confocal microscope system Cell Voyager CV6000 (Yokogawa Inc., Ratingen, Germany)

Equipment	Specifications	Company
Objective	20x water immersion 40x water immersion	Olympus, Germany
Lamp	488 nm excitation laser 561 nm excitation laser	Coherent
Filter sets	BP 522/35 BP 600/37	Semrock
Detector	Four EMCCD cameras	Hamamatsu Photonics
Software	CV 6000 Analysis Software	Yokogawa

3.1.2 Consumables

Table 7: List of consumables

Consumable	Manufacturer
Blotting papers	Macherey Nagel
Cell culture dishes, Ø 6 cm, 10 cm	TPP
Cell culture flasks, 75 cm^2	TPP
Cell culture plates, 6-well	TPP
Centricon centrifugal filter (30 kDa cutoff)	Millipore
Centrifugation tubes (15ml and 50ml)	Falcons or TPP
Clear 96 – well – plate	Greiner
Coverslips for confocal microscopy, Ø 13 mm, No. 1	VWR
Coverslips for epifluorescence microscopy, Ø 25 mm, No. 1	Marienfeld
Coverslips for STED microscopy, 22x22 mm, No. 1.5	Marienfeld

(high precision)	
Disposable cuvettes, 1 ml	Roth
Hamilton Syringes	Sigma-Aldrich
Membrane filter paper, thickness 1 mm	Sigma-Aldrich
Microscope slides, 75x25 mm	VWR
Ni-NTA agarose, bead size 45-165 nm	Qiagen
Nitrocellulose paper	Whatmann
Parafilm	Roth
Petri dishes, Ø 6 cm, 10 cm	Faust
Pipette tips, 0.1-10 µl, 2-200 µl, 50-1000 µl	Eppendorf and Peske
Reaction tubes, 1.5 ml and 2 ml	Eppendorf or Sarstedt
Serological pipettes (2 ml, 5 ml, 10 ml, 25 ml, 50 ml)	Sarstedt
Streptactin High Capacity beads, cat#: 2-1208-010	Iba
Subcellular Protein Fractionation Kit	Thermo Fisher
Syringes	Braun
TetraSpeck beads, 100 nm	Thermo Scientific
Vivaspin Turbo15 concentration falcons	Sartorius

3.1.3 Chemicals and Reagents

Table 8: List of Chemicals and (bio-)reagents

Substance	Manufacturer
Acetic acid	Roth
Acetone	Roth
Acrylamide – Bisacrylamide solution (37.5 : 1)	Roth
Agar	Roth
Ampicillin, cat#:69-53-4	Sigma-Aldrich
Ammoniumperoxidesulphate (APS)	Roth
β-Mercaptoethanol	Roth
Bradford Assay Reagent, cat#: 5000006	BioRad
Bromophenol blue	Merck
BSA	Sigma-Aldrich
Chloramphenicol	Sigma-Aldrich

Coomassie Brilliant Blue R250	Biorad
Dimethylsulphoxide (DMSO)	Fluka
Dithiotreitol	Roth
DraQ5, nuclear dye	Thermo Fisher
EGF, cat#: CYT-217	Peprotech
Ethylendiaminetetraacetic acid (EDTA)	AppliChem
Ethanol	Roth
G-418 Sulfate / Geneticin, 20ml, cat# 10131027	Thermo Fisher
Glutamine	PAN
Glycine	Roth
HEPES	Roth
Hydrochloric acid	VWR Chemical
Imidazole	Roth
Isopropanol	Roth
Isopropyl β-1-thiogalactopyranoside (IPTG)	Carbolution Chemicals
Kanamycin, cat# T832.4	Roth
Lipofectamine LTX PLUS	Thermo Fisher
Magnesium chloride	Acros organics
Methanol	Roth
Mounting Solution Aqua Polymount	Polysciences Inc.
N,N,N´,N´- Tetramethylendiamine (TEMED)	Merck
PAGE Ruler Prestained Plus	Thermo Scientific
Penicillin/Streptomycin	PAN
ProLong Gold Antifade Mountant	Thermo Fisher
Protease Inhibitor Cocktail	Roche
Protein Assay Dye Reagent Concentrate (5x)	BioRad
Sodium bicarbonate	Merck
Sodium chloride	Roth
Sodium cholate	Sigma-Aldrich
Sodium dodecyl sulphate (SDS)	Roth
Sodium orthovanadate	AppliChem
Thimerosal	AppliChem
TMA-DPH, cat#: T204	Thermo Scientific

Trifluoracetic acid	Roth
Tris	Roth
Triton X-100	AppliChem
Tween 20	AppliChem
Urea	Roth

3.1.4 Buffers and Solutions

Table 9: Buffer compositions and solutions

Buffer	Composition
Protein purification	
Lysis / Washing buffer I	50 mM Tris-HCl pH 7.8 at 4 °C 300 mM NaCl 20 mM Imidazole 10 % v/v Glycerol
Elution buffer SBP-Tag	Lysis / Washing buffer I + 2.5 mM Desthiobiotin
Elution buffer His-Tag	Lysis / Washing buffer I + 250 mM Imidazole
TEV digest buffer	50 mM Tris-HCl pH 7.8 at 4 °C 300 mM NaCl
TEV wash buffer	TEV digest buffer + 20 mM Imidazole
HEPES buffer for storage	20 mM HEPES 150 mM NaCl
SDS-PAGE	
4x Stacking gel buffer	500 mM Tris-HCl, pH 6.8 13.87 mM SDS
4x Separating gel buffer	1.5 M Tris-HCl, pH 8.8 13.87 mM SDS
6x Sample buffer	50 mM Tris-HCl, pH 6.8 30 % Glycerol 15 % w/v SDS

	600 mM DTT 1 mg Bromophenol blue
Coomassie staining	
Staining solution	30 % v/v methanol 10 % v/v acetic acid 700 mg/l Coomassie Brilliant Blue R250
Destaining solution	30 % v/v methanol 10 % v/v acetic acid
Western Blot	
1x Lysis Buffer II	20 mM Tris-HCl, pH 7.5 150 mM NaCl 1 mM EDTA 1 mM EGTA 2.5 mM sodium pyrophosphate 1 mM β-glycerophosphate 1 mM sodium vanadate 1 % (v/v) Triton-X 100
10x Wetblot buffer	250 mM Tris 1.92 M Glycine
Blocking buffer (5% BSA in TBST)	20 mM Tris-HCl pH 7.4 136 mM NaCl Tween 20 0.1 % v/v BSA 5 % w/v
10x PBS	1.37 M NaCl 27 mM KCl 80 mM Na_2HPO_4 20 mM KH_2PO_4
4x Sonication buffer	80 mM HEPES-KOH, pH 7.2 480 mM potassium glutamate 80 mM potassium acetate 40 mM EGTA
Quenching buffer	50 mM NH_4Cl in PBS
LB medium	20 g LB broth / 1 l ddH_20
LB agar solution	LB medium supplemented with 15 g/l agar

PLL Stock solution	2 mg/ml in ddH_2O

3.1.5 Biological materials

3.1.5.1 Antibodies

Table 10: List of antibodies

Antigen	Catalog #	Host species	Fluorophore	Dilution	Manufacturer
EGFR	SC-03	Rabbit	-	1:50 – 1:100 IF	Santa Cruz
EGFR	CS4267	Rabbit	-	1:1000 WB 1:50 IF	Cell Signaling
EGFR	PA1-1110	Rabbit	-	1:100	Abcam
EGFR pY1086	Ab32086	Rabbit	-	1:1000	Abnova
SBP-Tag	SC101595	Mouse	-	1:50	Santa Cruz
ARNO	Ab56510	Mouse	-	1:500	Abnova
Lamin	SC-7292	Mouse	-	1:1000-2000	Santa Cruz
GAPDH	SC-25778	Rabbit		1:1000	Santa Cruz
Rabbit IgG	A-21206	Donkey	Alexa 488	1:200	Thermo Fisher
Mouse IgG	A-21203	Donkey	Alexa 594	1:200	Thermo Fisher
Rabbit IgG	Ab150064	Donkey	Alexa 594 (STED)	1:200	Abcam
Mouse IgG	50185	Goat	Atto 647N (STED)	1:200	Sigma
Mouse IgG	CS5257	Goat	DyLight800	1:15000	Cell Signaling
Rabbit IgG	926-32213	Donkey	IR800CW	1:20000	LiCOR

3.1.5.2 Organisms

Table 11: List of Organisms

Organism	Source
E.coli BL21DE3	Famulok group (V. Fieberg)

E.coli XL10-Gold	Agilent technologies
HeLa (human cervix cancer cell) – adherent, cat#: CCL-2	ATCC
MDA-MB-468 (human mammary gland / breast cancer cell), cat#: HTB-132	ATCC

3.1.5.3 Plasmids

Table 12: List of Plasmids for protein expression*

Construct	Temperature	Induction time	Antibiotic
pET28ST-ARNO-PH clone 20	20 °C	Over night	Kanamycin
pET28ST-ARNO-Sec7	37 °C	4 h	Kanamycin
pET28ST-ARNO	20 °C	Over night	Kanamycin
pET28ST-ARNO E156K	20 °C	Over night	Kanamycin
pET28ST-ARNO R280C	20 °C	Over night	Kanamycin
pET28HT-ARNO-mEGFP	20 °C	Over night	Ampicillin
pET28HT-ARNO-PH-mEGFP	20 °C	Over night	Ampicillin
pET28HT-ARNO-Sec7-PH-mEGFP	20 °C	Over night	Ampicillin
pET28HT-ARNO-deltaCC-mEGFP	20 °C	Over night	Ampicillin
pET28HT-Gen4Lz-Sec7-PH-mEGFP	20 °C	Over night	Ampicillin
pET2828HT-ARNO-ΔPBR-mEGFP	20 °C	Over night	Ampicillin

all plasmids were a kind gift from Dr. Anton Schmitz (AG Famulok)

Table 13: List of Plasmids for mammalian expression*

Construct	Antibiotic resistance
pGFP-PK	Zeocin
pGFP-EGFRJM-PK	Zeocin
pCMVTag2-ARNO	-
pCMVTag2	-

all plasmids were a kind gift from Dr. Anton Schmitz (AG Famulok)

3.1.5.4 Culture medium

Table 14: Culture media

Medium	Manufacturer
DMEM	PAN
Fetal Calf Serum (FCS)	Biochrom
LB Medium	Roth
MEM	PAN
RPMI	PAN
1x PBS	PAN
Trypsin/EDTA (10x)	PAN

3.2 Methods

If not specified otherwise, experiments were performed at room temperature. All experiments involving living mammalian cells were carried out under sterile conditions.

3.2.1 Protein methods

3.2.1.1 Transformation of plasmid DNA into E. coli

An aliquot of competent *E. coli* strain BL21DE3 was thawed on ice. 500 ng of plasmid were added to 45 µl of bacteria and incubated on ice for 30 min followed by a heatshock of 42 °C for 45 sec. Subsequently, the mixture was put on ice immediately and cooled down for 10 min. Addition of 300 µl LB medium was followed by incubation in a thermoblock at 37 °C shaking at 800 rpm for 1 h to allow for the development of the antibiotic resistance. Then the mixture was plated on an agar plate containing 50 µg/ml kanamycin or 100 µg/ml ampicillin which was then incubated at 37 °C overnight.

3.2.1.2 Expression of proteins

200 ml of LB medium containing 50 µg/ml of the appropriate antibiotic were inoculated with a pipette tip which had been dipped into a colony on the agar plate and incubated overnight at 37 °C, shaking. Next, this preculture was added to 2 l LB medium containing 5 µg/ml antibiotic and grown until the optical density at 800 nm was 0.2. Protein expression was induced by addition of 0.5 mM IPTG. For temperature and induction time see **Table 12**. Bacteria were harvested by centrifugation for 20 min at 4000 rcf and a temperature of 4 °C in the JA25.5 rotor. The pellets were either directly subjected to protein purification or stored at -80 °C.

3.2.1.3 Purification of Streptavidin-binding-peptide (SBP)-tagged proteins

The streptavidin-binding-peptide is composed of 38 amino acids and binds to the tetrameric protein streptavidin with an affinity of 2.5 – 4.9 nM. This interaction can therefore be employed for protein purification [99]. To protect the protein of interest from degradation, all purification steps were performed with precooled buffers at 4 °C.

The *E.coli* pellet obtained from 2 l of culture was thoroughly resuspended in 10 ml Lysis buffer. 4 ml of a 50 % Streptactin High Capacity beads solution was equilibrated in Lysis buffer and centrifuged at 4 °C and 1900 rcf for 10 min.
The bacterial cell membranes were disrupted by passing them twice through a French press with a pressure between 1200 and 1500 bar. Next, the lysate was separated from the cell debris by centrifugation for 30 min at 20000 rcf at 4 °C (rotor JA 25.5). Pellets were discarded and the supernatatant was incubated with the equilibrated affinity beads in a 15 ml falcon for 1 h in the overhead tumbler to allow the SBP-tag to bind to the Streptactin beads. Afterwards, the beads were centrifuged for 5 min at 1900 rcf at 4 °C and, after discarding the supernatant, resuspended in 12 ml pre-cooled lysis buffer. This washing step was repeated three times before the beads were loaded onto a disposable column and a peristaltic pump was employed for three more wash steps with lysis buffer.
Elution of the protein of interest was achieved by three subsequent incubations of the beads with elution buffer for 5 min.

3.2.1.4 Size exclusion chromatography (SEC) with FPLC

All eluates, except for those of the SBP-PH-construct, were concentrated to 3 – 5 ml using a Vivaspin concentrator falcon with the appropriate molecular cutoff. Then, the eluates were loaded onto a HiLoad^{TM} 16/600 Superdex 200 pg SEC column which had previously been equilibrated with HEPES buffer for storage. The flow of the Ekta Pure FPLC was set to 1 ml/min. Peak fractions were collected, concentrated with a Vivaspin concentrator and the concentration was determined. Typically, the volume was about 2 ml with a concentration of 50-100 µM. The protein was then aliquoted, flash frozen in liquid nitrogen and stored at -80 °C.

3.2.1.5 Purification of hexa–histidine-tagged proteins

The basic protein purification steps are the same as described in chapters **3.2.1.1 - 3.2.1.4**, except for the use of 3 ml Protino Ni-NTA Agarose affinity beads slurry per 1 l of *E. coli* culture and the Lysis buffer I + 250 mM imidazole for elution.

3.2.1.6 Tobacco etch virus digest

In case of the GFP-constructs, the His-tag was fused to the protein chain by a linker containing a recognition site for the tobacco etch virus (TEV) protease allowing for cleavage to separate the tag from the protein.

The eluate was centrifugated for 15 min at 4 °C at 14000 rcf and the supernatant was injected into the Ekta Pure FPLC to change the buffer and get rid of the imidazole before the TEV digest. Peak fractions were collected and pooled. Per ml eluate, 1 µl of 0.5 M EDTA and 2 µl β–mercaptoethanol and one aliquot of TEV protease, which was homemade in the AG Famulok, were added.

The samples were incubated over night in the overhead tumbler @4 °C.

To remove the cleaved tag, 3 ml of Ni-NTA Agarose affinity beads slurry were equilibrated with TEV digest buffer. The solution was added and incubated for 30 – 60 min at 4 °C in the overhead tumbler. The mixture was then added to a disposable column and subjected to gravity flow. The protein of interest was in the flowthrough, while the cleaved his-tags as well as uncleaved constructs remained bound to the beads. One wash step was performed with 3 ml washing buffer and the wash flowthrough was combined with the initial flowthrough.

Subsequently, the protein solution was concentrated using Centricon centrifugal filters with the appropriate cutoff and the concentration was determined using the nanodrop. Typically, the volume was about 2 ml with a concentration of 50-100 µM.

3.2.1.7 SDS-PAGE

SDS-polyacrylamide-gel-electrophoresis (SDS-PAGE) is the separation of proteins based on their molecular weight by application of an electric field to a gel. The anionic detergent SDS binds to proteins in a ratio of 1.4 g SDS per 1 g protein thus dominating the protein´s overall charge. Therefore, separation of the proteins is charge independent from their isoelectric point [100].

Samples were diluted in 6x sample buffer and boiled for 5 min before loading them onto a gel with the appropriate acrylamide percentage.

Table 15: Pipetting scheme for SDS PAGE gels

Component	Composition Separating gel [µl]				Composition Stacking gel [µl]
	8 %	**10 %**	**12.5 %**	**15 %**	**4 %**
Acrylamide	1333	1667	2083	2500	213
Water	2379	2045	1629	1212	975
Separating gel buffer	1250				-
Stacking gel buffer	-				400
TEMED	8				2
APS	30				10.4
Total	5000	5000	5000	5000	1600.4

On each gel 5 µl of the PAGE Ruler Prestained Plus were loaded as a standard ladder indicating the running height of proteins.

Gels were run at 170 V for 50 – 60 min in 1x running buffer using a BioRad electrophoresis apparatus.

For protein visualization, the gels were incubated in Coomassie staining solution (see **Table 9**) for at least 30 min, gently shaking. The staining solution was recovered, and the gel rinsed once with destaining solution. Next, the gels were generously covered with destaining solution, shortly heated in the microwave and shaken for about 20 min. The gels were imaged using the Odyssey Imager.

Destaining solutions were recycled by passing them through a funnel that had been lined with filter paper and filled with active charcoil.

3.2.1.8 Westernblot

Proteins can be transferred from SDS-PAGE gels to nitrocellulose membranes by use of an electromagnetic field. Two sponges, two pieces of Whatman paper, one nitrocellulose membrane and the SDS-PAGE gel were equilibrated in Wetblot buffer. The blot was assembled as depicted in **Figure 8** within the buffer in the equilibration basin.

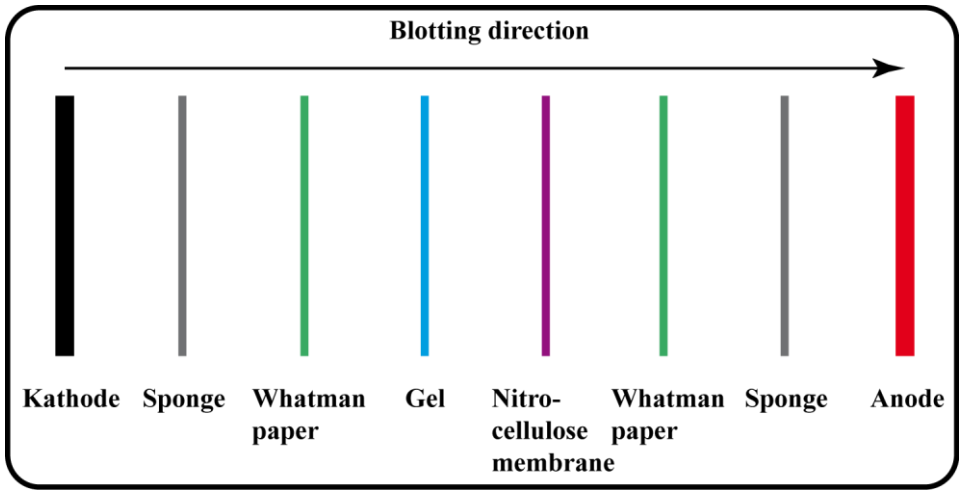

Figure 8: Building scheme of a wet westernblot system. *All components of the wetblot had been equilibrated in wetblot buffer at 4 °Cprior to construction.*

Then, the blot was placed into the wetblot chamber together with a coolpack and an electromagnetic field of 100V and 2 Ampere (A) was applied for 1 hour while the buffer was stirred by a magnetic stirrer.

Afterwards, unspecific binding of antibodies to the nitrocellulose membrane was blocked with 5 % BSA in TBST except for the ARNO blots that were blocked with 5 % milk powder in TBST. If necessary, the westernblots were cut according to the molecular weight standard and incubated separately with primary antibodies diluted in 5 % BSA in TBST at dilutions as stated in **Table 10** overnight at 4 °C, shaking gently. The primary antibodies were recovered and stored at 4 °C to be reused twice at maximal. The blots were washed three times for five minutes with TBST and then incubated with the secondary antibody diluted in 5 % BSA in TBST at dilutions as stated in **Table 10** for 1 hour at room temperature.

Having recovered the secondary antibodies, the blots were washed three times for five minutes with TBST and imaged using the Odyssee reader. Quantification of the bands was done with the Image Studio Lite Ver. 3.1.

3.2.2 Cell Culture

3.2.2.1 Cleaning and PLL-coating of coverslips

For some experiments, cells were plated onto glass-coverslips. Prior to using them for cell culture and microscopy, residual oil and other soiling from the production process needed to be removed.

To this end, 500 coverslips were rinsed five times with dH_2O in a 1 l beaker. Swirling of the coverslips was done manually to avoid mechanical damage. Afterwards, the coverslips were washed with 1 M HCl for 1–2 hrs swirling them every twenty minutes before being rinsed ten times with dH_2O. Afterwards, the coverslips were rinsed three times with 100 % EtOH (p.a.) and then kept with 100 % EtOH (p.a) overnight. On the next day, the EtOH was removed and the coverslips sterilized in an oven at 180 °C.
For subsequent sheeting experiments, it was necessary to enable the cells to adhere firmly to the coverslips. In order to achieve this, the coverslips were coated with poly–L–Lysine (PLL).
First, the PLL–stock solution at a concentration of 2 mg/ml was filtered and diluted 20-fold in ddH_2O. One coverslip in a well of a cell culture 6–well plate was covered with 500 µl of the PLL–solution, which forms a meniscus due to the water´s surface tension, and incubated for 30 min. Subsequently, the PLL-solution was removed and the coverslips were dried for at least 1 h before they were sterilized by irradiation with UV light for 20 min. Coated coverslips were stored within the 6-well-plates at 4 °C.

3.2.2.2 Passaging and counting of HeLa and MDA-MB-468 cells

Growth medium was removed from the cells and the flask was rinsed with 10 ml of PBS to remove residual medium. Per 75 cm^2 cell culture flask, 2 ml of Trypsin/EDTA reagent was added and it was ensured that the complete surface was covered. After incubation for 5 min at 37 °C, 8 ml of growth medium was added and pipetted up and down several times to detach all cells. Approximately 9.8 ml cell suspension was then taken out of the flask and 25 ml growth medium was added.
Ten µl of the cell suspension was diluted 10-fold in PBS and the cells were counted in a Neubauer chamber. Cell concentration could then be calculated by the formula

$$C = N / S * 10^5$$

Where C is the concentration of cells in #/ml, N is the cell count of the 10-fold dilution and S signifies the number of squares that had been used for counting in the Neubauer chamber. Usually, all eight squares were counted.
Consequently, appropriate numbers of cells could then be plated for subsequent experiments.

3.2.2.3 Preparation of stable HeLa cell lines

First, the plasmids were transfected into HeLa cells that had been seeded into 6-well-plates at a density of 3.75 x 10^5 cells/dish the day before.

Table 16: Transfection of HeLa cells with Lipofectamine LT1 kit

Component	Amount
DMEM	250 µl
Plasmid DNA	2.5 µg
LT1	12.5 µl

The transfection mixture was incubated for 25 min at room temperature before being added to the cells. 48 hours later, the transfected cells were transferred to a 15 cm^2 cell culture dish. For selection of successfully transfected cells, the antibiotic G-418 was added leading to a final concentration of 800 µg/ml. The G-418-supplemented medium was renewed daily for ten days. Then, single colonies were picked by local trypsination of the colonies and transfer into 6-well-plates. After verification of the correct subcellular localization of the fluorescent constructs by microscopy, the cell populations were sorted by fluorescence activated cell sorting (FACS) to obtain monoclones. Subsequently, the cell lines derived from these monoclones were always cultured in DMEM containing 10 % FCS and 800 µg/ml G-418 to prevent loss of the construct.

3.2.2.4 Membrane sheets

To be able to access the inner leaflet of the plasma membrane of the cell, so-called membrane sheets were prepared from cells grown on glass-coverslips.

About 1.5 * 10^5 cells were plated per coverslip and grown over night. One coverslip at a time were placed at the bottom of a petri dish completely filled with sonication buffer that had been precooled to 4 °C. The cells were facing up and 5 mm distant from the sonicator tip. A 0.1 s ultrasound pulse was applied to “unroof” the cells so that only the basal plasma membrane remained attached to the coverslip. The coverslip was taken out of the petri dish, briefly dried from excess sonication buffer by touching its rim with a soft paper towel and then subjected to protein incubation.

Unless specified otherwise, the membrane sheets were incubated with a 1 µM protein solution in sonication buffer face down on parafilm for 5 min at room temperature.

3.2.3 Experiments with HeLa cells

3.2.3.1 Transfection

DNA delivery into eukaryotic cells can be facilitated by formation of complexes between the plasmid DNA and cationic lipids used as transfection reagents. These complexes form micelles that then interact with the cells and trigger endocytosis.

One day before transfection, 0.75-1 * 10^6 cells were plated per 6-cm-dish.

The mixtures of plasmid and transfection reagent were prepared as indicated in **Table 17**.

Table 17: Scheme for transfection of mammalian cells using the Lipofectamine LTX PLUS kit

Component	Mixture A	Mixture B
RPMI	225 µl	225 µl
Lipofectamine LTX	13.5 µl	
Mock plasmid	-	3.75 – x µg
Plasmid of interest	-	x µg
PLUS Reagent	-	3.75 µl

Mixture B was added to mixture A and incubated for 5 min. Then, the mixture was added dropwise to the culture medium of the cells for incubation overnight.

3.2.3.2 Stimulation and lysis

One day before stimulation, the culture medium, still containing transfection reagent, was exchanged for starving medium that is medium not supplemented with FCS. The objective for this is to be able to perform the experiment with completely unstimulated EGFRs which then can be stimulated in a precisely defined way as opposed to working with an equilibrium of stimulated and unstimulated EGFRs in FCS-containing medium.

For stimulation, the starving medium was replaced by medium supplemented with 50 ng/ml EGF for 5 min. Cells were kept on ice and scraped off in ice in 2 ml ice-cold PBS. The cells in the suspension were harvested by centrifugation for 8 min at 800 rcf

at 4 °C. Then, the cell pellet was resuspended in 50-100 µl Lysis buffer supplemented with proteinase inhibitor at a 1:100 dilution. The mixture was incubated on ice for 20 min and thoroughly vortexed every 5 min. Afterwards, it was centrifugated for 30 min at 4 °C at maximum speed and the supernatant, the lysate, was transferred to a new tube for subsequent westernblot analysis.

3.2.3.3 Bradford assay for protein concentration in cell lysates

The Bradford assay relies on the absorbance shift of the dye Coomassie Brilliant Blue G-250 upon binding to different amino acids, which can be detected by a plate reader [101].

A BSA standard with concentrations ranging from 167 mg/ml to 3000 mg/ml was prepared and 2 µl of each concentration was pipetted into a transparent 96 – well – plate in duplicates. The lysate samples were 10-fold diluted and 2 µl of the dilutions was pipetted into the plate in triplicates. The Bio-Rad Protein Assay Reagent Concentrate was diluted 5-fold with ddH_20 and 150 µl of the resulting solution were added to each well of the 96 – well – plate. After 5 min of incubation at room temperature, the absorbance at 595 nm was measured using a Tecan M1000 Pro Infinite plate reader.

The BSA standard values were used to produce a linear regression line in Microsoft Excel. If the coefficient of determination, R^2, was ≥ 0.98, the line was accepted for further analysis of the samples. Sample concentrations were calculated with reference to the regression line.

3.2.3.4 Subcellular fractionation

To assess the subcellular localization of proteins, cytoplasmic, membrane and nuclear proteins were separated. For this, all buffers were taken from the Subcellular Protein Fractionation Kit, manufactured by Thermo Fisher. The complete procedure was performed on ice with precooled buffers and the centrifuges had been cooled to 4 °C. Cell pellet obtained after scraping the cells from 6 cm cell culture dishes were thoroughly resuspended in 100 µl cytoplasmic extraction buffer (CEB), supplemented with proteinase inhibitor (PI) at a 1:100 dilution. The sample was incubated in an overhead tumbler for 20 min at 4 °C, centrifuged for 8 min at 800 rcf and the supernatant was transferred to a fresh tube before being centrifuged for 10 min at 21130

rcf. The resulting supernatant, which was kept on ice until analysis by westernblot, was the cytoplasmic extract (CE).

The pellet was washed with 800 µl ice-cold PBS supplemented with PI at a 1:100 dilution and centrifuged for 8 min at 800 rcf. The pellet was resuspended in 100 µl membrane extraction buffer (MEB), with added PI and incubated for 20 min in an overhead tumbler. Afterwards, the samples were centrifuged for 10 min at 3000 rcf. The supernatant was transferred to a new tube and centrifuged for 10 min at maximum speed. The resulting supernatant was the membrane extract (ME), which was kept on ice until further analysis by westernblot.

To reduce contamination of the nuclear extract (NE), the pellets were washed with 800 µl PBS supplemented with PI at a 1:100 dilution, centrifuged for 10 min at 3000 rcf. Afterwards, the pellets were thoroughly resuspended in nuclear extraction buffer (NEB), supplemented with PI, vortexed for 15 sec and incubated in an overhead tumbler for 45 min. Then, the samples were centrifuged for 10 min at 5000 rcf and the supernatant was transferred to a fresh tube that then was centrifuged for 10 min at maximum speed. This supernatant equaled the nuclear extract (NE) and kept on ice until further analysis by westernblot.

3.2.4. Preparation of samples for microscopy

3.2.4.1 Epi-fluorescence microscopy

After protein incubation (see chapter **3.2.2.4**), the coverslips were transferred from the parafilm to 6-well-plates with the membrane sheets facing up. They were then fixed by incubation with 4 % PFA in PBS for 20 min, shaking gently. Since PFA creates background fluorescence, it needed to be quenched. For this, the solution was replaced by 50 mM NH_4Cl in PBS for 30 min, shaking gently. Afterwards, the quenching solution was removed, and the coverslips were washed three times for 5 min with 2 ml PBS. The GFP-constructs could be imaged immediately afterwards. Coverslips that were to be subjected to immunostaining were blocked in 2 ml 3 % BSA in PBS for one hour, shaking gently. Immunostainings were performed in a sequential manner. First, the antibody against the SBP-tag was diluted 1:50 in 3 % BSA in PBS and the coverslips were incubated with 100 µl of this solution for 1 h face down on parafilm in a wet chamber. Afterwards, they were transferred back to the 6-well-plate, washed 3 times for 5 min with 2 ml PBS and then incubated with 100 µl of secondary antibody

solution, diluting the antibody as indicated in **Table 10** in 3 % BSA in PBS, for 1h face down on parafilm in a wet chamber. Prior to use, the antibody solution was centrifuged for at least 10 min at 21130 rcf. After washing the coverslips in 6-well-plates three times for 5 min with 2 ml PBS, the entire staining procedure was repeated with the antibodies against the EGFR or the TFR, respectively. Coverslips were stored at 4 °C in PBS overnight.

3.2.4.2 STED microscopy

The coverslips were fixed, quenched and subjected to immunostaining as described in chapter **3.2.4.1**. For membrane staining, the coverslips were incubated for 10 min with 2 ml of a dilution of 400 µg/ml FastDiO in PBS, which had been sonicated for at least 15 min. Then, the coverslips were washed 3 times for 5 min with PBS. The coverslips were mounted onto microscope slides face down in 15 µl ProLong Gold Anifade Mountant solution and left to dry in the dark for 24 hrs. Afterwards, the rims of the coverslips were sealed using clear nail polish to prevent the sample from drying out. After the nail polish had hardened, the coverslips could be stored at 4 °C for several weeks.

3.2.4.3 Confocal microscopy

About 25000 cells were seeded per glass coverslip located in 24-well-plates. The next day, the medium was exchanged by medium without FCS to starve the cells overnight.
The following day, for stimulation, the starvation medium was exchanged by 500 µl medium containing 50 ng/ml EGF and the cells were incubated for 20 min at 37 °C. Fixation of the cells was achieved by adding to the 500 µl medium an additional 500 µl of 8 % PFA in PBS to each well and incubation at 37 °C for 15 min. Then, the coverslips were washed three times with PBS. For permeabilization, the PBS was replaced by 500 µl 0.5 % Triton X-100 in PBS. After 20 min incubation at room temperature, the coverslips were washed three times for 5 min with PBS. Then, the coverslips were blocked with 5 % Goat Serum and 0.3 % Triton X-100 in PBS for 1 h at room temperature. Having washed the coverslips three times for 5 min with PBS, the coverslips were transferred face up to a wet chamber and incubated with 50 µl primary antibody diluted in PBS containing 0.3% Triton X-100, as indicated in **Table 10**, per coverslip overnight at 4 °C.
The primary antibody solution was removed from the coverslips and they were washed by dipping them consecutively into three beakers containing PBS. Per coverslip, 50 µl

of secondary antibody diluted in 1 % Goat Serum and 0.3 % Triton X-100 in PBS was pipetted onto each coverslip and they were incubated for 1 hour at room temperature in the dark. The secondary antibody solution was removed, and the coverslips washed consecutively in three beakers containing PBS. For nuclear staining, 50 µl DraQ5, diluted 1:1000 in PBS was added to each coverslip that were incubated for 15 min in the dark before the coverslips were washed again. Then, the coverslips were mounted face down on microscopic slides, dried overnight in the dark and stored at 4 °C.

3.2.4.4 Cell Voyager

6500 cells in 100 µl medium were seeded per well of a 96-well plate and grown overnight. On the next day, the cells were either incubated with the compounds of interest or directly fixed. Fixation and nuclear staining was achieved by addition of 100 µl of a 1:2000 dilution of DraQ5 in 8 % PFA in PBS to each well and incubation for 15 min at 37 °C. Afterwards, the medium was replaced by PBS and the plates were stored at 4 °C in the dark.

3.2.5 Microscopy

3.2.5.1 Epifluorescence microscopy

The coverslips were placed face up in a microscopy chamber and covered with 2 ml of a 1:10 dilution of a saturated TMA-DPH solution in PBS. If colocalization analysis was planned, 100 µl of a 1:1000 dilution of Tetraspeck beads was added to the imaging solution.

Imaging was performed with a 60x oil immersion objective employing an additional 4x magnification lens.

The membrane sheets for imaging were chosen in the TMA-DPH channel based on their quality and integrity. Subsequently, the images in the fluorescent channels were taken. GFP and Alexa 488 fluorescence were detected using the EGFP filter set, Alexa 594 fluorescence was imaged employing the TRITC filter set and the Tetraspeck beads were imaged additionally with the Cy5 channel filter set. For every set of experiments, the image acquisition parameters such as exposure time and gain were kept constant.

3.2.5.2 STED microscopy

The membrane sheets were selected for imaging based on their quality and integrity by evaluation of the FastDiO staining which was excited with a pulsed 488 laser and detected with the 500-520 nm filter. For super-resolution imaging, a pixel size of 15 nm x 15 nm was used. The Atto647N fluorophore was excited with a pulsed 640 nm laser (1.95 mW), depleted with a 775 STED laser (2.57 mW) and detected with the 620-720 nm filter set. For the Alexa594 fluorophore, a pulsed 561 nm excitation laser (1.81 mW) and de-excited by a 775 STED laser (2.58 mW) was used. Its fluorescence was detected using the 580-630 nm filter set. The time-gate width was 8 ns with a delay of 1.094 ns for the line accumulation of the Alexa594 signal and a delay of 1.172 ns for the Atto647N signal. The width of the pinhole was set to 25 µm.

3.2.5.3 Confocal microscopy

The cells were selected for imaging based on their morphology. GFP fluorescence was excited by the 488 nm laser and the emitted signal was collected using the 525/40 nm filter set. DraQ5 staining was imaged by excitation with the 640 nm laser and detection with the DAPI/Cy5 dual dichroic mirror (MHE 46660). The Alexa594 fluorophore was excited by the 562 nm excitation laser and imaged using the 650-720 nm filter set. Confocal images were obtained using the 40x oil immersion objective (0.11 µm/pixel), while the 20x low working distance objective (0.459 µm/pixel) was used for the bright field images.

3.2.5.4 Cell Voyager

The automated confocal microscope was operated by Dr. Philip Denner. A 20x water immersion objective with a magnification of 0.75 was employed. GFP fluorescence was excited with a 488 nm excitation laser and detected using the 522-535 nm filter set. DraQ5 was excited by the 561 nm laser and the fluorescence was detected employing the 600-637 nm filter set.

3.2.6 Image Analysis

3.2.6.1 Epi-fluorescence

The images were exported as TIF files using the Olympus imaging software. All further analysis was performed using the open source ImageJ software version 1.51. The images were stacked and the channels overlaid. Square regions of interest (ROIs) with a size of 50 pixels were defined in the TMA-DPH channel based on the membrane quality and integrity.

For determination of the mean fluorescence intensity, background ROIs were defined in the regions without membrane and the mean fluorescence intensity measured in the background ROIs was substracted from the mean fluorescence intensity in the membrane ROIs.

For colocalization studies, the overlaid channels were manually aligned employing the Tetraspeck beads as points of reference.

The macros “Gero_coloc_ROIs_in_composite_stack_corrected_160314_B” as well as “Gero_coloc_ROIs_in_composite_stack_corrected_160314_B_flip”, both written by Dr. Jan Gero Schloetel (AG Lang), were employed to calculate the pixel-wise PCC by correlating the red and green fluorescence signals of each pixel within the ROIs. Since it has to be ensured that the PCC of samples with high cluster density significantly differs from the PCC calculated from a ROI with the same cluster density but random distribution, the second macro flips the second channel vertically as well as horizontally and then determines the PCC.

3.2.6.2 STED microscopy

Images were exported in the TIF format by the Imspector software version 0.14.11640. Image analysis was performed using the open source ImageJ software. The regions of interest (ROIs) were set manually with reference to the membrane staining documenting the integrity of the membrane. For further analysis, several macros written by Dr. Jan Gero Schloetel (AG Lang) were employed. First, the macro “combine_ROIs_03_simple” was used to alternate the ROIs on the membrane with those in the background.

Next, the macro “macro_gero_spot_analysis_NN_v46_FWHM_1Dvar_update2” was employed to perform the nearest neighbor analysis as well as the cluster size and density calculations. This macro first finds the local maxima in the two channels,

enhances spot identification by employment of a mexican hat filter and then removes very weak spots based on the minimum ratio of their intensity divided by their intensity in the other channel to address channel crosstalk. Subsequently, the nearest neighbor distances between the identified spots within as well as between the channels and the full-width at half maximum of the individual spots are calculated.

3.2.6.3 Cell Voyager

For image analysis the freeware software CellProfiler version 2.1.1 was employed. Using an algorithm written by Dr. Christoph Möhl (Image and Data Analysis Facility, DZNE), the software separated the nuclei from the cytoplasm in the images and measured the mean intensities in these regions. Since not the absolute fluorescence intensity, but the ratio between nuclear and cytoplasmic fluorescence was used for analysis, no background correction was needed. Exemplarily, one of the images after segmentation is shown in **Figure 9**.

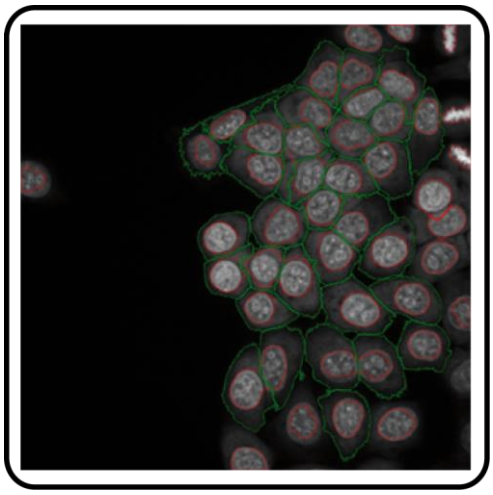

Figure 9: Example for automated cellular segmentation*. DraQ5 staining of HeLa cells. Nuclei and cytoplasms are recognized and separated by an algorithm of the CellProfiler software. The bleedthrough of the DraQ5 staining into the cytoplasm was used to determine the cell border.*
The automatized segmentation was controlled by eye and, if necessary, corrected manually.

4 Results

The spatiotemporal regulation of small GTPase activity is crucial for a plethora of cellular pathways. To achieve this, the activity as well as localization of GEFs like ARNO need to be controlled intricately. It has been shown that cytoplasmic ARNO is recruited to the inner leaflet of cell membranes via Arf1/6 and Arl4 [30]. The fact that ARNO contains a pleckstrin-homology (PH) domain which binds to phosphatidylinositol 4,5-bisphosphate [$PI(4,5)P_2$] and to phosphatidylinositol 3,4,5-trisphosphate [$PI(3,4,5)P_3$] indicates that ARNO can bind to the membrane independent of Arf 1/6 and Arl4 via phosphoinositide interaction [102]. Since the amount of PIP_2 is elevated in the plasma membrane as compared to other cellular compartments, a preferential recruitment of ARNO to the plasma membrane may be mediated by PIP_2 [40]. Moreover, the availability of PIP_2 binding sites may be regulated by the second messenger Ca^{2+} that has been shown to crosslink PIP_2 molecules [103]. Previous studies aimed for elucidating the binding of ARNO to artificial PIP_2-containing membrane systems, neglecting the complexity of native membranes [28,102]. Therefore, we wanted to study the contribution of the different ARNO domains to membrane binding on intact plasma membranes. These were prepared by unroofing HeLa cells with a brief ultrasound pulse leaving a basal plasma membrane sheet on the coverslip with the intracellular side facing up. This method preserves the composition of the membranes and avoids the need for detergents or other harsh treatments. Such membrane sheets have been proven to maintain many native functionalities from exocytosis to formation of endocytic vesicles [104,105].

4.1 Ca^{2+} impairs binding of ARNO to plasma membrane sheets

To verify that PIPs may play a role in membrane binding of ARNO and on top of that are regulated by Ca^{2+}, we first tested whether Ca^{2+} has any influence on the binding of ARNO to the native membranes. It should be noted that Ca^{2+}, even in traces, can mediate biological responses. To ensure Ca^{2+} concentrations lower than 100 nM, chelators like EGTA were added. First, we generated membrane sheets from Hela cells in a buffer without EGTA and incubated them for 5 min at room temperature without EGTA with 1 μM recombinant ARNO that carried a green fluorescent protein (GFP) tag. Then membranes were fixed and imaged. As shown in **Figure 10 a**, there is only a

minor amount of GFP-fluorescence (i.e. ARNO binding) detectable on membrane sheets. This observation suggests that the abundance of binding sites for ARNO is either very scarce or that the accessibility to the binding sites is limited.

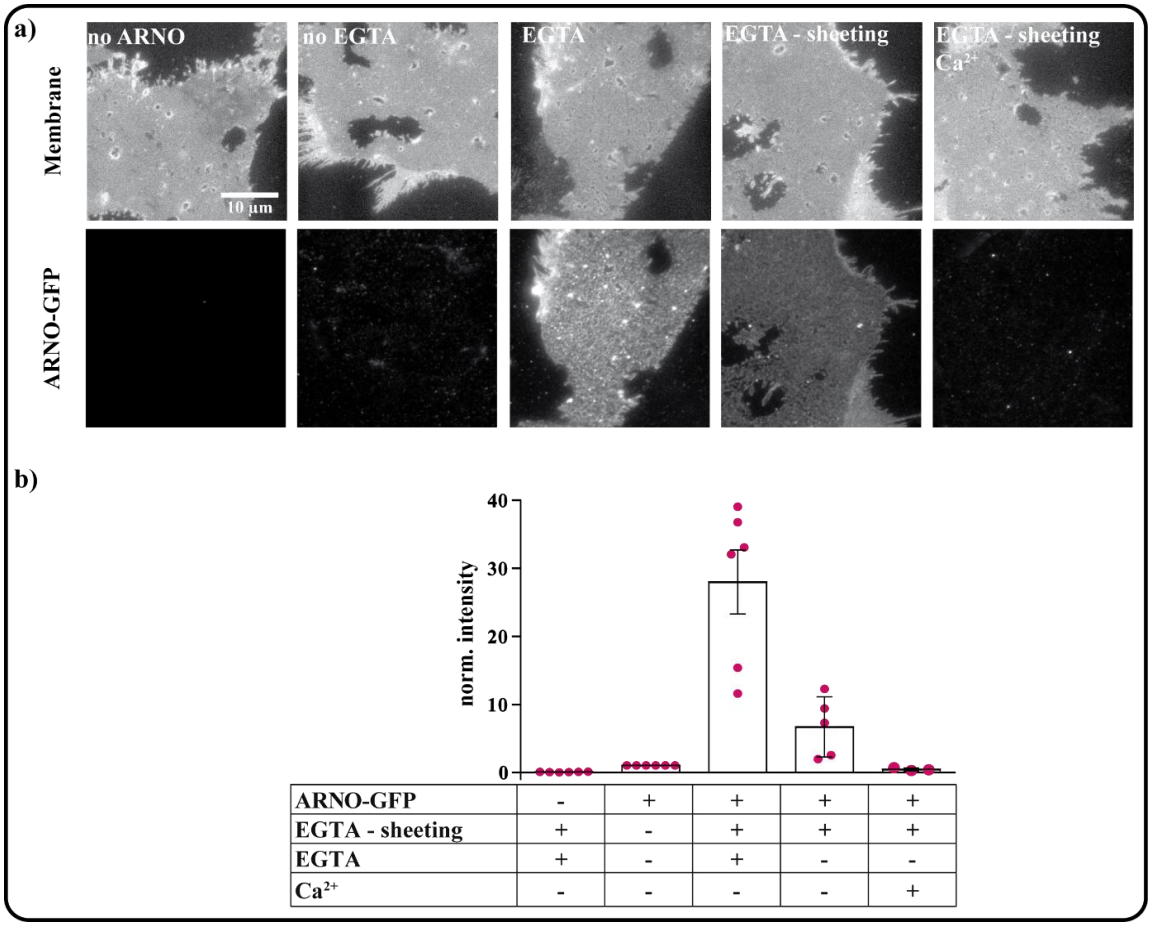

Figure 10: EGTA treatment increases ARNO-GFP recruitment to the plasma membrane. *Membrane sheets were prepared by a 0.1 sec ultrasound pulse at 4 °C and incubated with 1µM ARNO-GFP or only buffer for 5 min at room temperature. In the upper panel the TMA-DPH-staining is shown to document membrane integrity, the GFP-intensity can be seen in the lower panel.* ***a)*** *From left to right: Buffer control without ARNO-GFP, preparation of sheets and incubation with ARNO-GFP in the absence of the chelating agent EGTA, presence of 10 mM EGTA during the sheeting process as well as the protein incubation, presence of EGTA during sheeting but not protein incubation (≈ 30 sec), sheeting with EGTA, additional supplementation of the EGTA-free protein incubation buffer with $CaCl_2$.* ***b)*** *Quantification of the effects, shown is the mean ± SEM (n = 3-6 biological replicates) normalized to the condition without EGTA. GFP-fluorescence is scaled equally, membrane staining arbitrarily. Scale bar: 10 µm.*

For instance, as PIP_2 is a signaling molecule, most PIP_2 in a resting cell may be already occupied by other PIP_2-binding molecules and thus inaccessible for the added ARNO. Alternatively, the PIP_2-molecules might be inaccessible due to formation of PIP_2-

bridges, a phenomenon where Ca^{2+} ions tightly coordinate PIP_2-molecules. Henceforth, PH-domain-containing proteins cannot bind as easily to the PIP_2-molecules [103,106].

To disrupt such putative bridges, we supplemented the buffers with EGTA. EGTA is a strong Ca^{2+} chelator and able to extract Ca^{2+} from the preparation, either directly from the membrane or from the buffer solutions that may contain traces of Ca^{2+} or other bivalent cations. Addition of EGTA to the buffer in which the membrane sheets were prepared as well as to the buffer in which they were incubated with the recombinant ARNO-GFP produced a > 25-fold increase in ARNO fluorescence intensity compared to the EGTA-free experiment. Albeit to a much lesser extent, binding could be also increased adding EGTA only to the sonication solution (where membranes spend ≈ 30 s after sonication, followed by another 30 s washing step without EGTA) but omitting it from the ARNO binding buffer. This increase was reversed when adding excess Ca^{2+} to the ARNO binding buffer as shown in **Figure 10 b**.

Taken together, these data show that the accessibility of ARNO binding sites in the plasma membrane is limited but can be greatly enhanced by removal of bivalent cations such as Ca^{2+} which may increase the accessibility to PIP_2. This observation hints to a crucial role of the PH-PIP-interaction in recruiting ARNO to the plasma membrane.

4.2 The ARNO PH-domain is required, but not sufficient for membrane binding

Having discovered the conditions for optimal ARNO recruitment to the plasma membrane sheets, we tested two protein constructs for further investigation of the role of the PH-PIP_2-interaction for the membrane binding of ARNO. In one of the constructs a point mutation, changing the amino acid arginine 280 to cysteine (R280C), renders it incapable of binding to PIP_2 [28,107]. The other one is a deletion construct where only the PH-domain, without the rest of ARNO, binds to the membrane sheets.

In **Figure 11 a** and **c**, the fluorescence intensities of the ARNO protein constructs are shown. In this case, for visualization antibody-labeling of an N-terminal SBP-tag was employed. The PH-domain alone binds about 90 % less compared to the full–length ARNO. To exclude that this is caused by the SBP-tag of this short construct being embedded too deeply in the membrane to be accessed by the antibody, thus diminishing staining, we repeated this experiment employing GFP-labeling. As shown in **Figure 11**

b and **d**, the extent of binding diminishment was in the same range, excluding limited antibody accessibility as a cause for less immunostaining.

The R280C mutant was almost completely incapable of binding to the sheets (**Figure 11 a** & **c**).

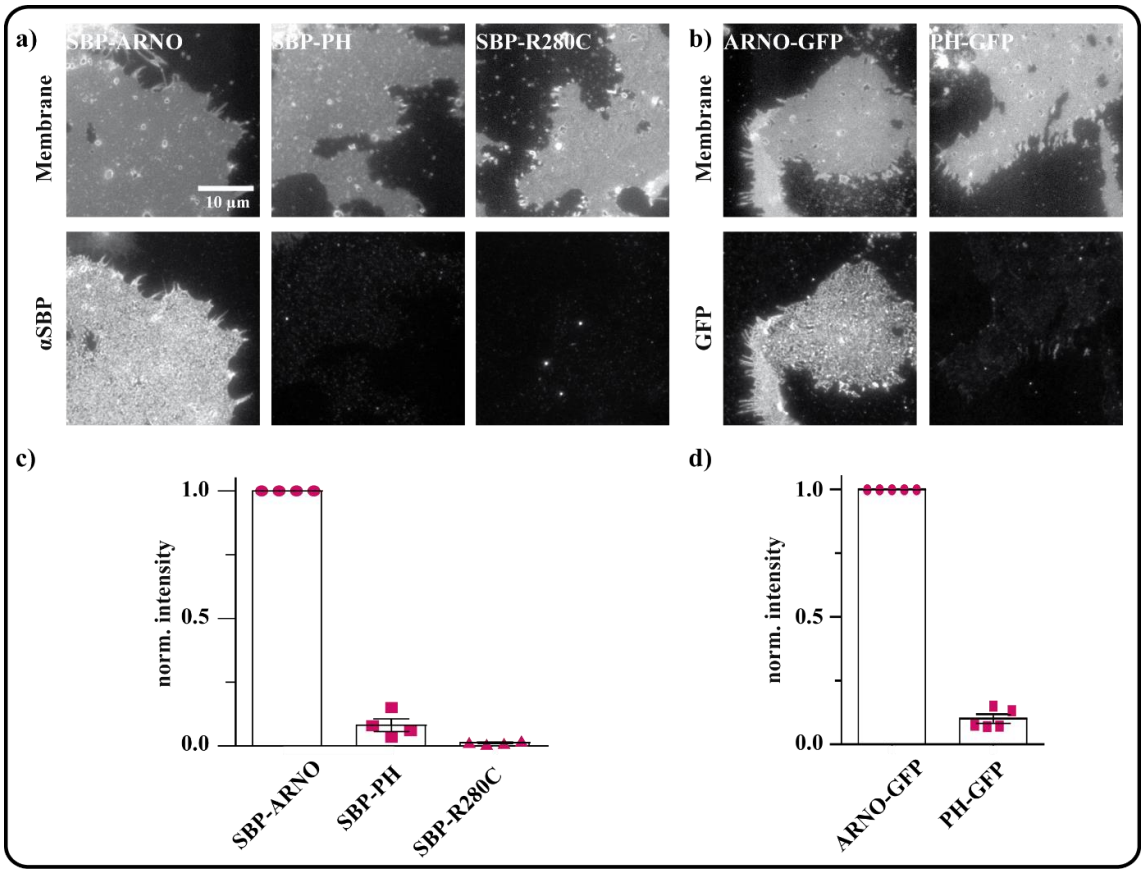

Figure 11: Role of the PH-domain in membrane recruitment. *Having prepared the plasma membrane sheets in sonication buffer, they were incubated with the indicated ARNO protein constructs. The GFP-constructs could be imaged directly, the SBP-tagged proteins were subjected to immunostaining.* ***a & b)*** *The lower panel depicts the SBP- or GFP-tag-signal, respectively. In the upper panel, the TMA-DPH-staining is shown as a control for the membrane integrity.* ***c & d)*** *Quantification of the signal intensities normalized to the full-length constructs, shown is the mean ± SEM 1 (n = 3-5 biological replicates). All images are scaled equally in the respective channels. Scale bar: 10 µm*

Together with the observation that Ca^{2+}, which crosslinks PIPs, diminishes ARNO binding, these data strongly indicate that the interaction of ARNO´s PH-domain and PIP_2 is crucial for binding to the plasma membrane. However, the fact that the PH-domain itself is only able to bind to a small extent points to a more complex binding mechanism, perhaps at a cooperative binding of the different ARNO domains. Therefore, the PH-PIP-interaction is essential but not sufficient for membrane

association of ARNO. This is in agreement with the previous studies employing artificial membrane systems [28,102].

4.3 The different ARNO domains bind to the plasma membrane in a cooperative manner

As previous studies have focused on the cooperative effect of the PH-domain and the polybasic region (PBR) [28,102], we wanted to systematically elucidate the possible contributions of all protein sections and therefore designed a variety of different ARNO constructs. A schematic overview of these constructs is shown in **Figure 12**. ARNO is comprised of the CC-domain, which can interact with other proteins and is responsible for dimerization, the Sec7 domain, which is the catalytically active part of the GEF, the PH-domain, which can interact with phosphoinositides as well as Arf proteins and the PBR-domain, which can bind to negatively charged lipids.

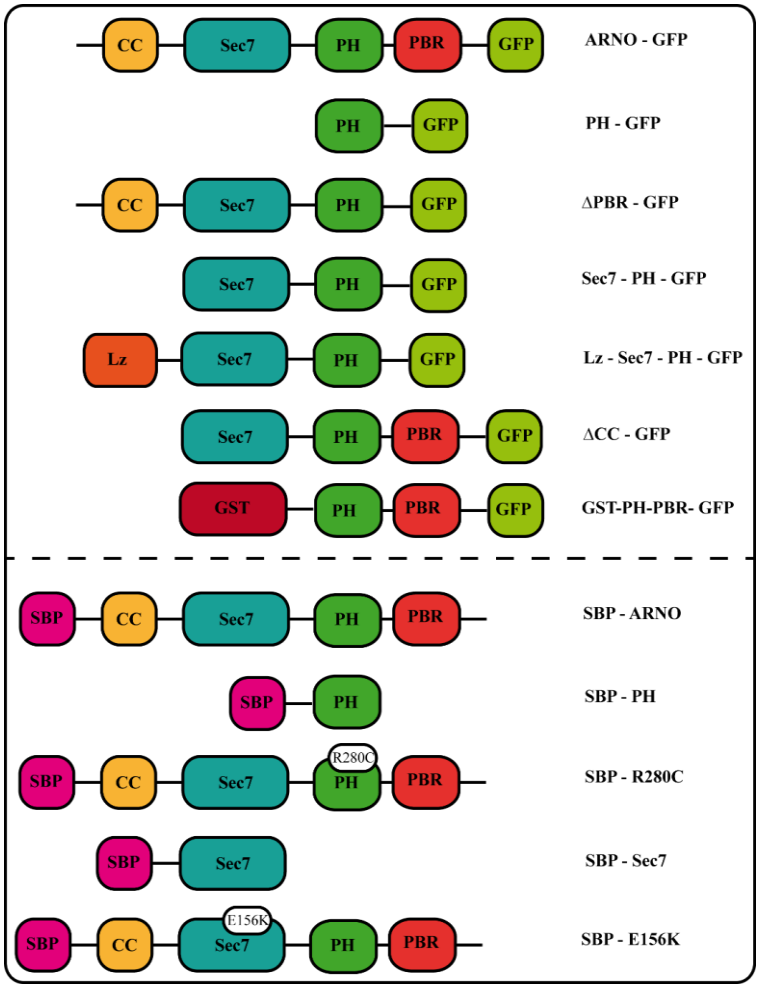

Figure 12: Overview of the different ARNO protein constructs. *Abbreviations: CC = coiled-coil-domain, Sec7 = seven-coiled-seven-domain, PH = pleckstrin-homology-domain, PBR = polybasic region, GFP = green fluorescent protein, Lz = Leucine*

zipper, GST = glutathione-S-transferase, SBP = streptavidin-binding-peptide. The ΔCC-GFP and GST-PH-PBR-GFP constructs were kind gifts by Volkmar Fieberg.

Because ARNO´s function is defined by the Sec7-domain, we first focused on the Sec7-domain. We found that the Sec7-domain alone does not bind to the membrane sheets (**Figure 13 a** and **c**). The E156K point mutant of the full-length protein produces a loss of function of the Sec7-domain because this mutant is unable to coordinate the Mg^{2+} ion in the Arf GDP/GTP-binding groove and therefore cannot catalyze the release of GDP that is necessary for the activation of Arfs [24]. This construct binds to the membrane sheets as strong as the wildtype protein, demonstrating that the catalytic activity of the Sec7-domain is not involved in recruitment of ARNO to the membrane sheets (**Figure 13 a** and **c**).

However, the PH-Sec7 segment binds two-fold stronger than the PH-domain alone, which indicates some contribution of the Sec7-domain to the membrane binding affinity (**Figure 13 b** & **d**). Deletion of the PBR segment (ΔPBR-GFP) reduces binding by about 35 % and deletion of the coiled-coil-domain (ΔCC-GFP) leads to a loss of more than 60 % of the binding (**Figure 13 b** & **d**). To determine whether the contribution of the coiled–coil-domain to membrane binding was a result of protein–protein-interactions or of an increase in avidity achieved by ARNO dimerization via the coiled–coil domain, we fused the weakly binding Sec7-PH-GFP construct with the leucine zipper of Gcn4 (Lz-Sec7-PH-GFP). This leucine zipper, as does the CC-domain, promotes dimerization of the construct but does not interact with the binding partners of the genuine coiled–coil domain of ARNO. This increases the binding by about 3-fold and may hint to an avidity-based contribution of the coiled-coil-domain (**Figure 13 b** & **d**). To further investigate this, we replaced the CC-domain as well as the Sec7-domain with the constitutively dimerized glutathione S-transferase (GST-PH-PBR-GFP). Here, the Sec7-domain was replaced to keep the domain composition and size more similar to ARNO. This construct exhibited about 80 % membrane binding affinity as compared to ARNO (**Figure 13 b** & **d**), which supports the suggestion that dimerization might stabilize membrane anchoring via the PH-domain.

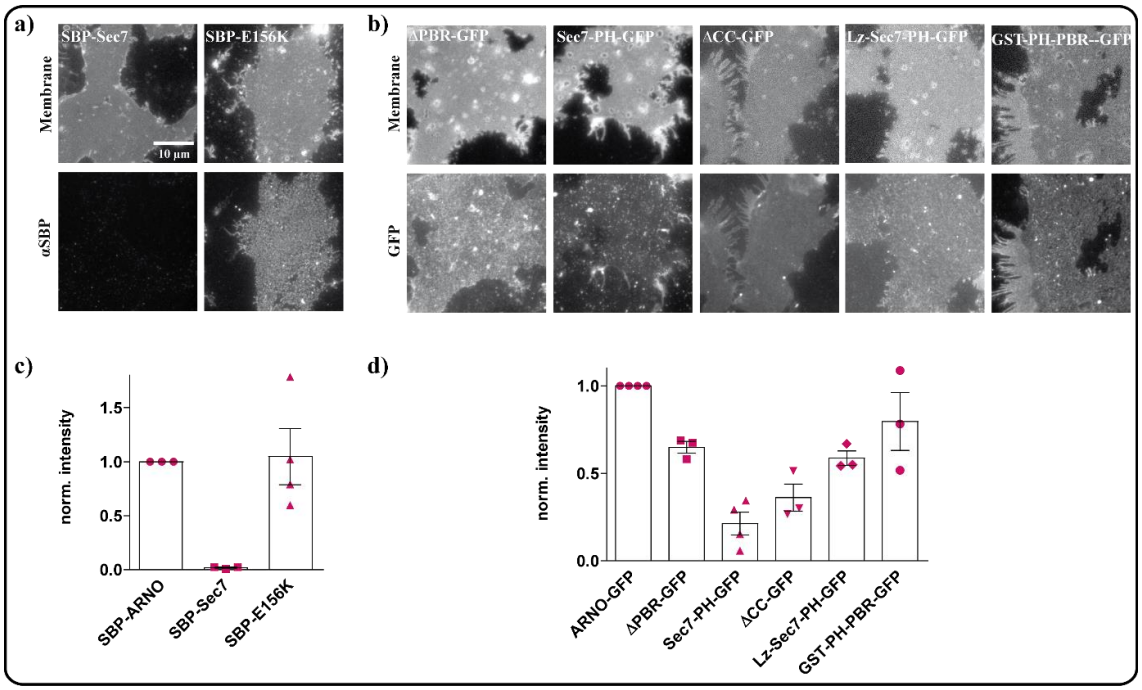

Figure 13: All ARNO domains contribute to membrane recruitment*. Membrane sheets were incubated with 1µM of the indicated protein constructs. GFP-fluorescence was imaged directly, while SBP-tagged constructs were subjected to immunostaining. The integrity of the membrane sheets was verified by staining with TMA-DPH.* ***a)*** *Representative images of the membrane sheets (upper panels) and the SBP-tagged protein constructs bound to the membrane sheets (lower panel).* ***b)*** *Representative images of the membrane sheets (upper panels) and the GFP-tagged proteins bound to the membranes.* ***c*** *&* ***d)*** *Quantification, shown is the mean ± SEM (n = 3-6 biological replicates) normalized to the signal of full-length ARNO. All images are scaled equally for each fluorescence channel, membrane stainings are scaled arbitrarily. Scale bar: 10 µm.*

In conclusion, we show that all ARNO domains, namely PH, Sec7, PBR and CC contribute to binding to the plasma membrane. It is of note, that the effects are not only additive, but cooperative. In the case of the CC-domain, dimerization of the protein may be the mechanism underlying the increase in binding.

4.4 Endogenous EGFR clusters colocalize with bound recombinant SBP-ARNO

Comparing the membrane stainings to the staining patterns of the constructs, it becomes obvious that the recombinant proteins do not uniformly bind to all membrane locations. Instead, they prefer special sites resembling microdomains.

We tested whether these microdomains may be defined by protein clusters formed by the EGF receptor. The EGFR was selected for the following reasons:

First, several studies have shown that EGFR clustering is influenced by PIPs [60,62]. Since ARNO binds to PIPs, it may be recruited to PIPs which are enriched at sites of EGFR clusters.

Second, several indications point to a direct interaction between ARNO and the JM-domain of the EGFR [108,109].

Third, ARNO may be involved in EGFR signaling [39].

To elucidate whether ARNO binds to EGFR clusters, we costained the membrane-bound SBP-tagged ARNO protein constructs and the endogenous EGFR.

Here, it should be noted that there is accumulating evidence pointing to quality issues concerning antibodies. Insufficient industrial validation standards and high batch-to-batch variation contributes to a shockingly high number of non-reproducible results. This problem has been coined the "reproducibility crisis" [110–112].

To ensure the specificity of the EGFR antibody used in our experiments, Dr. Jeff Hannam (AG Famulok) labeled the EGFR small molecule inhibitor PD168393 with the fluorophore Alexa594 (MH-50). This tool was used as a standard for the EGFR antibody validation. Membrane sheets were then costained with the EGFR antibody SC-03 as well as the fluorescent inhibitor and colocalization was assessed. Exemplary images are shown in **Figure 14**.

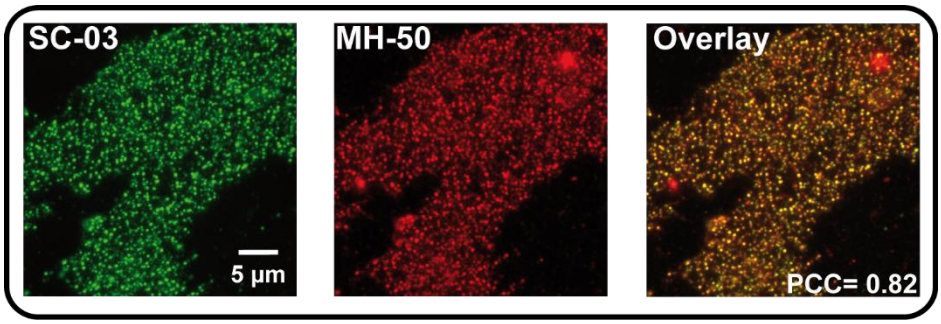

Figure 14: Validation of the EGFR antibody. *Epifluorescent images of HeLa membrane sheets stained for the EGFR costained with the SC-03 antibody (green) and the Alexa-594-labeled inhibitor PD168393 (MH-50, red). Overlay of the two channels results in the intermediate color yellow for almost all EGFR clusters. The calculated PCC equals 0.82. n = two biological replicates including about 60 membrane sheets, SD ± 0.007.*

Visual analysis of the resulting stainings already suggests a high degree of overlap. The Pearson Correlation Coefficient of 0.82 provided the mathematical verification of this impression. It should be noted, that a value of 0.82 suggests a nearly perfect overlap as for technical limitations always lower values than 1 are found even in the case of perfect colocalization [113].

Consequently, we concluded that the used batch of SC-03 antibody indeed selectively and specifically stained the EGFR.

The results of the costaining of the SBP-ARNO constructs and the EGFR are presented in **Figure 15**.

Visual examination of the images reveals a great extent of overlap between the EGFR and the full-length protein as well as the E156K mutant. For the other constructs, no cluster overlap is obvious at least by visual examination.

Colocalization between two fluorophores consists of two components: Co-occurence, that is the presence of both fluorophores within individual pixels, and correlation which means proportional codistribution of two probes [114]. Subjectively, colocalization can be identified visually by superimposing the two image channels. However, the gained insight is qualitative at best and poses the additional problem that an intermediate color, for example yellow for the combination of a red and green channel, can only be observed if the intensities of the fluorescence signals are in a comparable range [115]. In the Pearson Correlation Coefficient (PCC) analysis, the intensities of red and green fluorescence are measured for each pixel to determine the correlation coefficient across a region of interest. In the case of perfect correlation, the PCC equals +1, no correlation results in a PCC of 0 and a PCC of -1 indicates an inversely related distribution of probes [116].

While interpretation of PCC values in absolute terms of overlap is difficult, it serves as an indicator for relative colocalization between the different protein constructs. It also should be noted that colocalization is no evidence for a direct protein-protein interaction. It only hints to an either direct or indirect interaction between the two proteins or just spatial proximity. As shown in **Figure 15 b**, the PCC between the EGFR clusters and recombinant SBP-ARNO bound to the sheets equals approximately 0.3, indicating a significant but not strong correlation. The SBP-PH construct colocalizes with the EGFR to a weaker extent of about 0.18 which may be due to the lower binding affinity of the PH-domain alone. However, the difference between the PCC values of the two constructs is statistically significant (student´s t-test, $p = 0.009$). This suggests that the colocalization between SBP-ARNO and the EGFR is not only due to the proximity between the EGFR clusters and PIP_2 [62].

For the SBP-tagged E156K point mutant approximately the same PCC as for full-length ARNO is obtained indicating that exchange function of the Sec7 domain is not necessary for the spatial proximity of ARNO and the EGFR.

The recombinant SBP-R280C mutant as well as the SBP-Sec7-domain do not exhibit colocalization with the endogenous EGFR clusters, which is not surprising since these constructs hardly bind to the membrane. Compared to the PH-domain, which displays roughly 10 % of the intensity, the Sec7-domain and the R280C mutant are in a range of 1–2 % what may preclude the detection of overlapping structures.

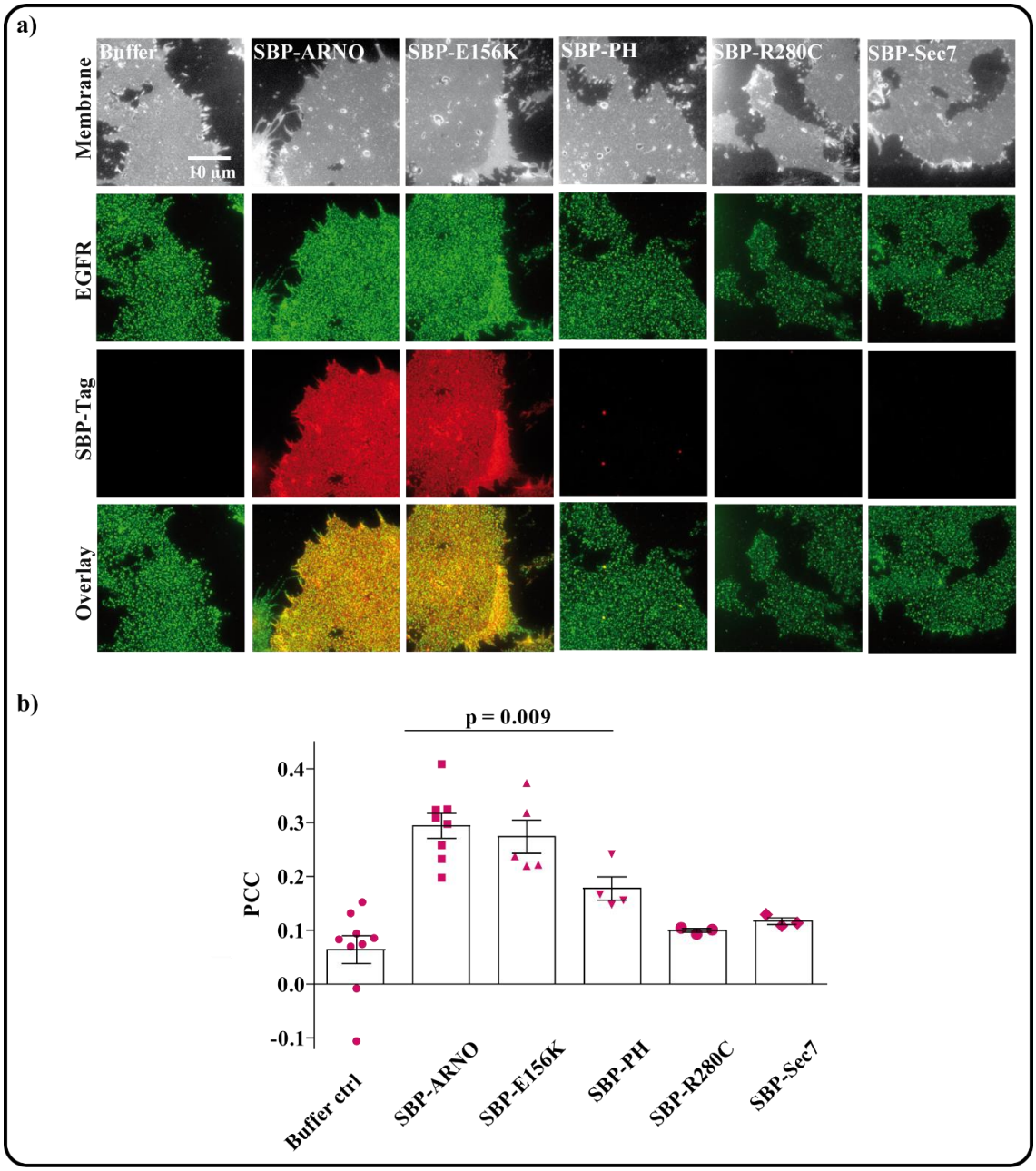

Figure 15: Colocalization of SBP-ARNO constructs and the endogenous EGFR. *Membrane sheets were incubated with a 1 µM solution of SBP-tagged ARNO constructs, before being subjected to sequential immunostaining against the SBP-tag (Alexa 594, third panel) and the endogenous EGFR (Alexa 488, second panel). The membrane sheet integrity was controlled by staining with TMA-DPH during imaging (first panel). The overlay of the EGFR and the ARNO channel is shown in the fourth panel.* ***a)*** *Representative images of the stainings for the EGFR (green), the different*

SBP-tagged protein constructs bound to the membrane (red) and the overlay of the two fluorescence channels (yellow). ***b)*** *The Pearson Correlation Coefficient indicates the extent of colocalization between endogenous EGFR and SBP-tagged ARNO protein constructs. Shown is the mean ± SEM (n = 3-8 biological replicates). Statistical analysis: Student´s t-test. Scale bar: 5 µm.*

4.5 The spatial proximity of SBP-ARNO and EGFR clusters is not an artefact of cluster density

The resolution of conventional epifluorescence microscopy is limited by the Abbe diffraction limit, which defines the minimal distance two objects must have to be separated from each other. This distance is dependent on the wavelength of the light and the numerical aperture of the microscope objective. In practice, this distance ranges between 200 – 300 nm. Therefore, two objects, e.g. an EGFR cluster and an ARNO binding site, overlapping in epi-fluorescence microscopy may be separated from each other by more than 100 nm, which would exclude a direct molecular interaction between the EGFR and ARNO. To reduce this uncertainty, we employed super-resolution microscopy [117].

On immunostained samples the distances between EGFR clusters and the sites to which SBP-ARNO binds were analyzed.

For this, an ImageJ Macro programmed by Dr. Jan Gero Schloetel (AG Lang) was used that first sharpens the raw images by application of a Mexican Hat Filter to then localize the clusters´ centers by their fluorescence intensity maxima. Only clusters for which the Gaussian fit obtained an $R^2 \geq 0.9$ were included in the analysis. Then, the software calculates the distances between one channel´s maxima and the closest maximum in the respective other channel. As a reference channel, the SBP-ARNO signal is employed so the distance from SBP-ARNO binding site to the next EGFR cluster is calculated.

To determine the distances at randomized cluster distribution at the given density, the analysis was as well performed after the EGFR channel had been flipped horizontally and vertically, in the following referred to as “flip ctrl” analysis.

In **Figure 16 b** the distance distribution histogram between the SBP-ARNO sites and their adjacent EGFR cluster is shown. To exclude that the observed proximity was rather the consequence of the number of EGFR clusters per area than an indication of an attraction between ARNO and EGFR clusters, we performed the nearest neighbor analysis with the endogenous Transferrin receptor (TFR) which has approximately the same cluster density as the EGFR (**Figure 16 d** & **g**). The histogram of the flip control

for the Transferrin receptor is shifted to the right (**Figure 16 d**, black), but the difference between the flipped and unflipped (turquoise) distance distribution histograms is not as pronounced as for the EGFR nearest neighbor analysis (**Figure 16 b**) In other words, the distance distribution of SBP-ARNO has a stronger resemblance of the random distribution for the TFR analysis than for the EGFR analysis.

An overlay of the distance distribution histograms for SBP-ARNO clusters in relation to the EGFR (magenta) and the Transferrin receptor (turquoise) is shown in **Figure 16 e**. Clearly, the latter histogram is shifted to the right which indicates a smaller population of SBP-ARNO clusters in close and a larger population in further distance to the next endogenous TFR cluster.

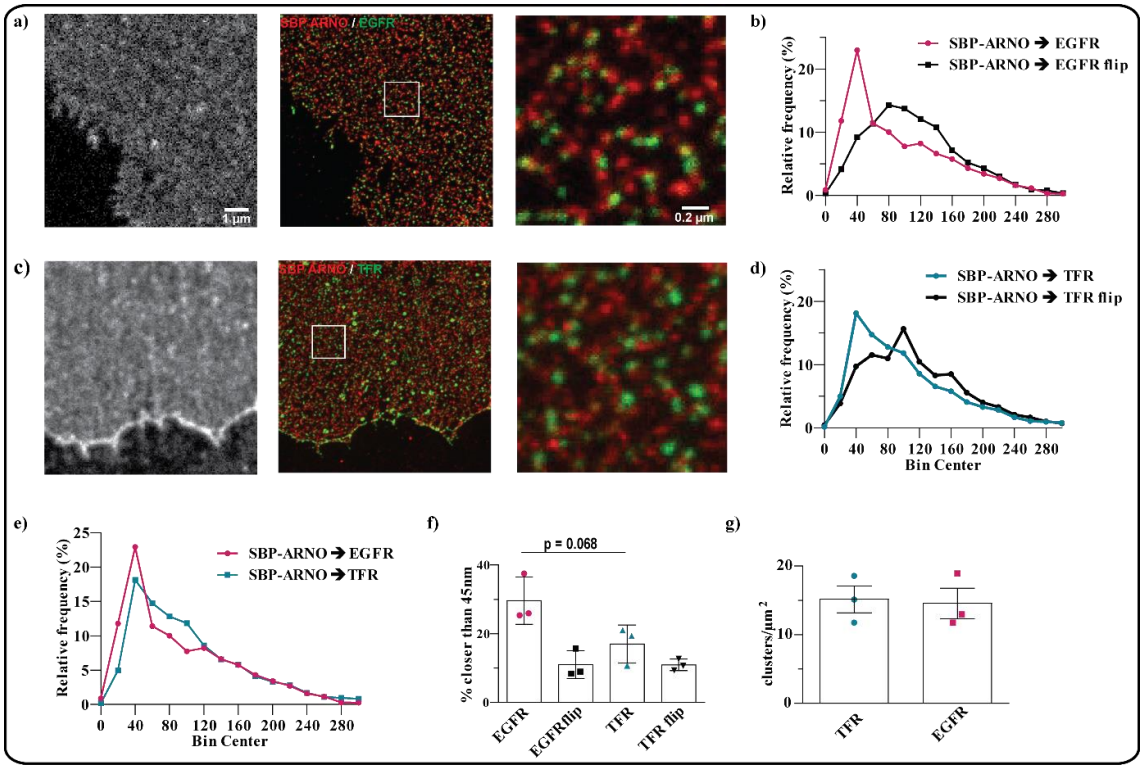

Figure 16: Comparison of the nearest neighbor analysis between SBP-ARNO and the EGFR or Transferrin-Receptor (TFR), respectively*. **a/c)** Representative confocal images of membrane sheets stained with Fast-DiO (left panel) and STED images of SBP-ARNO (red) and the EGFR or TFR (green) (middle panel) and magnified image sections (right panel). **b)** Frequency distribution of distance between SBP-ARNO and its nearest EGFR clusters (magenta) **d)** Frequency distribution of the distances between SBP-ARNO clusters and the TFR clusters (turquoise). Flip ctrl shown in black. **e)** Direct comparison of the distance distributions between ARNO and the EGFR (magenta) and TFR (turquoise), respectively. **f)** Percentage of ARNO clusters per ROI that are closer than 45nm to their next neighboring EGFR cluster or the next TFR cluster, respectively. Mean values are shown ± SEM. **g)** Cluster densities of EGFR and TFR. Three biological replicates with 11 – 15 ROIs per day were included into the analysis.*

As seen in **Figure 16 f**, performance of the nearest neighbor analysis of SBP-ARNO and the TFR and comparing it to the previous analysis with the EGFR reveals that less than 20% of SBP-ARNO clusters are closer than 45 nm to their next TFR neighbor compared to the about 30% of clusters closer than 45 nm to the neighboring EGFR cluster. Even though employment of the student´s t-test for statistical evaluation did not proof this difference to be significant ($p = 0.068$), the power of the test was very low due to the low n of three. This is synonymous with a high probability of a false negative testing result.

Analysis of a randomized cluster distribution (flip ctrl) accounts for approximately 10% of the neighbors in very close proximity. Subtraction of this value leads to the result that SBP-ARNO sites are twice as often closer than 45 nm to the next EGFR than they are to the next TFR cluster.

Conclusively, the control of the nearest neighbor analysis with the Transferrin receptor supports the presumption that the overlap of SBP-ARNO and endogenous EGFR clusters exists due to a molecular interaction, being it direct or indirect, and not due to random spatial distribution and cluster densities.

4.6 STED imaging suggests that many ARNO clusters bind very close to the EGFR

Having determined the proximity distribution of SBP-ARNO and the EGFR, the nearest neighbor analysis was performed for the other ARNO constructs. The STED images as well as the nearest neighbor distance distribution histograms are depicted in **Figure 17**. In all cases a peak at around 40 nm distance was observed, which was most prominent for SBP-ARNO and SBP-E156K, which is expected from the epifluorescence data (see **Figure 13**). Different from the overlap determined in epifluorescence microscopy, the differences between the constructs was more subtle, suggesting that binding of all constructs occurs in principle to the same locations. Because constructs lacking domains bind with a lower affinity, the reduction of their PCC is more pronounced. Except for the SBP-R280C construct, the median distance values for all protein constructs are approximately 75 nm and the histograms visualize similar median distances. In all cases, the median distance of the flip control, shown in black, was significantly larger than for the sample, shown in magenta, indicating that the spatial cluster distribution is not random.

Minor differences in their distribution can be explained by the different signal densities. While for SBP-ARNO more than 3500 clusters could be analyzed, only 450 SBP-R280C clusters were included into the analysis (**Table 18**).

Table 18: Number of clusters per SBP-protein construct analyzed in nearest neighbor analysis

Protein construct	Number of clusters analyzed
SBP-ARNO	3554
SBP-E156K	3260
SBP-Sec7	713
SBP-R280C	450
SBP-PH	1007

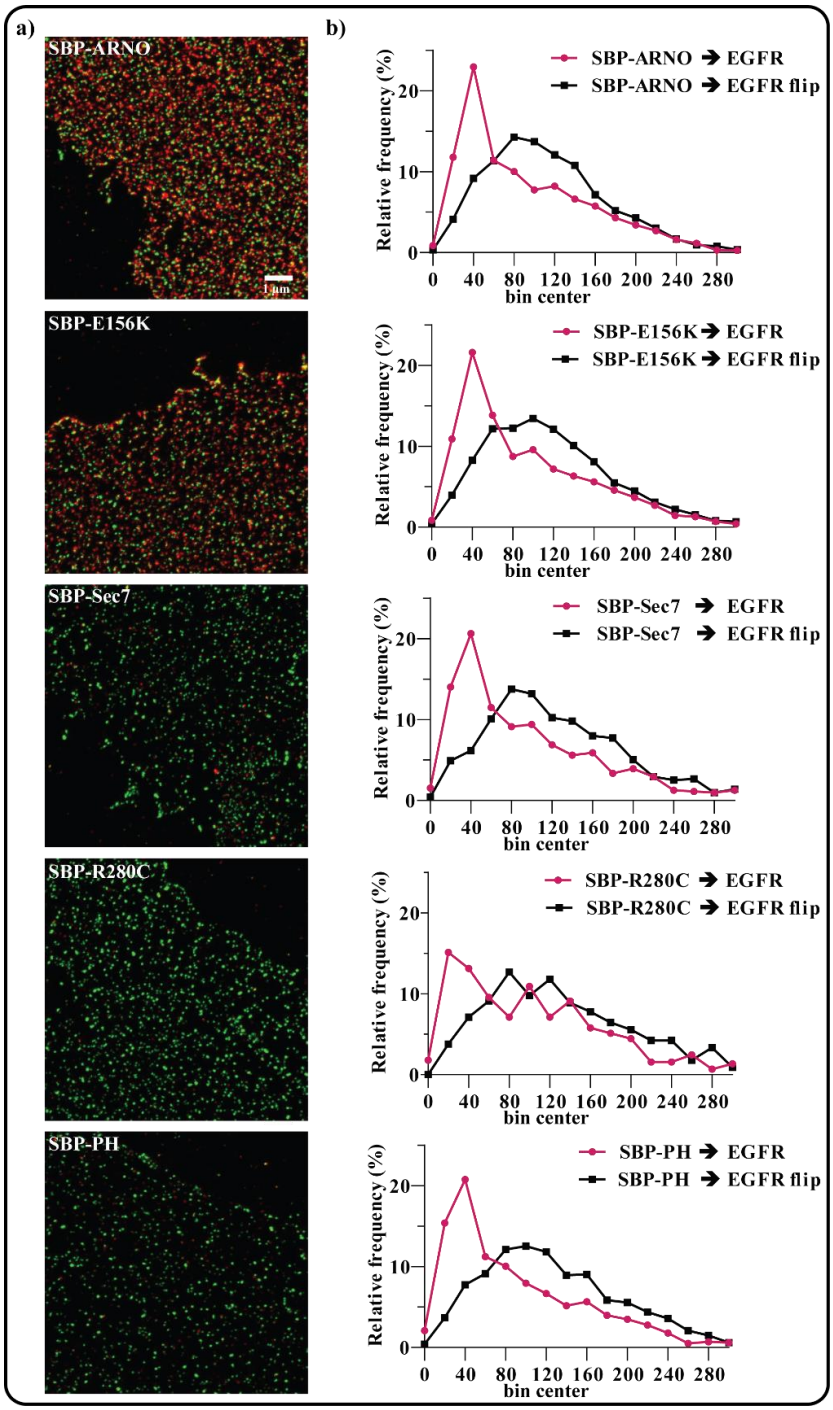

Figure 17: Nearest Neighbor analysis between the EGFR and membrane-bound recombinant SBP-ARNO-constructs. *Membrane sheets were incubated with a 1 µM solution of SBP-ARNO-construct for 5 min before PFA fixation, quenching and immunostaining. Membranes were stained with Fast-DiO and selected for analysis based on membrane integrity (for exemplary images see* ***Figure 16****). The nearest neighbor analysis was performed using an ImageJ-Macro written by Dr. Jan Gero Schloetel (AG Lang). Scale bar: 1 µm.* ***a)*** *The left panel shows the STED images of recombinant ARNO constructs (red) and endogenous EGFR clusters (green).* ***b)*** *In the right panel, histograms of the distance distributions of the nearest neighbor analyses for the different SBP-ARNO constructs (magenta) with flip controls (black) are presented. Three biological replicates were pooled, resulting in 450 (SBP-R280C) to 3554(SBP-ARNO) analyzed clusters.*

Altogether, the high-resolution image analysis narrows down the minimal distance between EGFR and ARNO binding site to a value smaller than 45 nm: A close proximity of EGFR and SBP-ARNO clusters can be observed and quantified. While being a prerequisite for an interaction, existence or even the nature thereof is not addressed.

4.7 Physical size of the clusters

Cluster sizes were determined to clarify whether the short distances between the centers of the SBP-ARNO and EGFR clusters may indicate physical contact between clusters. As schematically depicted in **Figure 18 a**, cluster sizes were defined as the full width at half-maximum (FWHM) of the Gaussian fit to the clusters´ intensity profiles [118,119].

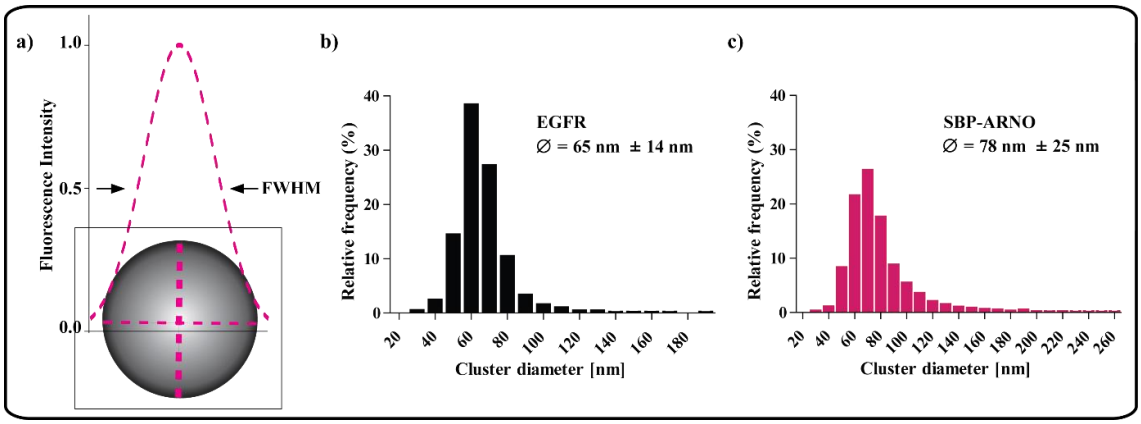

Figure 18: Size determination of EGFR and SBP-ARNO clusters. a) *Schematic representation of a cluster´s fluorescence intensity profile (magenta, dotted line). Cluster diameters were determined by measurement of the full width at half maximum of two Gaussian fits with different line widths of the individual clusters.* ***b)*** *Frequency distribution histograms of the FWHM of the endogenous EGFR clusters (black) and* ***c)*** *SBP-ARNO (magenta). Three biological replicates were pooled for the analysis, for the EGFR 2621 and for SBP-ARNO 3554 clusters were analyzed.*

Figure 18 b shows that the size distribution of the EGFR clusters has a rather narrow profile with a mean of 65 nm ± 14 while the histogram of SBP-ARNO´s size distribution is slightly broader and has a mean of 78 nm ± 25.

Therefore, distances between EGFR and SBP-ARNO clusters closer than 71.5 nm, which equals the sum of the cluster radii, may indicate binding that both proteins locate to the same membrane structure or that two different entities exist that are in physical contact.

4.8 The fraction of ARNO/ARNO construct clusters closer than 45 nm to EGFR clusters is the same for all constructs

Having observed similar nearest neighbor distance distribution histograms for the SBP-tagged protein constructs (**Figure 17**), we took a closer look at the clusters with a distance closer than 45 nm. The reasoning for choosing this value was two-fold. First, the distance distributions have a peak at this value, indicating the existence of a defined population. Second, such distances indicate close physical proximity even for the very small clusters.

In a defined region of interest (ROI), the number of ARNO/ARNO-construct clusters with an EGFR cluster closer than 45 nm was expressed as percentage of all clusters (**Figure 19 a**).

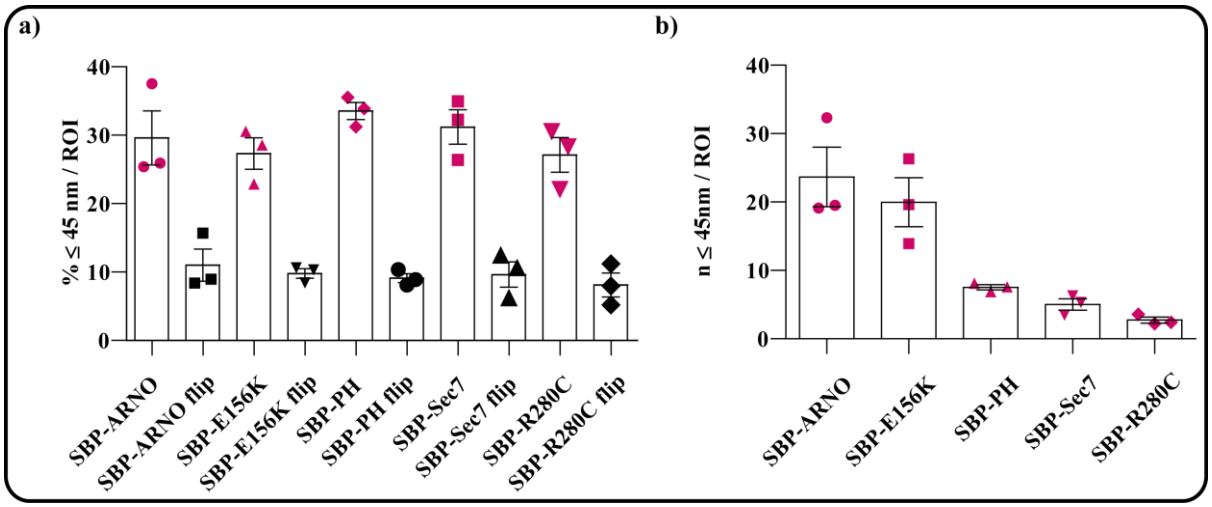

Figure 19: Portion of SBP-construct clusters in very close proximity to the EGFR clusters. a) *The number of spots per region of interest that are closer than 45nm to the next endogenous EGFR cluster.* ***b)*** *The percentage of spots per ROI that are nearer than 45nm to an EGFR cluster. Flip controls are depicted in black. Three biological replicates with 15 ROIs each were included in the analysis. Shown are mean values ± SEM.*

Interestingly, **Figure 19 a** shows that the percentage of clusters closer than 45 nm to its next EGFR neighbor is in the same range for all constructs. Comparison with the flip control, shown in black, reveals that this percentage of approximately 30 % is about three times as high as for randomly distributed clusters.

Consequently, in case of a binding event between ARNO and the EGFR, all domains might be contributing to the interaction by fitting into distinct binding sites.

Note that, due to the different binding efficiencies, the number of ARNO/ARNO construct clusters varied largely between the constructs (**Table 18**) and so does the

absolute number of clusters which are closer than 45 nm to their next EGFR cluster per ROI (**Figure 19 b**).

4.9 Impairment of ARNO-GFP membrane binding by EGFR antibodies

Close proximity of proteins can lead to mutual exclusion of their antibody staining in double staining experiments. Likewise, this fact can be explored to test whether two proteins are close to each other. Hence, we assessed whether binding of ARNO-GFP to the membrane sheets could be impaired by coincubation with antibodies against the EGFR. Three different antibodies against the EGFR, namely CS4267, PA1-1110 and SC-03, were added to the ARNO-GFP solution at a dilution of 1:100. The incubation time was 5 minutes. As a control, an antibody against the Transferrin receptor was used because the Transferrin receptor has the same cluster density as the EGFR (**Figure 16 b**), so this antibody is supposed to decorate the membrane sheets equally well as the EGFR antibody.

Figure 20 shows that there is a trend for decreased ARNO-GFP binding to the membrane sheets in all conditions to which EGFR antibody had been added. Addition of the primary antibody against the TFR does not decrease binding.

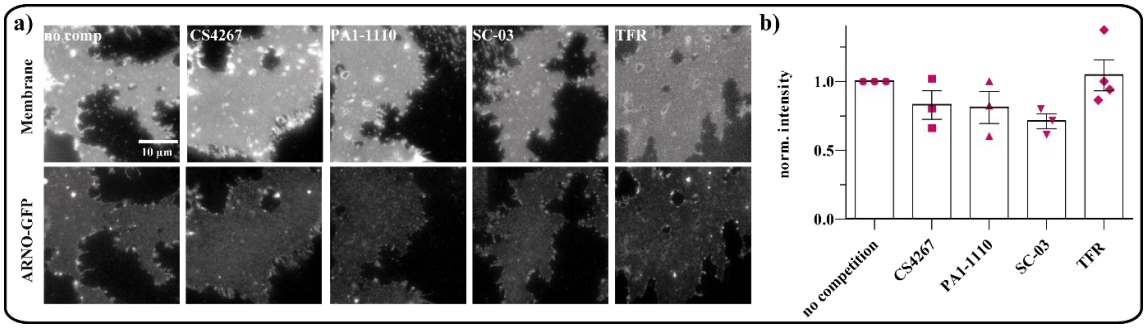

Figure 20: Competition of ARNO-GFP with EGFR antibodies. *Membrane sheets were incubated with 1µM ARNO-GFP in either buffer or a 100-fold dilution of EGFR antibody for 5 min. As a control, the antibody against the Transferrin receptor is employed. The sheets were imaged on the day of the experiment.* ***a)*** *Representative images of the different conditions. Membrane integrity was controlled with TMA-DPH staining (upper panel). The GFP-signal is shown in the lower panel. All images are scaled equally in the GFP channel and arbitrarily in the TMA-DPH channel.* ***b)*** *Quantification of the effect, shown is the mean ± SEM (n = 3-4 biological replicates).*

The result of this competition binding experiment provides an additional hint that a fraction of ARNO and EGFR proteins are very close to each other on the plasma membrane.

4.10 The staining pattern of the EGFR is altered only after SBP-ARNO binding

As previously described (**Figure 15**), for the colocalization study, the membrane sheets were incubated with different SBP-tagged ARNO constructs for five minutes, subsequently fixed with PFA and quenched of background fluorescence with 50 mM NH_4Cl. Then, they were stained for the SBP-tag before being incubated with the SC-03 antibody against the EGFR and its secondary antibody.

Interestingly, the staining intensity of the EGFR is influenced depending on which protein construct the membrane sheets were incubated with. **Figure 21 a** illustrates the EGFR intensity normalized to the buffer control. Incubation with SBP-ARNO led to a more than 1.2-fold increase in EGFR stainability. SBP-E156K also increases the EGFR staining intensity, though the effect is not as pronounced as for the wildtype. A Kruskal-Wallis one-way analysis on ranks treating each sheet as a replicate calculates a p value smaller than 0.001 for both conditions. Incubation with the SBP-R280C construct, decreases the staining intensity of the EGFR, significantly (Kruskal-Wallis one-way analysis $p = 0.016$). The other ARNO protein constructs do not have an effect. At first it might be surprising that ARNO-binding does not lead to a diminished binding, because of the decrease of ARNO binding upon coincubation with EGFR antibodies (***Figure 20***).

A plausible reason for this might be a conformational change of the flexible C-terminal tail of the EGFR making it more accessible for the SC-03 antibody after ARNO binding. Alternatively, incubation with ARNO might lower the packing density of the EGFR clusters, which could decrease steric hindrance of antibody binding thus leading to an increase of staining intensity.

The coefficient of variation, or Relative Standard Deviation (RSD) can serve as a measure for the degree of clustering or cluster size. In our case, it is defined as the standard deviation of the signal within the membrane ROI σ divided by the mean fluorescence intensity μ [120]:

$$RSD = \frac{\sigma}{\mu}$$

After incubation with SBP-ARNO or SBP-E156K, the RSD of the EGFR is significantly lowered (Kruskal-Wallis one-way analysis, $p < 0.001$), indicating a lower degree of clustering of the EGFR molecules. In contrast, the RSD is increased after incubation of the sheets with SBP-R280C (Kruskal-Wallis one-way analysis, $p < 0.001$) (**Figure 21 b**).

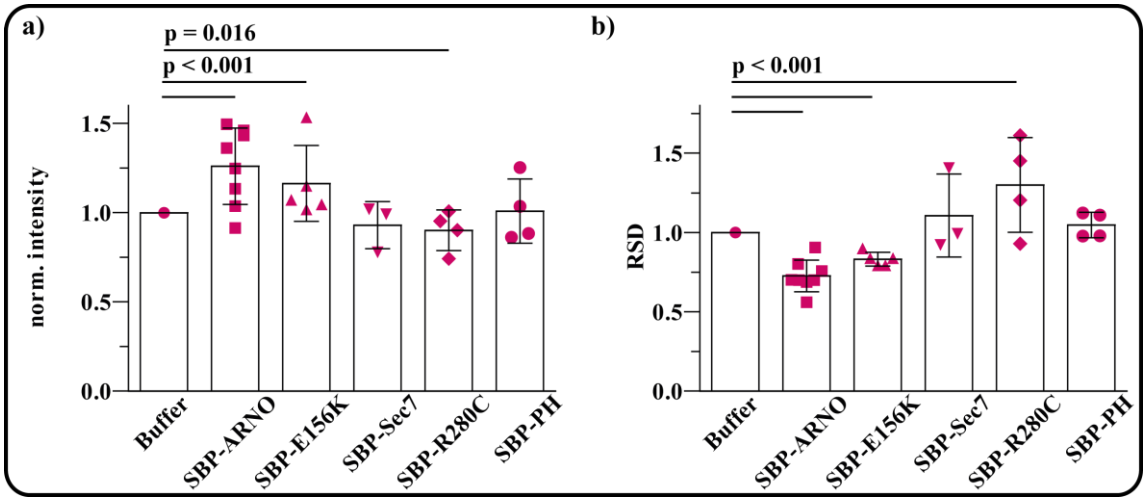

Figure 21: Influence of ARNO constructs on EGFR staining intensity and clustering. *The sheets were incubated for 5 min with either buffer or 1 µM of the SBP-tagged protein construct, and immunostained against the SBP-tag followed by immunostaining for the EGFR. Analysis is performed on the data already presented in* ***Figure 15****.* ***a)*** *Intensity of the EGFR staining values normalized to the buffer condition.* ***b)*** *The relative standard deviation (RSD) of the EGFR clusters, shown is the mean ± SEM (n = 3-8 biological replicates). The values are normalized to the buffer condition.*

Altogether, the analysis of the EGFR staining pattern suggests that ARNO influences the arrangement or conformation of EGFR molecules.

4.11 Influence of SecinH3 on membrane recruitment of SBP-ARNO and clustering of the EGFR

Being one of the small GEFs for Arf 1&6, ARNO is insensitive to Brefeldin A. However, it can be inhibited by the small molecule inhibitor SecinH3 as could be shown in a variety of studies [25,121,122]. We tested in how far addition of SecinH3 during incubation of the sheets with the SBP-ARNO affects the ability of SBP-ARNO to bind to the membrane.

Indeed, as shown in **Figure 22**, incubation with 15 µM SecinH3 impairs the ability of ARNO to bind to the sheets which is indicated by a decrease in signal intensity as compared to the DMSO control (Rank Sum test, $p < 0.001$, see panel a). In good agreement with the results described in **Figure 21**, inhibition of ARNO leads to a decrease in EGFR staining intensity or, in other words, a loss of ARNO mediated increase (Rank Sum test, $p = 0.02$, panel b) and a higher degree of clustering (Rank Sum test, $p = 0.021$, panel c).

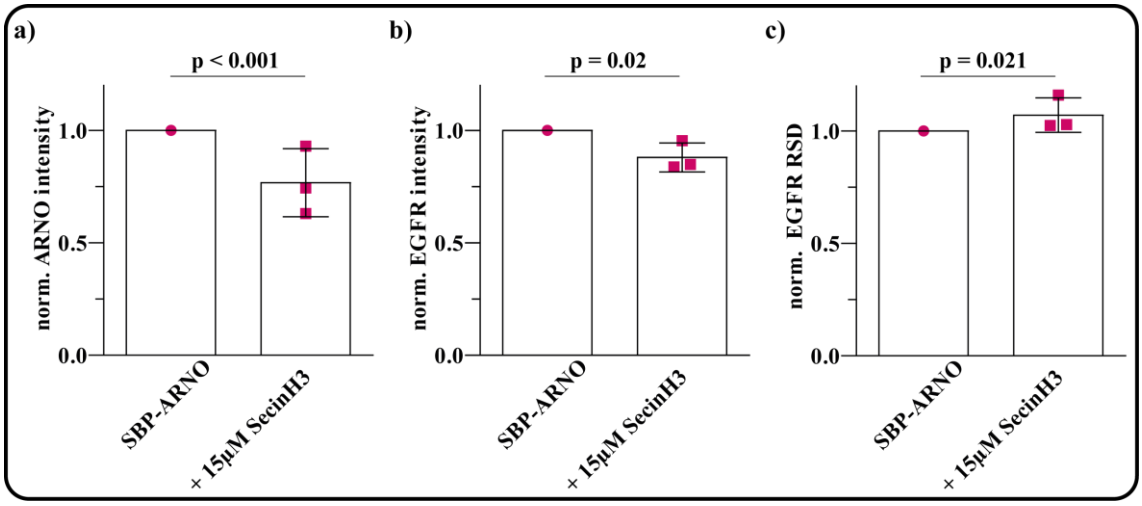

Figure 22: Effect of SecinH3 on ARNO binding and EGFR staining pattern. *The membrane sheets were incubated for 5 min with 1 µM SBP-ARNO either in the presence of 0.4% DMSO or 15µM SecinH3 before being immunostained subsequently for the SBP-tag and the EGFR. Shown are mean values ± SD (n = 3 biological replicates, 98 SBP-ARNO and 96 SecinH3 membrane sheets).* ***a)*** *The intensity of the ARNO staining is decreased upon coincubation with SecinH3.* ***b)*** *The EGFR intensity is decreased to about 90% after treatment with SecinH3 during SBP-ARNO incubation.* ***c)*** *The EGFR´s RSD is slightly increased for the sheets treated with 15 µM SecinH3 during the 5 min of protein incubation.*

This is especially interesting, since the GTPase-inactive mutant E156K does not behave differently from the wild-type ARNO in terms of binding and influence on the EGFR. Thus, this is a hint at another functional relationship between ARNO and SecinH3 or between the Sec7–domain of ARNO and the EGFR.

Altogether, the data support the notion that incubation with ARNO influences the EGFR clustering and/or its conformation. However, it should be noted that this does not prove a direct interaction.

4.12 Overexpression of ARNO in HeLa cells leads to a trend for stronger activation of the EGFR

Having observed a colocalization with and possible influence on the clustering of the EGFR, we aimed at investigating in how far changes in the intracellular ARNO concentration might impact the EGFR´s activation to determine a possible functional relevance of the findings.

As a measure for receptor activation, we chose the phosphorylation status of Tyrosin 1086, because it is known to be phosphorylated in early receptor activation and serves as an important binding site for downstream effectors like the Cbl-Grb2-complex [123].

HeLa cells were transfected with different amounts of an ARNO–coding plasmid, starved overnight in medium without FCS, stimulated with 50 ng/ml EGF for 5 min, lysed and analyzed via Westernblot.

A representative example of these Westernblots is shown in pseudocolor in **Figure 23 a**. As expected, the EGFR content is decreased upon stimulation of the cells (upper panel) [124]. Phosphorylation of the tyrosine residue 1086 is greatly enhanced after stimulation. A tendency for a further increase of phosphorylation in the cells transfected with 1µg or 2µg ARNO-plasmid can be observed as well (second panel). In the bottom panel, the ARNO blot is shown, indicating that the transfection of the ARNO strongly increases the ARNO concentration strongly above the endogenous level. The quantification of the pY1086 bands normalized to the EGFR content and the loading control Lamin is shown in **Figure 23 b**.

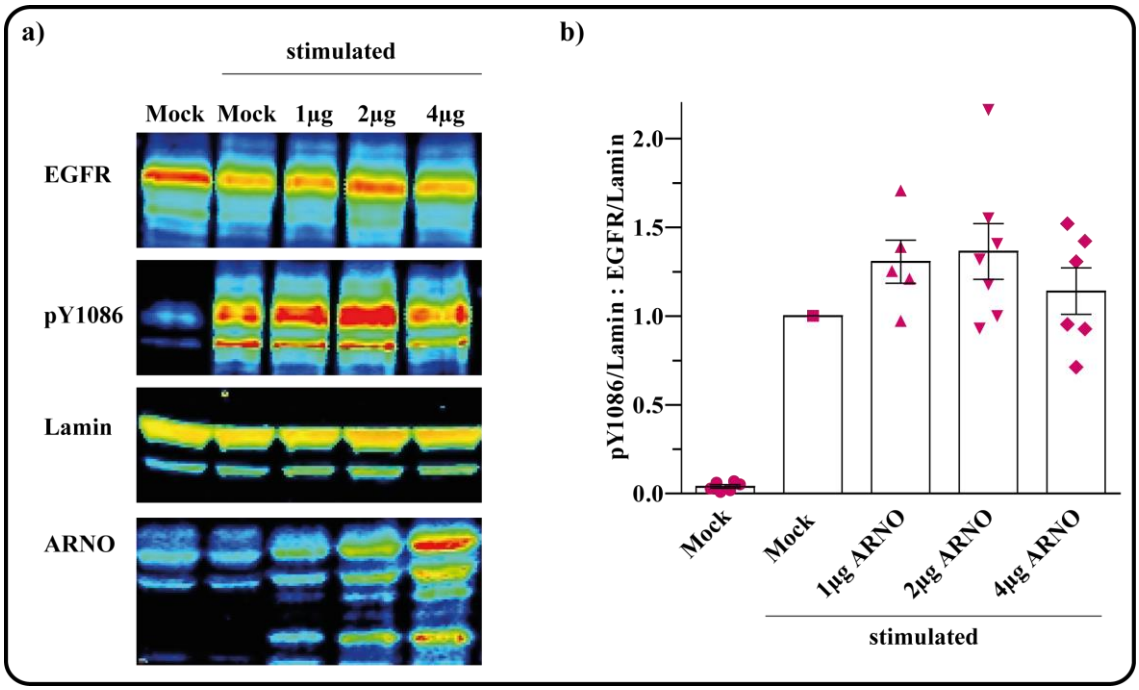

Figure 23: Influence of the overexpression of ARNO on EGFR activation. *HeLa cells were transfected with a plasmid coding for ARNO, grown for 24h starved overnight, stimulated and analyzed by westernblot. A transfection of empty plasmid (mock) was included as a reference.* ***a)*** *Westernblot in pseudocolor (blue: low signal intensity, red: high intensity). EGFR phosphorylation, indicated by staining against pY1086 (second panel) increases upon stimulation with EGF. The gel loading control Lamin (third panel) is shown only for one of the blots. The transfection-dependent increase of the cells´ ARNO content can be seen in the bottom panel.* ***b)*** *Quantification of Westernblot bands. EGFR and pY1086 signals were normalized to their respective Lamin loading control yielding pY1086/Lamin and EGFR/Lamin. Finally the pY1086 was divided by EGFR/Lamin. Shown are mean values ± SEM (n = 5-7 biological replicates).*

For the cells transfected with 1 µg or 2 µg ARNO plasmid, the mean values are about 30 % higher than that of the Mock transfected cells. However, the signal variability between the different days is quite high so that statistical testing does not prove this tendency to be significant (Kruskal-Wallis-test on ranks; $p = 0.935$). Transfection of 4 µg ARNO plasmid did not alter phosphorylation of the tyrosine residue 1086 much compared to the Mock transfected condition.

Even though a tendency towards a correlation between intracellular ARNO concentration and an enhanced EGFR activation can be observed, it does not hold up to rigorous statistical testing.

4.13 Immunostaining reveals nuclear translocation of the EGFR after stimulation with EGF

Full-length EGFR originating from the plasma membrane within the nucleus has been observed in a variety of tissues, tumors and cancer cell lines. Nuclear translocation of the EGFR has been reported to be initialized by stimulation with growth factors like EGF, irradiation in radiotherapy or treatment with EGFR antibodies [125]. One method to analyze this is the immunostaining of the EGFR with antibodies prior to microscopic imaging.

Here, we employ immunostaining of the EGFR with two different antibodies (CS4267 & SC-03) to show the EGFR´s translocation into the nuclei of HeLa cells. Exemplary images of Hela cells that had been starved overnight, optionally stimulated with 50 ng/ml EGF for 20 minutes, fixed, permeabilized and stained for the EGFR (red) as well as the nuclei (blue) are seen in **Figure 24**. Unstimulated cells (upper rows) are compared to stimulated cells (lower rows). These images taken by a CLSM are the central optical sections of stacks that were recorded from the top to the bottom of the nuclei to ensure that possibly observed intranuclear EGFR staining is not due to out of focus fluorescence from above or below the nuclei.

In the left panels, the EGFR staining is depicted (**a**: stained with CS4267, **b**: stained with SC-03). Strikingly, the staining pattern of the two antibodies differs greatly. This might be yet another example of the limitations of commercial antibodies and the lack of validation by the producers and distributors. However, for both staining conditions, vesicular internalization upon stimulation can be observed.

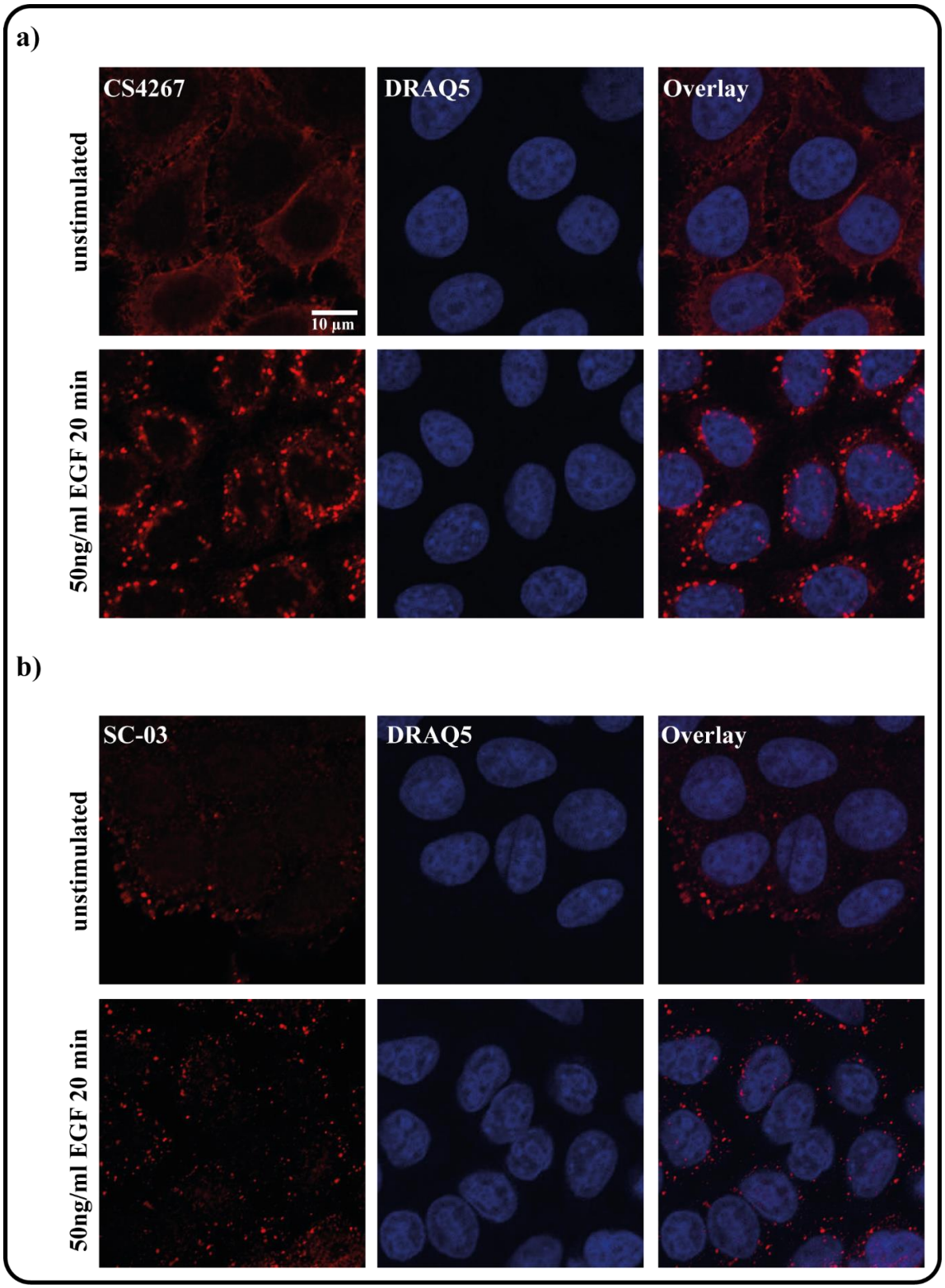

Figure 24: Detection of EGFR by immunofluorescence before and after stimulation. *HeLa cells were starved overnight and either left unstimulated or stimulated with 50ng/ml EGF for 20 minutes, fixed with 3.7% PFA and immunostained for the EGFR (red, left panel) and the nuclei (blue, middle panel). An overlay of both channels is shown in the right panel.* ***a)*** *The EGFR was stained with the CS4267 antibody.* ***b)*** *EGFR staining with the SC-03 antibody. Scale bar: 10µm. For each staining, the red channel is scaled equally. The experiment was performed twice.*

Both EGFR antibodies detect a strong stimulation-dependent accumulation of EGFR in the perinuclear periphery. Occasionally, some spots appeared to be present within the nuclei.

4.14 Subcellular fractionation of HeLa cells hints at nuclear translocation of the EGFR

Having found preliminary evidence for the EGFR´s nuclear translocation by fluorescence microscopy, we wanted to verify this result by cellular fractionation. For this, HeLa cells were starved overnight, stimulated with 50 ng/ml EGF for 5 minutes or left unstimulated and underwent subcellular fractionation by cell lysis using buffers with different salt concentrations and centrifugation, yielding three fractions: cytoplasm, membrane and nucleoplasm.

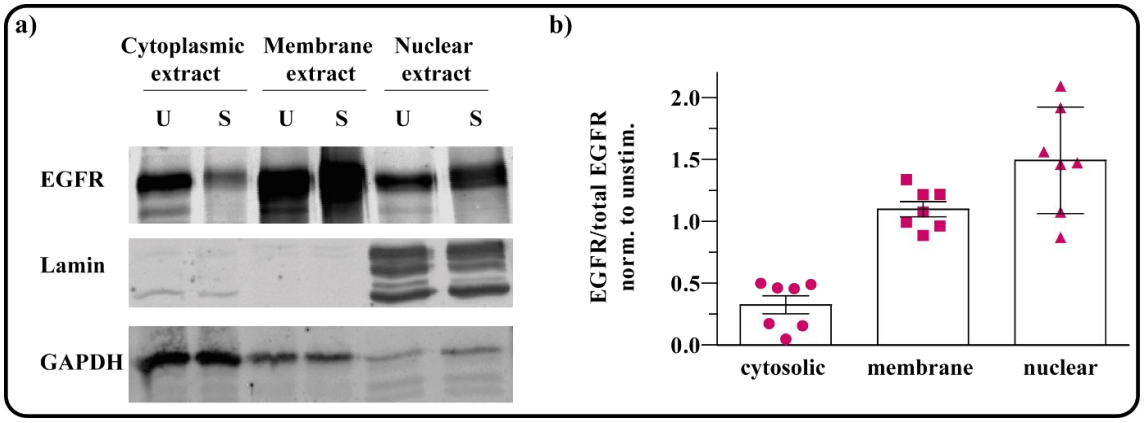

Figure 25: EGFR distribution analyzed by subcellular fractionation. *Subcellular fractionation of Hela cells that, after overnight starvation, were either left unstimulated (U) or stimulated with 50 ng/ml EGF for 5 min (S).* ***a)*** *Westernblot of the obtained extracts. EGFR (upper panel), Lamin (middle panel) as a marker protein for the nuclear fraction and GAPDH (bottom panel) as the marker for the cytoplasmic extract.* ***b)*** *Quantification of the EGFR divided by the total EGFR content. The data of each extract was normalized to its unstimulated condition, shown are the mean values ± SEM (n = 7 biological replicates). Statistical analysis: Rank Sum test performed with values before normalization, p = 0.383 for the nuclear extract.*

Figure 25 a shows a representative westernblot of the subcellular fractionation. In the upper panel the EGFR signal is shown. The middle panel indicates the nuclear filament Lamin to control for the destruction of nuclei in earlier fractionation steps, what does not seem to happen to a great extent. The cytoplasmic protein GAPDH is blotted to check for spillover from the cytoplasmic extract into the other fractions.

Though additional washing steps were added to the kit protocol, some spillover is observed. However, since it happened to the same extent for both conditions, it is not considered to distort the result.

Stimulation-dependent decrease of the EGFR is seen in the cytoplasmic extract, which probably is the result from translocation as well as degradation. A double band appears in the nuclear extract and both bands were included in quantification. This double band has regularly been observed in our experiments and could, for example, originate from different phosphorylation patterns.

A quantification of the portion of the EGFR in the different fractions is depicted in **Figure 25 b**. In the mean, the proportion of nuclear EGFR in stimulated cells is about 1.5 times higher than in unstimulated ones. However, the variance between the different days was too high to withstand statistical testing (Rank Sum test, $p = 0.383$). Yet, the double band in the stimulated cells´ nuclear extract is a clear sign for changes in nuclear EGFR content.

4.15 The role of ARNO in the nuclear translocation of the EGFR

We asked whether ARNO regulates EGFR translocation to the nucleus. The rational for this was two-fold: First, the three clusters of basic amino acids (RRRHIVRKRTLRR) within the EGFR´s JM-domain were identified as its nuclear localization sequence (NLS) and the JM-domain was identified as a putative binding region for ARNO [108,126]. Second, EGFR nuclear translocation can be triggered by its activation through EGF stimulation and we had observed a tendency for increased EGFR phosphorylation after ARNO transfection (see **Figure 23**).

4.15.1 Overexpression of ARNO has no influence on the nuclear translocation of the EGFR

HeLa cells were transfected with different amounts of ARNO plasmid, starved serum-free overnight, stimulated with 50 ng/ml EGF for 5 min and subjected to subcellular fractionation before being analyzed by westernblot. In **Figure 26 a**, a representative westernblot is shown. For all stimulated conditions, a characteristic double band can be observed in the nuclear extract. However, no clear differences between the cells that had

been transfected with empty vector (Mock) and the ones transfected with different ARNO concentrations can be observed.

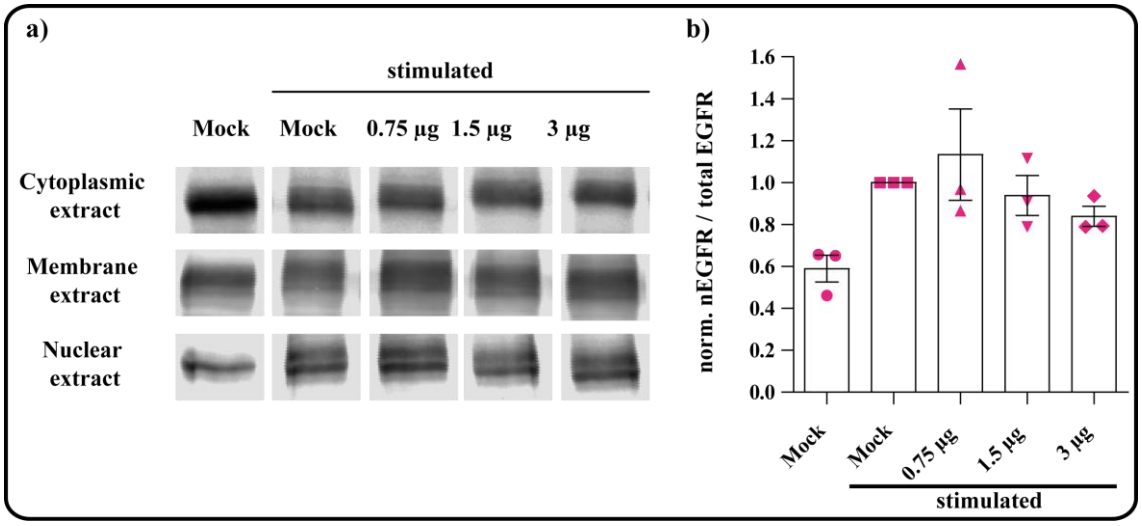

Figure 26: Influence of the overexpression of ARNO on the nuclear translocation of the EGFR. *Subcellular fractionations were performed after transfection with empty vector (Mock) or different amounts of ARNO and stimulation with 50 ng/ml EGF for 5 min.* ***a)*** *Western blot of the EGFR content of the different extracts. EGFR content of the cytoplasmic extract (upper panel), membrane extract (middle panel) and nuclear extract (bottom panel).* ***b)*** *Quantification of the ratio of nuclear EGFR to total EGFR content, normalized to the Mock-transfected. Depicted is the mean value ± SEM (n = 3 biological replicates).*

This visual observation is underlined by quantification and statistical analysis of the westernblots which is shown in **Figure 26 b**. Neither does the one-way Anova analysis detect a significant difference between the conditions (p=0.597), nor is a clear tendency observed.

4.15.2 Establishment of reporter cell lines for the nuclear translocation of the EGFR

We set up a system allowing to reproduce the basic finding, that the JM-domain is responsible for the nuclear translocation of the EGFR.

A schematic depiction of the constructs used for further analysis is shown in **Figure 27 a**: Since GFP is known to accumulate in the nucleus, the cytoplasmic protein pyruvate kinase (PK) was chosen as a component of the fusion constructs to ensure a clear distinction between the cytoplasmic protein construct and the one that is actively imported into the nucleus. It was either coupled to a monomeric GFP protein (PK-GFP,

left) or to the monomeric GFP and the EGFR´s JM-domain (PK-JM-GFP, right). So, we suspected the first protein construct to be located cytoplasmatically and the latter one to be translocated into the nucleus.

To assess and quantify this, we used the automated high throughput confocal imaging platform Cell Voyager for image acquisition and employed the Cell Profiler Software for analysis. As a measure for the extent of nuclear localization of the fusion proteins, we calculated the Nuclear Localization Index (NLI) as a ratio of the fluorescence signal within the nuclei (NFI) divided by total fluorescence being the sum of the fluorescence intensity within the nuclei plus the fluorescence intensity within the cytoplasm (CFI):

$$NLI = \frac{NFI}{NFI + CFI}$$

The values of the NLI can range from 0, indicating a completely cytoplasmic protein localization and +1 which means a 100 % nuclear localization.

Figure 27 b shows representative images of the stable cell lines. In the upper row of pictures, epifluorescent and in the bottom row confocal images are presented. For each cell line the GFP channel (left panel), the nuclear DRAQ5 staining (blue, middle panel) and the overlay of the two (right panel) is shown. The cell line expressing PK-GFP is shown on the left and the cytoplasmic localization can be observed distinctly. On the other hand, the PK-JM-GFP fusion protein is clearly located predominantly in the cells´ nuclei (right side).

The relative frequency distributions of the cell lines´ Nuclear Localization Indices are shown in **Figure 27 c.** For the cell line stably transfected with the PK-GFP fusion protein (left), the distribution has a relatively sharp peak with a maximum of about 0.5 and a mean value of 0.48 ± 0.04. The unexpectedly high content of nuclear PK-GFP can be explained by two phenomena: First, the correct subcellular localization of proteins might be obscured by overexpression, a phenomenon which has been described before [127], and, secondly, since the nucleoplasm has a smaller volume than the cytoplasm, a given amount of nuclear fluorescent protein has a bigger effect on the NLI than the same amount of protein would have when located in the cytoplasm.

On the right side, the frequency distribution histogram of the cell line stably transfected with PK-JM-GFP is shown. Clearly, a population right from the one of PK-GFP can be observed. The NLI values of this cell line have a mean value of 0.64 ± 0.08.

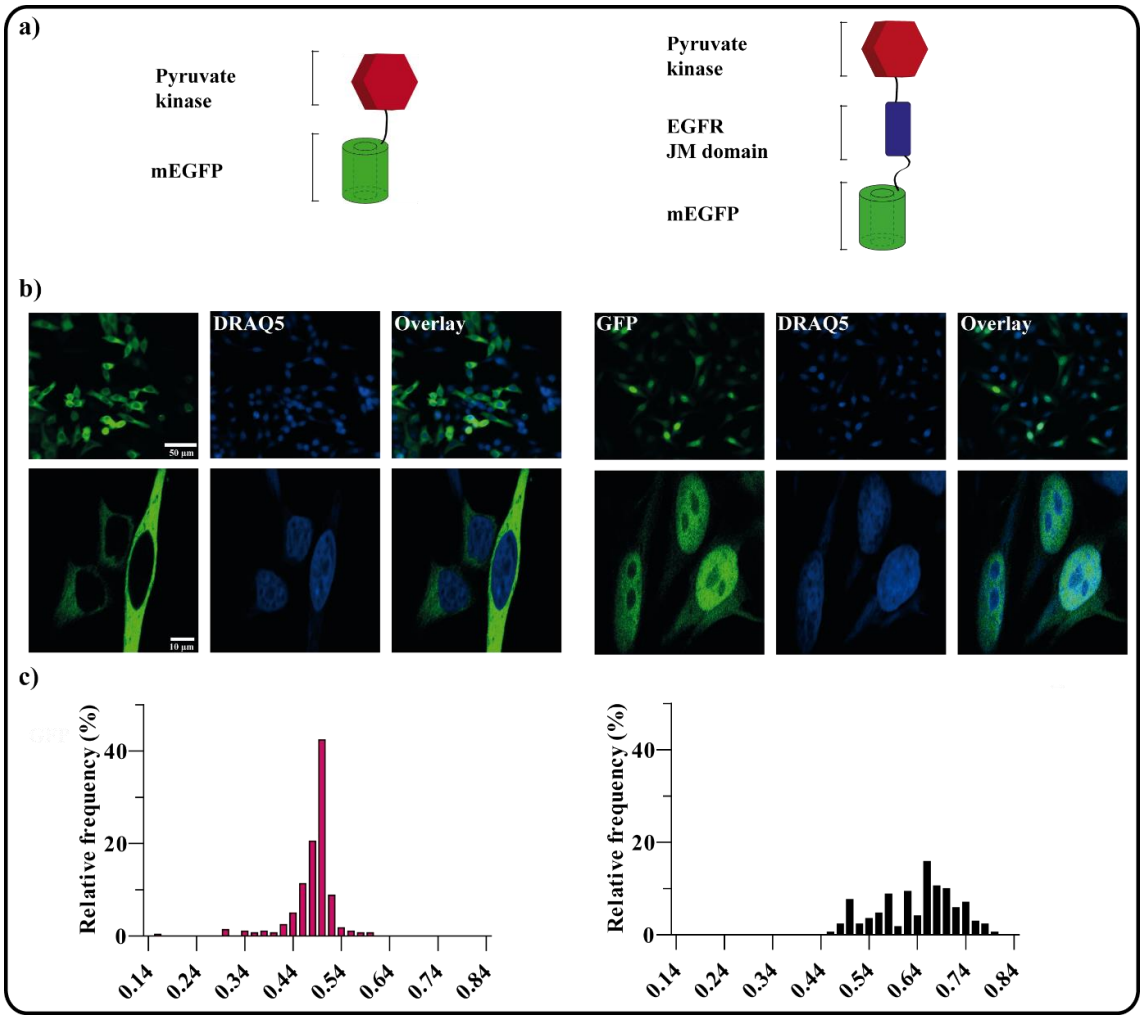

Figure 27: The NLS is located in the JM-domain of the EGFR. *Stable Hela cell lines were created by transfection of the different constructs and subsequent selection of the cells with Zeocin. The cells were fixed with 3.7% PFA, permeabilized and the nuclei were stained with DRAQ5. Analysis was performed with the Cell Profiler Software.* ***a)*** *Schematic representation of the transfected constructs. The cytoplasmic protein pyruvate kinase was fused to mEGFP (PK-GFP, left side) as a control. Secondly, the EGFR´s JM domain was inserted into the pyruvate kinase-mEGFP fusion protein (PK-JM-GFP, right side).* ***b)*** *Microscopic images of the PK-GFP cell line (left) and PK-JM-GFP (right). Depicted is the GFP-channel, the DRAQ5-channel and the overlay of the two. In the upper row epifluorescent (scale bar 40 µm) and in the lower row confocal images (scale bar 10 µm) are shown.* ***c)*** *Relative frequency distributions of the cells´ localization indices. Higher values indicate a higher proportion of intranuclear protein. On the left side, the PK-GFP´s histogram has a mean value of 0.48 ± 0.04. The PK-JM-GFP´s mean value equals 0.64 ± 0.08 (right side). (Two biological replicates, 171 and 283 cells were analyzed).*

Conclusively, we were able to reproduce Hsu and Hung´s findings and found an analysis that is able to read out and quantify differences in subcellular protein localization.

4.15.2.1 Transfected ARNO-mCherry is not cotranslocated into the nuclei with the EGFR

Since the JM-domain has been reported to interact with ARNO, we assessed whether ARNO might be cotranslocated into the nucleus together with the PK-JM-GFP construct. Therefore, ARNO-mCherry was transfected into the HeLa reporter cell line. Exemplary confocal images are shown in **Figure 28**.

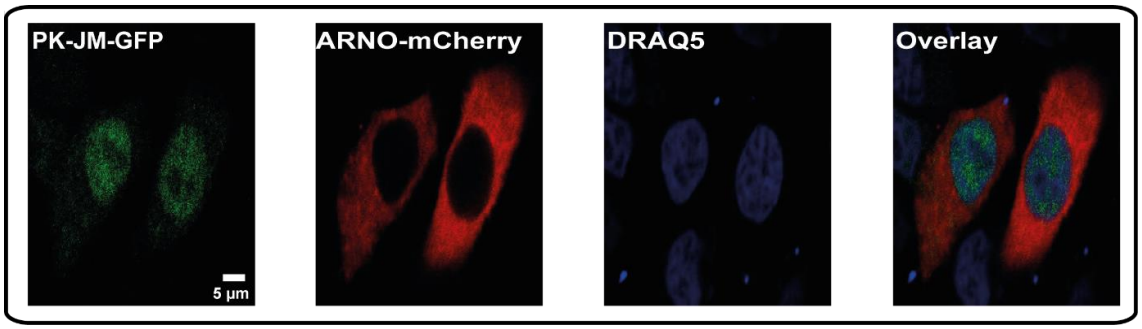

Figure 28: Localization of ARNO co-expressed with PK-JM-GFP. *Confocal images of the fixed Hela cell line stably expressing PK-JM-GFP (green, left panel). The cellular localization of the transiently transfected ARNO-mCherry (red) is cytoplasmic. Nuclei are shown in blue, an overlay of all three channels can be seen in the far-right panel. Scale bar 5 µm.*

Despite the clear nuclear localization of the JM-domain-containing protein construct, the cytoplasmic localization of ARNO-mCherry is maintained.

4.15.2.2 Influence of Importazole on the subcellular localization of PK-GFP and PK-JM-GFP

To take a closer look at the mode of nuclear translocation of the EGFR and to evaluate in how far the stable cell lines are a sensitive and suitable readout for change thereof, we employed two different small molecule inhibitors and assessed their influence on the subcellular localization of the established protein constructs.

Previous studies found that the EGFR colocalizes and interacts with Importin α/β, a class of proteins that directly interact with nucleoporins thus mediating the transport of cargo through the nuclear pores [128,129]. The 2,4-diaminoquinazoline compound Importazole has been described as a membrane-permeable small molecule capable of interrupting Importin-mediated nuclear import [130,131]. Consequently, we incubated the HeLa cell lines stably expressing PK-GFP or PK-JM-GFP with either 63 µM Importazole or 0.4 % DMSO for 10 hours.

A distinct effect on the relative frequency distribution of the Nuclear Localization Index of the cell line transfected with PK-JM-GFP, but not the one transfected with PK-GFP is observed (**Figure 29 a & b**): The PK-JM-GFP cell line´s histogram is shifted towards smaller NLIs indicating a profoundly reduced proportion of nuclear protein. In fact, a peak can be observed around 0.52 which is approximately the mean value of the cell line expressing PK-GFP. These data support the hypothesis that the construct containing the EGFR´s JM-domain, and therefore its NLS, is imported into the nucleus in a controlled and regulated way while the nuclear presence of the PK-GFP is most probably only an overexpression artefact.

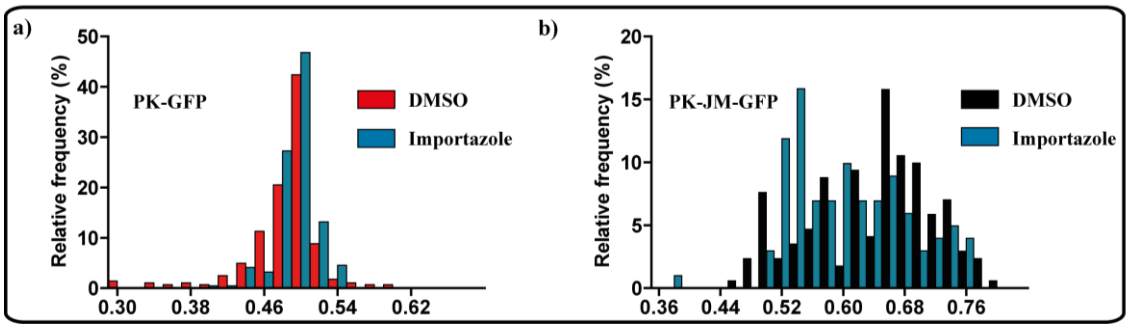

Figure 29: Influence of Importazole on PK-GFP and PK-JM-GFP. *Frequency distribution histograms of the stable cell lines after treatment with Importazole.* ***a)*** *HeLa cells stably expressing PK-GFP were treated with either DMSO (red) or Importazole (blue).* ***b)*** *Treatment of the PK–JM-GFP cell line with Importazole (blue) in comparison to the cells that have been treated with DMSO only (black) (2 biological replicates, between 101 and 283 cells per condition).*

In summary, the dependency on Importin for nuclear import could be reproduced and measured with our reporter cell lines.

4.15.3 Influence of Secin compounds on the nuclear translocation of the EGFR

Since incubation with SecinH3 is able to reverse the impact of recombinant ARNO on endogenous EGFR clusters in plasma membrane sheets (**Figure 22**). we consequently addressed the impact of incubation with 15 µM SecinH3 prior to stimulation on the subcellular localization of the EGFR.

The westernblot in **Figure 30 a** shows the subcellular fractionation of the analyzed HeLa cells. From left to right, the EGFR signals of starved, unstimulated (U), stimulated cells that had been treated with 0.4 % DMSO (S) and cells that had been incubated with 15µM SecinH3 prior to stimulation (H3) are shown.

By visual examination of the westernblot bands, no difference between the DMSO control and the condition treated with SecinH3 can be noticed.

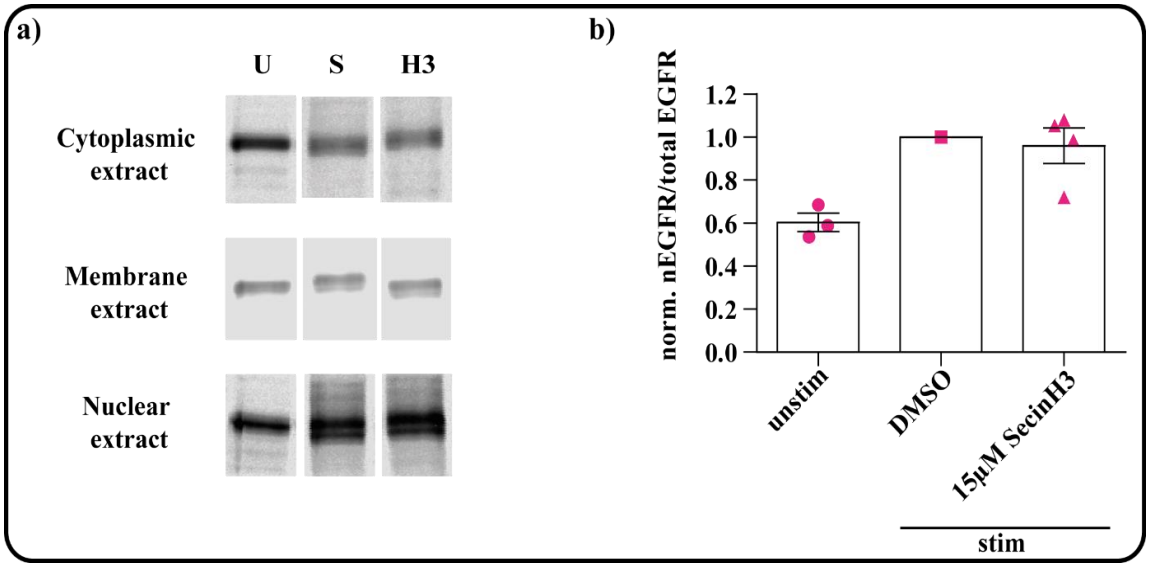

Figure 30: Influence of SecinH3 on the nuclear translocation of the EGFR. *Subcellular fractionation of starved and stimulated HeLa cells that had been either incubated with 15 µM SecinH3 or 0.4 % DMSO.* ***a)*** *Representative westernblot of the different fractions of unstimulated cells (U), cells that have been stimulated with 50 ng/ml EGF for 5 min (S) and cells that have been incubated with 15 µM SecinH3 prior to stimulation (H3).* ***b)*** *Quantification of the ratio of nuclear EGFR to total EGFR normalized to the DMSO control. Depicted are the mean values ± SEM, normalized to the stimulated DMSO ctrl. Statistical test: Student´s t-test, difference between DMSO and SecinH3 not significant (p = 0.724). 3-4 biological replicates.*

This observation is verified by quantification and statistical analysis of the westernblot signal, which is seen in **Figure 30 b**. Analysis of the ratio of nuclear EGFR to total cellular EGFR reveals almost no difference in the mean value. This is reflected in the student´s t-test p-value of 0.724.

To verify and extend this finding, we once again employed the Cell Voyager system for assessment of a variety of Secin compounds´ influence on the subcellular distribution of PK-GFP or PK-JM-GFP, respectively. Subsequently, for every imaged cell, the Nuclear Localization Index (NLI) was calculated and analyzed.

In **Figure 31 a**, the resulting frequency distribution histograms for the cell line stably expressing the PK-GFP fusion protein and in panel **b** the ones for the cell line expressing PK–JM-GFP are depicted.

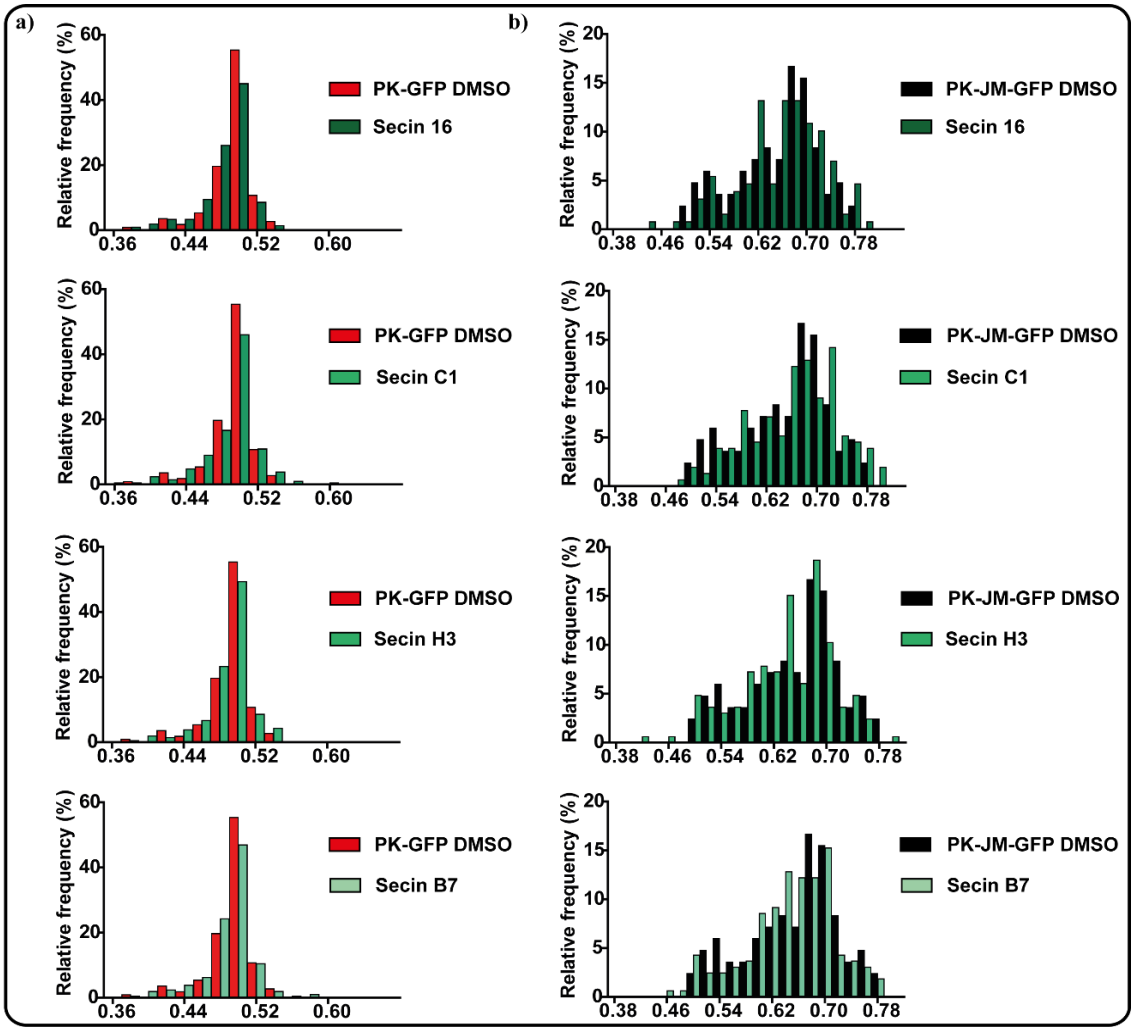

Figure 31: Treatment of PK-GFP and PK-JM-GFP cell lines with Secin compounds. *Frequency distribution histograms of the Nuclear Localization Indices of the cell lines stably transfected with PK-JM-GFP or PK-GFP, respectively after incubation with either DMSO (black/red) or a Secin compound (shades of green).* ***a)*** *Frequency distribution histograms of the PK-JM-GFP-transfected cell line´s NLI.* ***b)*** *Frequency distribution histograms after incubating the PK-GFP-transfected cell line with different Secin compounds. 1 biological replicate, between 84 and 184 cells analyzed.*

None of the compounds has a discernible effect on either of the cell lines what is in line with the other findings.

Overall, in this study, no influence of ARNO on the nuclear translocation of the EGFR could be observed.

5 Discussion

5.1 Membrane binding of ARNO

In the first part of this study, we assessed the contribution of the different domains of ARNO to plasma membrane binding, since this recruitment is required for many of ARNO´s major functions. Among these functions, the activation of the small GTPase Arf6 that in turn does not only recognize and bind to preferred sites of effector proteins but assembles them into multi-valent membrane-binding platforms held together by multiple protein-membrane and protein-protein interactions, is well established [132]. Consequently, vesicle formation and packing as well as membrane remodeling is initiated [19]. On top of that, Arf6 is involved in cytoskeletal rearrangement thus playing a role in cell migration and adhesion [133].

5.1.1 The role of the ARNO coiled-coil domain

Active participation in recruitment of ARNO to the plasma membrane from the cytoplasm has, for example, been reported for Arf6 and Arl4. Membrane-associated Arf6 and Arl4 molecules can bind to ARNO´s PH-domain. The cooperative binding of the PH-domain to Arf6 as well as PIP_2 is thought to relieve the autoinhibition of ARNO thus leading to the activation of more Arf proteins [134].

However, in some cases ARNO does not freely translocate between cytoplasm and plasma membrane but has been reported to be actively shuttled towards the plasma membrane, for example bound to CCDC120 in vesicles of growing neurites [135].

As described, Arf can be activated by directly recruiting ARNO. Besides this direct interaction of ARNO and Arf, sometimes the activation is mediated by third party proteins like RLIP1 or CNK1 [136,137]. Binding to these proteins has been shown to be conveyed by ARNO´s coiled-coil-domain.

The coiled-coil domain is structurally similar to a leucin zipper and can therefore interact with other proteins containing similar domains as well as lead to homodimerization [138].

In agreement with the findings reporting the facilitation of membrane recruitment by coiled-coil domain-binding proteins like CNK1, as indicated in **Figure 13**, we found that loss of the coiled-coil domain impaired ARNO´s binding of the basal plasma membrane by approximately 60 %.

ARNO´s preference for dimerization due to its coiled-coil domain has clearly been demonstrated [139]. Artificial dimerization of a Sec7-PH-GFP-construct by a leucin zipper was able to restore the membrane binding ability in part, but not totally. Dimerization of the PH-PBR-construct by fusion with GST lead to a similar result (**Figure 13**). This suggests that the coiled-coil domain´s contribution to membrane binding might be partly due to the interaction with other proteins and partly due to an increased avidity facilitating the protein-membrane-interaction for the other domains.

Contradictory, Hiester and his colleagues performed subcellular fractionations and found less full-length ARNO in the membrane fraction than of an ARNO construct lacking the coiled-coil domain. They then performed several bead-based binding assays and concluded that the coiled-coil domain bound to the other ARNO domains adding yet another autoinhibitory mechanism impairing membrane binding [32]. However, neither did they control for equal expression levels of the transfected protein constructs, nor does their model of autoinhibitory coiled-coil domain-binding take the coiled-coil domain´s role in dimerization of ARNO into account.

5.1.2 The availability of PIP_2 for PH-domain-containing proteins

Since our data cement the importance of the PIP-PH-domain-interaction for plasma membrane binding of ARNO (**Figure 11**), it is self-evident that the availability of PIPs for binding is an important factor for ARNO´s plasma membrane association.

Regulation of the availability of PIPs for their binding partners is strictly regulated in a spatio-temporal manner. This is a prerequisite for the coordinated orchestration of the many signaling pathways PIPs are involved in. Since studies have shown that the total concentration of PIP_2 does not change much in response to extracellular stimuli, this regulation seems to be achieved largely independent from synthesis and turnover [141].

Interestingly, one of the key regulators of the amount of free PIP_2 in the plasma membrane is the concentration of intracellular cations such as Ca^{2+} and Mg^{2+}.

However, many different mechanisms come into play determining the influence of these cations. On the one hand, the anionic head groups of the PIP_2 molecules attract cations from the cytoplasm forming an ionic double layer. This ion cloud electrostatically shields the PIPs from their potential binding partners.

For example, intracellular Mg^{2+} and other multivalent cations can decrease the interaction between certain K^+-channels (KCNQ) and PIP_2 and even impair the membrane recruitment of rat Synaptotagmin-1 [106,142]. Furthermore, a phenomenon called "Ca^{2+}-PIP_2-bridges" has been coined, a very strong binding between Ca^{2+}-ions and the anionic head groups of PIP_2 molecules preventing the interaction of PH-domains and PIP_2. The biological relevance of the Ca^{2+}-dependent inhibition of the membrane recruitment of PH-domain-containing proteins has been shown in hepatocytes during obesity and hyperlipidemia that have a chronically attenuated Ca^{2+}-level [143].

These effects on the availability of PIPs are a possible explanation for the necessity of the chelator EGTA in the binding assays (**Figure 10**) and might also explain why, after incubation with EGTA, such a high amount of recombinant ARNO could be bound to the sheets compared to the amount of plasma membrane-bound endogenous ARNO in steady state [36]. This might also be the reason why overexpression of ARNO leads to a predominantly cytoplasmic localization (**Figure 28**), something that had also been observed before [144].

Compared to EDTA, EGTA has a higher sensitivity for Ca^{2+}, but a much lower affinity for Mg^{2+}. To explain why chelation of Ca^{2+} is more relevant for the availability of PIPs for binding by PH-domains than chelation of Mg^{2+}, the physicochemical properties of the different cations need to be taken into consideration. Since in the aqueous solution of the cytoplasm the cations are surrounded by a hydration shell, formation of an ionic interaction or bridge requires the release of a water molecule from that shell.

Though equal in net charge, other characteristics determine the differences in the energetic barriers that need to be overcome for this process.

The coordination number defines the number of a central atom´s neighbors in a crystal or molecule. While Mg^{2+} coordinates its neighbors favorably in a strict sixfold octahedral complex and therefore has a coordination number of six, Ca^{2+} prefers coordination numbers between six and eight and has a wider range of energetically low ligand atom bond lengths [145]. Since the radius of Mg^{2+} is smaller than that of Ca^{2+}, its charge–to–radius–ratio is bigger. These factors contribute to the relatively high hydration energy of Mg^{2+} and a water exchange rate that is about 3000 times lower than that of Ca^{2+} [146]. In summary, these properties may explain why Ca^{2+} forms tight bridges with the PIP_2 molecules while Mg^{2+} associates more loosely in ion clouds.

However, it is of note that cations are not the only factors influencing the availability of PIPs in the plasma membrane. Myristoylated alanine-rich C kinase substrate (MARCKS) are natively unfolded proteins, meaning that they are not structured in a specific way. A single MARCKS molecule is able to nonspecifically and electrostatically sequester multiple PIP_2 molecules. Therefore, they are able to sequester and concentrate pools of PIP_2 in specific regions of the plasma membrane, for example in ruffles [147,148]. This interaction is reversible. Calmodulin, that is activated by high intracellular Ca^{2+} levels, leads to dissociation of MARCKS from the membrane freeing the previously sequestered PIP_2 molecules [149]. So, in the part of the membranes in which PIP_2 had been bound to MARCKS, elevation of the intracellular Ca^{2+} concentration results in more binding sites for PH-domain-containing proteins instead of less.

Taken together, this means that the spatiotemporal fluctuations of Ca^{2+} concentration at the plasma membrane might regulate ARNO recruitment, differentially.

5.2 Ca^{2+} plays a central role in the network of PIP_2, ARNO and the EGFR

Ca^{2+} ions have been known to ubiquitously regulate a plethora of cellular functions. Not only exists a concentration gradient over four orders of magnitude between the intra- and extracellular milieu, but tight spatiotemporal control of the intracellular Ca^{2+} level enables the cell to use this cation as a versatile tool for the specific regulation of various signaling pathways [140].

5.2.1 The intracellular Ca^{2+} level can be regulated stimulus-dependent by the EGFR

Since Ca^{2+} acts as such an important cofactor in cell signaling, its intracellular concentration is subject to intricate regulation.

Activation of the Phospholipase C is one of the downstream effects of EGFR signaling [150]. It breaks down PIP_2 into two second messengers: Diacylglycerol (DAG) and Inositol(1,4,5)triphosphate (IP_3). IP_3 diffuses into the cytoplasm, binds to specific receptors at the membrane of the endoplasmic reticulum which serves as the cell´s Ca^{2+} storage organelle. Consequently, a substantial amount of Ca^{2+} is released into the cytoplasm within a very short period of time.

This rapid increase in cytoplasmic Ca^{2+} concentration is downregulated by dephosphorylation of IP_3 to IP_2, phosphorylation of IP_3 to IP_4 and actively pumping the Ca^{2+} ions into the extracellular space. DAG on the other hand remains in the plasma membrane where it can either be involved in eicosanoid synthesis or activation of the protein kinase C (PKC) [151].

In addition to the subsequent Ca^{2+} release from intracellular stores, an influx from the extracellular space can be triggered. The extent and proportions of these two different mechanisms influencing the intracellular Ca^{2+} concentration is dependent on the strength and duration of the EGF stimulus [152]. Massive influx of extracellular Ca^{2+} through ion channels leads to local Ca^{2+} microdomains around the channel adding to the heterogeneity of Ca^{2+} concentrations across the plasma membrane [140]. As already described in **Chapter 1.6**, the interaction between the EGFR´s JM-domain and PIP_2 is crucial for the receptor´s activity. It has not yet been elucidated whether free Ca^{2+} ions can impair this interaction. Nevertheless, the Ca^{2+}-Calmodulin-complex is able to bind directly to the EGFR´s JM-domain if all four Ca^{2+} binding sites of the Calmodulin molecule are occupied resulting in impairment of the EGFR–PIP_2–interaction [153]. On top of that, certain Calmodulin–dependent kinases like the CaMKII phosphorylate the EGFR leading to its deactivation and increased endocytosis [152]. Given that the studies reporting that the EGFR–PIP_2–interaction is required for the receptor´s activation seem more convincing than those claiming the opposite, the augmented Ca^{2+} level would lead to a negative feedback [47,60,62].

5.2.2 G-protein coupled receptors are important mediators of Ca^{2+} signaling

Among the most prominent regulators are G-protein coupled receptor (GPCR)-induced PIP_2 signaling pathways. GPCRs constitute the largest family of plasma membrane receptors and can be activated by a multiltude of different stimuli like neurotransmitters, light or the extracellular Ca^{2+} level [154].

Structurally, GPCRs consist of seven transmembrane units with an extracellular ligand binding site and an intracellular G-protein interaction surface and can be found in either active, active-like or inactive conformation. Ligand binding induces, in cooperation with other factors, the conformational change from the inactive to the active state in which the GPCR can act as a GEF for heterotrimeric G-proteins, exchanging bound GDP for GTP [155].

The activated G-protein then dissociates from the receptor and in turn kicks off several signaling pathways. One of the major ones includes activation of the Phospholipase C-β resulting in a pronounced increase of the intracellular Ca^{2+} concentration.

5.2.3 The signaling pathways of GPCRs and small GTPases are interwoven

It has been widely accepted that small GTPases play a role in the trafficking of GPCRs from the ER to the plasma membrane thus providing spatio-temporal regulation of the hundreds of different GPCRs. For example, inhibition of the five human Arf GTPases demonstrated that they differentially modulate the cell surface targeting of the GPCRs like the α_{2B}-adrenergic receptor, the angiotensin II type 1 receptor and the chemokine receptor 4. Expectedly, manipulation of Arf1 shows the strongest effect [156]. Recycling times and therefore resensitization vary between different GPCRs [157].

In addition to the broad control of GPCR signaling through trafficking by small GTPases, there is evidence for a direct interaction between certain amino acids in the C-terminal tail of GPCRs and small GTPases [158]. This can lead to the exchange from GDP to GTP and therefore activation of the small GTPase and propagate signaling. Consequently, the GPCR has direct influence on its own trafficking. For example, the angiotensin type 1 receptor causes the activation of Rab5a thus increasing endocytosis. Rab8 is reportedly the first example for a small GTPase to influence the inositol phosphate signaling of the metabotropic glutamate receptor 1a (mGLuR1a) leading to the attenuation of the Ca^{2+}-level in primary hippocampal neurons [159].

Another phospholipase that can be activated by many Ca^{2+}-mobilizing GPCRs is the phospholipase D (PLD). Mitchell and colleagues showed that its activation could be inhibited by the Arf protein inhibitor Brefeldin A and were able to coimmunoprecipitate Arf and Rho GTPases with certain GPCRs of the Rhodopsin family. Conclusively, they proposed a model in which direct interaction between GPCRs and Arf as well as Rho GTPases leads to a stronger activation of the PLD independently from heterotrimeric G-proteins [160].

Desensitization of GPCRs can be achieved by phosphorylation and subsequent binding of β-Arrestins. These proteins occupy the G protein binding site thus terminating active signaling via G-proteins. However, this initiates G-protein independent signaling pathways. [161]. On top of that, they link the receptor to Clathrin and other endocytic proteins.

Several groups demonstrated that Arf6 as well as ARNO directly interact with and are regulated by GPCR-associated Arrestin β, providing a direct link between the desensitization of Ca^{2+} concentration-regulating GPCRs and ARNO [162,163].

These findings, together with our results concerning the notion that the binding of ARNO to the plasma membrane strongly depends on the availability of PIP_2 and can be impaired by the formation of Ca^{2+} -PIP_2-bridges (**Figure 10**), may raise speculations in how far this might be a relevant positive feedback for GPCRs delaying their desensitization. On the other hand, in those regions of the plasma membrane where the PIP_2 molecules had been sequestered by MARCKS, more binding sites for ARNO might be available leading to increased endocytosis of the GPCRs.

Among many others, these findings sparked a discussion in the scientific field about the depth and extent of the crosstalk between classical GPCR and small GTPase signaling pathways. For Arf proteins as well as GPCRs, the view develops from the understanding of individual signaling molecules to members of signaling platforms in the membrane consisting of an ensemble of crosstalking molecules [132,164].

5.2.4 The EGFR-GPCR relationship

During about one and a half decades, solid evidence has accumulated that the signaling networks of GPCRs and the EGFR crosstalk [165]. The modes of transactivation of the EGFR by GPCRs can basically be divided into two mechanisms:

Firstly, many GPCRs directly increase the activity of membrane-embedded matrix metalloproteases (MMP). These shed ligands like HB-EGF from the membrane leading to the EGFR´s activation, a process that has been shown to be relevant for many physiological processes and diseases including cancer [166,167].

Secondly, GPCRs can activate intracellular protein tyrosine kinases (PTK), for example of the Src family, promoting the phosphorylation of the EGFR [168].

Thus, once again, the extent of complexity of the signaling pathways´ meshwork in cells is underlined.

5.3 Plasma membrane compartmentalization

Having analyzed numerous factors that are important for ARNO´s binding to the plasma membrane, high resolution STED imaging provided a more detailed look at the way ARNO molecules are organized once they are bound.

Generally, most proteins that are either transiently bound to or permanently integrated in the plasma membrane do not diffuse randomly but exist in an equilibrium between free monomers and clusters or microdomains, respectively.

5.3.1 The meaning of protein clustering and micropatterning

Our view on membranes has changed during the course of the last decades from simple barriers between cellular compartments to the realization that lipids actively interact with the integrated proteins influencing their signaling. In terms of the organization of proteins within membranes, by today, there is no model that covers all observed phenomena in their entire complexity, but a variety of non–mutually exclusive ideas, each highlighting certain characteristics of the system [169].

5.3.1.1 The mobility of proteins in the plasma membrane is limited

Initially, Nicolson and Singer had proposed the “fluid mosaic model” in which membranes are a viscous two-dimensional solution formed by freely diffusing lipids and proteins [170]. However, this hypothesis was undercut by the finding that the diffusion of proteins in natural membranes was about 5-50 times slower than in artificial membranes [171]. Evidence accumulated that proteins and lipids are not distributed homogenously and advanced techniques like single-molecule tracking led to the “picket fence model”. It proposes that the movement of transmembrane proteins is restricted into so-called “confinement zones” by cytoskeletal proteins like actin. Transgression from one confinement zone into the other can only happen by so-called “hop-diffusion” [172,173]. On top of that, the existence of “lipid rafts” has been claimed: Sphingolipid microdomains that require cholesterol and are resistant to certain detergents though their existence and relevance has been subject to controversy in the field [174–176]. Nevertheless, it too supports the notion of a spatial compartmentalization of the plasma membrane itself. In 2006, Lillemeier and colleagues conducted electron microscopy studies of membrane sheets and were able to distinguish areas of high and low protein density.

They therefore proposed the idea of proteophilic regions in the membrane, so-called "protein islands" that have a diameter between 30 and 300 nm and probably develop due to protein-protein and protein–lipid-interactions [49].
Within these regions, the proteins self-organize into clusters and microdomains.
This notion would explain why our STED images do not show evenly distributed clusters, but regions with a high abundance of clusters and regions that were nearly devoid of them (**Figure 16**). Though relatively long-lived, clusters are fluctuating, non-rigid structures which means that the proteins exist in an equilibrium between its monomeric and clustered form [177].

5.3.2 The partial cluster overlap might indicate a functional connection between ARNO and the EGFR

The STED data in (**Figure 17**) show that there is nearly no concentric colocalization between ARNO and EGFR clusters, but rather a close proximity and partial overlap. This neither indicates a functional relationship between the two proteins, nor does it exclude direct interaction. Certain interacting proteins have been shown to form clusters exhibiting a similar pattern. For example, the microtubule end binding protein EB1 is well known to interact with the tumor-suppressor protein adenomatous polyposis coli (APC) in non-cholinergic cells. Yet, in nicotinic synapses, confocal microscopy imaging revealed an only partial overlap and very close proximity of the protein clusters [178].

Advances in microscopic techniques like the overcome of the diffraction barrier might lead to an increase in this kind of findings: Clusters, which can appear to be fully colocalized when analyzed with confocal or wide-field microscopy might be resolved to only partially overlap using advanced techniques like STED or PALM/STORM [179]. Likewise, in this study, the extent of protein cluster overlap becomes apparent in STED but not epifluorescent wide-field microscopy (**Figure 17** & **15**).
Interestingly, the PCC as well as the STED data of the different ARNO constructs may indicate that the overlap of ARNO construct and EGFR clusters rather depend on the ability to bind to the membrane than on the presence of a certain domain. The finding that for all membrane-bound constructs the percentage of clusters in very close proximity to the EGFR is about the same (**Figure 19**) may indicate that a putative binding to the EGFR might be achieved in a cooperative manner.

The ability of EGFR antibodies to compete with ARNO for plasma membrane binding is an additional indication for the great vicinity between ARNO and EGFR molecules in the membrane (**Figure 20**). It makes sense that membrane binding of ARNO-GFP was reduced, but not inhibited since only a fraction of ARNO is expected to be very close to the EGFR and therefore is impaired in its ability to bind.

5.3.2.1 What drives cluster formation?

To get a better understanding of the colocalization of ARNO and EGFR clusters, it is important to understand how protein clusters are formed.

The formation of clusters is driven by different forces: Electrostatic interactions between charged residues or (induced) dipoles as well as hydrophobic forces.

For example, PIP_2 sequesters the SNARE-protein syntaxin 1a by interaction with its positively charged polybasic region. Neutralization of the protein´s charge reduces the electrostatic repulsion between the proteins thus facilitating a higher packing density [180].

Similarly, the interaction between PIP_2 and the EGFR´s JM-domain is not only relevant for the structural conformation of its dimers, but also drives the formation of nanoclusters. Aberrant numbers and sizes of EGFR clusters have been found in lung cancer cells as compared to healthy cells suggesting a pathophysiological relevance [61].

However, the abundance of positively charged lipids in the plasma membrane is low. Therefore, neutralization of negative protein residues is achieved by cations like Ca^{2+}. Conclusively, supplementation of buffer with divalent cations induces protein clustering on membrane sheets [146].

Hydrophobic forces probably synergistically add to the formation of clusters, for example due to their involvement in coiled-coil formation [181].

Another determinant of clustering is the interaction between the membrane-associated and cytoplasmic proteins.

On the one hand, specific cytoplasmic interactions have been shown to directly influence formation and packing density of clusters. For example, tight clustering of syntaxin 1A has been reported to require the protein´s cytoplasmic domain while the transmembrane domain is sufficient for loose packing [182].

On the other hand, there is evidence that the density and size of the membrane´s confinement zones or protein islands, together with protein concentration, also is a factor determining clustering of transmembrane proteins like the EGFR [183].

Cluster size is limited, probably by short-range attractive and long range repulsive forces between the proteins. Abulrob and colleagues found a similar EGFR cluster size distribution as in this study with a mean diameter of 150 nm. Treatment with EGF resulted in an increased number of small and large clusters, while preincubation with EGFR inhibitors reversed the increase of large clusters to control cell level [118]. Typical cluster sizes of proteins in the plasma membrane are around 70 – 100 nm, so the sizes of the ARNO as well as the EGFR clusters determined in this study are in the usual range (**Figure 18**) [184]. This argues for a natural behavior of the added recombinant ARNO, since the high concentration does not lead to larger diameter, but to a higher number of clusters in the membrane, when compared to wildtype ARNO clusters. This phenomenon has also been observed for overexpressed syntaxin 1A constructs [182].

However, the flip control that was utilized in the colocalization studies to control for arbitrarily close clusters, does not account for restrictions of the clusters´ spatial distribution in the membrane. So, employment of the flip control alone, could not exclude that the observed proximity between EGFR and ARNO clusters is due to random island distribution. Because of this, the Transferrin receptor, which has the same cluster density as the EGFR, has been employed as a control protein. The nearest neighbor analysis of STED images observes less ARNO clusters in very close proximity to TFR clusters (**Figure 16**), while the flip control values are almost equal for the TFR – ARNO and EGFR – ARNO analysis. Thus, the results of the EGFR–ARNO nearest neighbor analysis are not due to random cluster distribution.

The Transferrin receptor mediates the endocytic intake of iron by binding to its ligand Transferrin. This uptake is dependent on $PI(4,5)P_2$, so a close proximity between PIP_2 and the TFR is likely [185]. Therefore, the fact that ARNO and the EGFR are closer to each other than ARNO and the TFR might be conveyed by more than only mutual sequestering by PIP_2. This is especially interesting, since the group of Michel Franco and others observed that Arf6 and its GEF EFA6 are directly involved in endocytosis as well as recycling of the TFR [186,187]. So, probably the close proximity between ARNO and the EGFR, as compared to the TFR, is not explained by binding of ARNO to Arf6.

5.3.3 The packing density of molecules within a cluster can be important for its functionality

The term cluster density defines the number of packed molecules per area within a cluster. This packing density depends on several factors like ion concentration, the protein conformation that might be influenced by e.g. ligand binding, posttranslational modifications and sequestering by other proteins or lipids. Its physiological relevance has been shown, for example, for α4 integrins that mediate cell adhesion. Tightening of its packing density by overexpression of CD82 positively correlated with an increase of cell adhesion [146,188].

Most studies focusing on EGFR clustering primarily analyzed the oligomerization state of the EGFR, being the ratio between monomers, dimers and oligomers.

Since stimulation of cells with EGFR as well as the incubation with inhibitors change EGFR clustering, there is a general agreement, that the degree of oligomerization is important for its signaling [189–191].

However, not much is known about the changes in the packing density of EGFR molecules within the clusters and its impact on signaling.

The data presented in **Figure 21** indicate, that incubation of the plasma membrane sheets with ARNO leads to a more intense antibody-staining of the EGFR. Since the total amount of EGFR molecules in the sheets cannot have changed, the accessibility of the C-terminal epitope, which is the binding site of the SC-03 EGFR antibody, must have increased. This might either be due to a conformational rearrangement of this C-terminal tail or due to changes in the degree of clustering or cluster density, respectively. A very dense packing of the proteins can mask the epitopes impairing binding of antibodies and therefore reducing the fluorescence intensity [182]. Thus, an increase of stainability might hint at looser packing of EGFR molecules. Future studies may elucidate the relationship between ARNO and EGFR clustering. Independent of whether the increased accessibility of the EGFR´s C–terminus is the result of reduced packing density or a conformational change, this might also be of physiological relevance since effector proteins such as Shc and Grb2 bind to this domain [192]. If the increased accessibility is not only true for the antibody, but also for effector proteins, a physiological relevance would be probable.

Also, some of the other ARNO constructs do influence the EGFR clusters´ RSD. Similarly to the full-length ARNO, the E156K construct decreases the RSD value while Sec7-and PH–domain do not have a significant effect and the R280C mutant increases it. On the other hand, cotreatment of the membrane sheets with the inhibitor SecinH3 reversed the effect of ARNO on the EGFR´s staining intensity and RSD (**Figure 22**). So, similar to the results concerning the colocalization with the EGFR, this influence seems to be dependent on the ability of the constructs to bind to the membrane.

5.4. The functional relationship between ARNO and the EGFR

Given the close proximity of ARNO and EGFR clusters and the influence of ARNO on the staining of the EGFR´s C-terminal tail, the second part of the study aimed at elucidating in how far ARNO and the EGFR functions are connected in a possibly biologically relevant way.

5.4.1 There might be evidence for a biological influence of ARNO on EGFR activation

After transfection of ARNO into HeLa cells a tendency of increased EGFR phosphorylation at the tyrosine residue 1086 (pY1086), and therefore activation, can be observed in comparison to mock–transfected cells (**Figure 23**). Here, increasing the number of biological replicates might lead to a result that withstands statistical testing.

In human embryonal kidney (Hek) cells, the increase of EGFR phosphorylation after transfection with ARNO was even more pronounced (personal communication Michael Famulok). Therefore, the effect could be observed in a tumor as well as an immortalized cell line hinting at a phenomenon that might be of relevance not only in a cancer context but also in healthy cells. Downstream effectors like Grb2 and Cbl bind to pY1086, so proving an influence of ARNO on these proteins would support the ARNO – pY1086 – relationship suggested in this study.

In vitro experiments assessing EGFR phosphorylation in presence or absence of ARNO were not able to detect differences [37]. The presence of different artificial membrane systems like nanodiscs and bicelles did not lead to different results [108].

In summary, the inability to detect an increase of EGFR stimulation in cell-free setups rather speaks for the involvement of additional players than for a direct interaction.

Therefore, future studies might aim at elucidating the effect of ARNO overexpression, knockout or inhibition by SecinH3 on proteins associated with EGFR signaling.

5.4.2 There is no evidence for an involvement of ARNO in the EGFR´s nuclear translocation

Given that, in a cellular context, there is a tendency for increased EGFR phosphorylation upon ARNO overexpression, and that the hypothetical binding site for ARNO in the JM-domain is congruent with the EGFR´s nuclear localization sequence, the question arose whether ARNO has an impact on the EGFR´s nuclear translocation [108,126].

While it was possible to observe the increased subcellular localization after EGFR stimulation with EGF in confocal microscopy as well as in westernblot analysis of subcellular fractionation extracts, in this study, no influence of ARNO overexpression or inhibiton on the nuclear translocation of the EGFR could be detected (**Chapter 4.15**). This might either be the case because there is none or due to an insensitivity of the analysis methods used.

While visually, the difference in the subcellular concentration of the PK-GFP and PK-JM-GFP constructs was strikingly apparent, the latter´s NLI was just 30 % higher. However, this might be because the NLI distribution histogram of the PK-JM-GFP expressing cell line shows a very wide population, which might blur the effect (**Figure 27**). Given this narrow range of the mean NLI values between two extremely distinct constructs, it is possible that smaller changes might not be distinguishable.

So, inhibition of Sec61β–mediated nuclear import by Importazole did lead only to a rather small shift in the PK-JM-GFP cell line´s histogram. Nevertheless, a peak could be observed at an NLI value of 0,52 which is close to the mean value of the PK-GFP cell line signifying an enrichment of protein in the cytoplasm confirming the previously reported involvement of Sec61β in the EGFR´s nuclear import (**Figure 29**) [128]. Consequently, future research might assess in how far Importazole might be a valuable therapeutic agent for inhibition of nucelar import of the EGFR, for example in addition to radiotherapy.

Live cell imaging and the analysis of individual cells could be a way of improving the sensitivity issues because different cells within the broad population and their reaction to stimuli can be distinguished.

Also, it could be interesting to compare ARNO overexpressing cells to ARNO knockout cells in regards of the subcellular distribution of either the PK-constructs or the EGFR itself. The knockout might provide further insight, because the Secin compounds only inhibit the GTPase activity of cytohesin Sec7-domains so GTPase–independent functions might be unaffected [193].

Hypothetically, if the lack of influence of ARNO activity on EGFR translocation is real, this might serve as an additional argument against the direct interaction between ARNO and the JM-domain since otherwise ARNO and Importin β would compete for the exact same binding site. However, the possibility of an interaction under special circumstances, e.g. a certain subcellular localization, specific stimuli etc. is conceivable.

5.4.3 CNK 1 might be a possible third player connecting ARNO with the EGFR

Another possible explanation for an influence of ARNO on the EGFR signaling cascade without the need for direct interaction might be that one or more proteins could be involved to convey the effects. So-called scaffolding proteins are key-components in the assembly of signaling platforms and multiprotein clusters.

One possible candidate for this is the Connector Enhancer of KSR1 (CNK1).

Mass spectrometry studies have identified cytohesins as major binding partners of CNK1 by interaction of the proteins´ coiled-coil-domains. In insulin signaling, CNK1 seems to facilitate the membrane recruitment of cytohesins and Arf1, resulting in increased PI3K/AKT signaling and the formation of PIP_2 - enriched microdomains in the membrane environment [136]. In *Drosophila*, the cytohesin homologue Steppke has been shown to be involved in insulin signaling as well as in MAPK activation downstream of the EGFR. The interaction of Steppke with dCNK, the only CNK homologue in *Drosophila*, is necessary for its function in the EGFR signaling [194]. Therefore, involvement of ARNO and the EGFR cascade in the CNK1 scaffolding complex could be an interesting subject for further studies.

Other scaffolding complexes cytohesins have been reported to be part of include GRP1–associated scaffolding protein (GRASP) [195]. The general receptor for 3–phosphoinositides (GRP1) is a GEF for Arf6 and activated downstream of the insulin receptor through phosphorylation by Akt, linking the complex to receptor tyrosine kinase signaling [196]. In *C.elegans*, GRP1 and Arf1 form functional complexes with

PIP5K regulating PIP2 production in the plasma membrane as part of the Insulin/IGF pathway [197].

So, even the lack of definite evidence for direct interaction does not exclude the existence of a biologically relevant relationship between ARNO and the EGFR.

5.5 Summary

The ARNO domains contribute to plasma membrane binding in a cooperative manner:

The interaction between the PH - domain and PIPs is crucial and can be regulated via the concentration of Ca^{2+} ions. However, this interaction is not sufficient for anchoring the protein in the membrane. Additional binding of the polybasic region to anionic phospholipids is required to secure the membrane association. Dimerization of ARNO through its coiled–coil–domain increases the ability to bind to the membrane. Absence of the Sec7–domain impairs binding to a small extent. However, functional GEF activity is not required.

In the plasma membrane, ARNO and EGFR clusters overlap partially.

The relative standard deviation of the EGFR clusters and their staining intensity is altered after incubation with ARNO suggesting an influence on cluster density or the C – terminal tail´s conformation.

In a cellular context, overexpression of ARNO results in a trend towards increased EGFR phosphorylation or activation, respectively. No effect on the EGFR´s nuclear translocation could be detected.

Overall, the data in this study reveal new insights in ARNO–membrane association and suggest a functional relationship with EGFR clusters, probably as parts of the same complex signaling platforms.

6 References

1. Stoeger, T., Battich, N. & Pelkmans, L. Passive Noise Filtering by Cellular Compartmentalization. *Cell* **164,** 1151–1161 (2016).
2. Schrum, J. P., Zhu, T. F. & Szostak, J. W. The origins of cellular life. *Cold Spring Harbor perspectives in biology* **2,** a002212 (2010).
3. Gabaldon, T. & Pittis, A. A. Origin and evolution of metabolic sub-cellular compartmentalization in eukaryotes. *Biochimie* **119,** 262–268 (2015).
4. Cavalier-Smith, T. Origin of the cell nucleus, mitosis and sex: roles of intracellular coevolution. *Biology direct* **5,** 7 (2010).
5. Blom, M., Reis, K. & Aspenstrom, P. RhoD localization and function is dependent on its GTP/GDP-bound state and unique N-terminal motif. *European journal of cell biology* (2018).
6. Derby, M. C. & Gleeson, P. A. New insights into membrane trafficking and protein sorting. *International review of cytology* **261,** 47–116 (2007).
7. Zouhar, J. & Sauer, M. Helping hands for budding prospects: ENTH/ANTH/VHS accessory proteins in endocytosis, vacuolar transport, and secretion. *The Plant cell* **26,** 4232–4244 (2014).
8. Mima, J. Reconstitution of membrane tethering mediated by Rab-family small GTPases. *Biophysical reviews* **10,** 543–549 (2018).
9. Yang, Y., Lee, M. & Fairn, G. D. Phospholipid Subcellular Localization and Dynamics. *The Journal of biological chemistry* (2018).
10. Pompa, A. *et al.* Unconventional Transport Routes of Soluble and Membrane Proteins and Their Role in Developmental Biology. *International journal of molecular sciences* **18** (2017).
11. Gomez-Navarro, N. & Miller, E. Protein sorting at the ER-Golgi interface. *The Journal of cell biology* **215,** 769–778 (2016).
12. Wennerberg, K., Rossman, K. L. & Der, C. J. The Ras superfamily at a glance. *Journal of cell science* **118,** 843–846 (2005).
13. Mizuno-Yamasaki, E., Rivera-Molina, F. & Novick, P. GTPase Networks in Membrane Traffic. *Annual review of biochemistry* **81,** 637–659 (2012).
14. Zhao, W. *et al.* Direct Targeting of the Ras GTPase Superfamily Through Structure-Based Design. *Current topics in medicinal chemistry* **17,** 16–29 (2017).
15. Spang, A., Shiba, Y. & Randazzo, P. A. Arf GAPs: gatekeepers of vesicle generation. *FEBS letters* **584,** 2646–2651 (2010).
16. Donaldson, J. G. & Jackson, C. L. ARF family G proteins and their regulators: roles in membrane transport, development and disease. *Nature reviews. Molecular cell biology* **12,** 362–375 (2011).
17. Koo, T. H., Eipper, B. A. & Donaldson, J. G. Arf6 recruits the Rac GEF Kalirin to the plasma membrane facilitating Rac activation. *BMC cell biology* **8,** 29 (2007).
18. McMahon, H. T. & Mills, I. G. COP and clathrin-coated vesicle budding: different pathways, common approaches. *Current opinion in cell biology* **16,** 379–391 (2004).

19. Casanova, J. E. Regulation of Arf activation: the Sec7 family of guanine nucleotide exchange factors. *Traffic (Copenhagen, Denmark)* **8,** 1476–1485 (2007).

20. Gamara, J., Chouinard, F., Davis, L., Aoudjit, F. & Bourgoin, S. G. Regulators and Effectors of Arf GTPases in Neutrophils. *Journal of Immunology Research* **2015,** 235170 (2015).

21. Wright, J., Kahn, R. A. & Sztul, E. Regulating the large Sec7 ARF guanine nucleotide exchange factors: the when, where and how of activation. *Cellular and molecular life sciences : CMLS* **71,** 3419–3438 (2014).

22. Nawrotek, A., Zeghouf, M. & Cherfils, J. Allosteric regulation of Arf GTPases and their GEFs at the membrane interface. *Small GTPases* **7,** 283–296 (2016).

23. Cherfils, J. *et al.* Structure of the Sec7 domain of the Arf exchange factor ARNO. *Nature* **392,** 101–105 (1998).

24. Beraud-Dufour, S. *et al.* A glutamic finger in the guanine nucleotide exchange factor ARNO displaces Mg2+ and the beta-phosphate to destabilize GDP on ARF1. *The EMBO journal* **17,** 3651–3659 (1998).

25. Hafner, M. *et al.* Inhibition of cytohesins by SecinH3 leads to hepatic insulin resistance. *Nature* **444,** 941–944 (2006).

26. DiNitto, J. P. *et al.* Structural basis and mechanism of autoregulation in 3-phosphoinositide-dependent Grp1 family Arf GTPase exchange factors. *Molecular cell* **28,** 569–583 (2007).

27. Stalder, D. & Antonny, B. Arf GTPase regulation through cascade mechanisms and positive feedback loops. *FEBS letters* **587,** 2028–2035 (2013).

28. Nagel, W., Schilcher, P., Zeitlmann, L. & Kolanus, W. The PH Domain and the Polybasic c Domain of Cytohesin-1 Cooperate specifically in Plasma Membrane Association and Cellular Function. *Molecular biology of the cell* **9,** 1981–1994 (1998).

29. Malaby, A. W., van den Berg, B. & Lambright, D. G. Structural basis for membrane recruitment and allosteric activation of cytohesin family Arf GTPase exchange factors. *Proceedings of the National Academy of Sciences of the United States of America* **110,** 14213–14218 (2013).

30. Cohen, L. A. *et al.* Active Arf6 recruits ARNO/cytohesin GEFs to the PM by binding their PH domains. *Molecular biology of the cell* **18,** 2244–2253 (2007).

31. Stalder, D. *et al.* Kinetic studies of the Arf activator Arno on model membranes in the presence of Arf effectors suggest control by a positive feedback loop. *The Journal of biological chemistry* **286,** 3873–3883 (2011).

32. Hiester, K. G. & Santy, L. C. The cytohesin coiled-coil domain interacts with threonine 276 to control membrane association. *PloS one* **8,** e82084 (2013).

33. Santy, L. C., Frank, S. R., Hatfield, J. C. & Casanova, J. E. Regulation of ARNO nucleotide exchange by a PH domain electrostatic switch. *Current Biology* **9,** 1173–1176 (1999).

34. Belov, G. A., Kovtunovych, G., Jackson, C. L. & Ehrenfeld, E. Poliovirus replication requires the N-terminus but not the catalytic Sec7 domain of ArfGEF GBF1. *Cellular microbiology* **12,** 1463–1479 (2010).

35. O'Rourke, S. M., Christensen, S. N. & Bowerman, B. Caenorhabditis elegans EFA-6 limits microtubule growth at the cell cortex. *Nature cell biology* **12,** 1235–1241 (2010).

36. Bill, A. *et al.* Cytohesins are cytoplasmic ErbB receptor activators. *Cell* **143,** 201–211 (2010).

37. Bill, A. *et al.* Retraction Notice to: Cytohesins Are Cytoplasmic ErbB Receptor Activators. *Cell* **165,** 1293 (2016).

38. Bill, A. *et al.* Anti-proliferative effect of cytohesin inhibition in gefitinib-resistant lung cancer cells. *PloS one* **7,** e41179 (2012).

39. Pan, T. *et al.* Cytohesins/ARNO. The function in colorectal cancer cells. *PloS one* **9,** e90997 (2014).

40. Stahelin, R. V., Scott, J. L. & Frick, C. T. Cellular and molecular interactions of phosphoinositides and peripheral proteins. *Chemistry and physics of lipids* **182,** 3–18 (2014).

41. Balla, T. Phosphoinositides: tiny lipids with giant impact on cell regulation. *Physiological reviews* **93,** 1019–1137 (2013).

42. Hammond, G. R. V. & Balla, T. Polyphosphoinositide binding domains: Key to inositol lipid biology. *Biochimica et biophysica acta* **1851,** 746–758 (2015).

43. Lemmon, M. A. Membrane recognition by phospholipid-binding domains. *Nature reviews. Molecular cell biology* **9,** 99–111 (2008).

44. van Weering, J. R. T. *et al.* Molecular basis for SNX-BAR-mediated assembly of distinct endosomal sorting tubules. *The EMBO journal* **31,** 4466–4480 (2012).

45. Heo, W. D. *et al.* PI(3,4,5)P3 and PI(4,5)P2 lipids target proteins with polybasic clusters to the plasma membrane. *Science (New York, N.Y.)* **314,** 1458–1461 (2006).

46. Jian, X., Gruschus, J. M., Sztul, E. & Randazzo, P. A. The pleckstrin homology (PH) domain of the Arf exchange factor Brag2 is an allosteric binding site. *The Journal of biological chemistry* **287,** 24273–24283 (2012).

47. McLaughlin, S., Smith, S. O., Hayman, M. J. & Murray, D. An electrostatic engine model for autoinhibition and activation of the epidermal growth factor receptor (EGFR/ErbB) family. *The Journal of general physiology* **126,** 41–53 (2005).

48. Picas, L., Gaits-Iacovoni, F. & Goud, B. The emerging role of phosphoinositide clustering in intracellular trafficking and signal transduction. *F1000Research* **5** (2016).

49. Lillemeier, B. F., Pfeiffer, J. R., Surviladze, Z., Wilson, B. S. & Davis, M. M. Plasma membrane-associated proteins are clustered into islands attached to the cytoskeleton. *Proceedings of the National Academy of Sciences of the United States of America* **103,** 18992–18997 (2006).

50. Saka, S. K. *et al.* Multi-protein assemblies underlie the mesoscale organization of the plasma membrane. *Nature communications* **5,** 4509 (2014).

51. Johannes, L., Pezeshkian, W., Ipsen, J. H. & Shillcock, J. C. Clustering on Membranes. Fluctuations and More. *Trends in cell biology* **28,** 405–415 (2018).

52. Arendt, K. L. *et al.* PIP(3) controls synaptic function by maintaining AMPA receptor clustering at the postsynaptic membrane. *Nature neuroscience* **13,** 36–44 (2009).

53. Milovanovic, D. *et al.* Calcium Promotes the Formation of Syntaxin 1 Mesoscale Domains through Phosphatidylinositol 4,5-Bisphosphate. *The Journal of biological chemistry* **291,** 7868–7876 (2016).

54. Chen, X. *et al.* Phosphatidylinositol 4,5-bisphosphate clusters the cell adhesion molecule CD44 and assembles a specific CD44-Ezrin heterocomplex, as revealed by small angle neutron scattering. *The Journal of biological chemistry* **290,** 6639–6652 (2015).

55. Al-Ejeh, F. *et al.* Treatment of triple-negative breast cancer using anti-EGFR-directed radioimmunotherapy combined with radiosensitizing chemotherapy and PARP inhibitor. *Journal of nuclear medicine : official publication, Society of Nuclear Medicine* **54,** 913–921 (2013).

56. Lemmon, M. A. & Schlessinger, J. Cell signaling by receptor tyrosine kinases. *Cell* **141,** 1117–1134 (2010).

57. Fichter, C. D. *et al.* A new model system identifies epidermal growth factor receptor-human epidermal growth factor receptor 2 (HER2) and HER2-human epidermal growth factor receptor 3 heterodimers as potent inducers of oesophageal epithelial cell invasion. *The Journal of pathology* **243,** 481–495 (2017).

58. Huang, Y. *et al.* Molecular basis for multimerization in the activation of the epidermal growth factor receptor. *eLife* **5** (2016).

59. Endres, N. F. *et al.* Conformational coupling across the plasma membrane in activation of the EGF receptor. *Cell* **152,** 543–556 (2013).

60. Abd Halim, K. B., Koldso, H. & Sansom, M. S. P. Interactions of the EGFR juxtamembrane domain with PIP2-containing lipid bilayers: Insights from multiscale molecular dynamics simulations. *Biochimica et biophysica acta* **1850,** 1017–1025 (2015).

61. Wang, Y. *et al.* Regulation of EGFR nanocluster formation by ionic protein-lipid interaction. *Cell research* **24,** 959–976 (2014).

62. Michailidis, I. E. *et al.* Phosphatidylinositol-4,5-bisphosphate regulates epidermal growth factor receptor activation. *Pflugers Archiv : European journal of physiology* **461,** 387–397 (2011).

63. Bauer, N. C., Doetsch, P. W. & Corbett, A. H. Mechanisms Regulating Protein Localization. *Traffic (Copenhagen, Denmark)* **16,** 1039–1061 (2015).

64. Kracikova, M., Akiri, G., George, A., Sachidanandam, R. & Aaronson, S. A. A threshold mechanism mediates p53 cell fate decision between growth arrest and apoptosis. *Cell death and differentiation* **20,** 576–588 (2013).

65. Henriksen, L., Grandal, M. V., Knudsen, S. L. J., van Deurs, B. & Grovdal, L. M. Internalization mechanisms of the epidermal growth factor receptor after activation with different ligands. *PloS one* **8,** e58148 (2013).

66. Laketa, V. *et al.* PIP_3 induces the recycling of receptor tyrosine kinases. *Science signaling* **7,** ra5 (2014).

67. Sorkin, A. & Goh, L. K. Endocytosis and intracellular trafficking of ErbBs. *Experimental Cell Research* **315,** 683–696 (2009).

68. Madshus, I. H. & Stang, E. Internalization and intracellular sorting of the EGF receptor: a model for understanding the mechanisms of receptor trafficking. *Journal of cell science* **122,** 3433–3439 (2009).

69. Ch'ng, T. H. *et al.* Activity-dependent transport of the transcriptional coactivator CRTC1 from synapse to nucleus. *Cell* **150,** 207–221 (2012).

70. Nakanishi, S. & Okazawa, M. Membrane potential-regulated Ca2+ signalling in development and maturation of mammalian cerebellar granule cells. *The Journal of physiology* **575,** 389–395 (2006).

71. Nonaka, M. *et al.* Towards a better understanding of cognitive behaviors regulated by gene expression downstream of activity-dependent transcription factors. *Neurobiology of learning and memory* **115,** 21–29 (2014).

72. Kamio, T., Shigematsu, K., Sou, H., Kawai, K. & Tsuchiyama, H. Immunohistochemical expression of epidermal growth factor receptors in human adrenocortical carcinoma. *Human pathology* **21,** 277–282 (1990).

73. Wang, Y.-N. *et al.* COPI-mediated retrograde trafficking from the Golgi to the ER regulates EGFR nuclear transport. *Biochemical and biophysical research communications* **399,** 498–504 (2010).

74. Wang, Y.-N. *et al.* Membrane-bound trafficking regulates nuclear transport of integral epidermal growth factor receptor (EGFR) and ErbB-2. *The Journal of biological chemistry* **287,** 16869–16879 (2012).

75. Brand, T. M., Iida, M., Li, C. & Wheeler, D. L. The nuclear epidermal growth factor receptor signaling network and its role in cancer. *Discovery medicine* **12,** 419–432 (2011).

76. Shi, Y. *et al.* Nuclear epidermal growth factor receptor interacts with transcriptional intermediary factor 2 to activate cyclin D1 gene expression triggered by the oncoprotein latent membrane protein 1. *Carcinogenesis* **33,** 1468–1478 (2012).

77. Hanada, N. *et al.* Co-regulation of B-Myb expression by E2F1 and EGF receptor. *Molecular carcinogenesis* **45,** 10–17 (2006).

78. Liccardi, G., Hartley, J. A. & Hochhauser, D. EGFR nuclear translocation modulates DNA repair following cisplatin and ionizing radiation treatment. *Cancer research* **71,** 1103–1114 (2011).

79. Wang, S.-C. *et al.* Tyrosine phosphorylation controls PCNA function through protein stability. *Nature cell biology* **8,** 1359–1368 (2006).

80. Eldredge, E. R. *et al.* Activation of c-fos gene expression by a kinase-deficient epidermal growth factor receptor. *Molecular and Cellular Biology* **14,** 7527–7534 (1994).

81. Lin, S. Y. *et al.* Nuclear localization of EGF receptor and its potential new role as a transcription factor. *Nature cell biology* **3,** 802–808 (2001).

82. Lo, H.-W. *et al.* Nuclear interaction of EGFR and STAT3 in the activation of the iNOS/NO pathway. *Cancer cell* **7,** 575–589 (2005).

83. Han, W., Carpenter, R. L., Cao, X. & Lo, H.-W. STAT1 gene expression is enhanced by nuclear EGFR and HER2 via cooperation with STAT3. *Molecular carcinogenesis* **52,** 959–969 (2013).

84. Hung, L.-Y. *et al.* Nuclear epidermal growth factor receptor (EGFR) interacts with signal transducer and activator of transcription 5 (STAT5) in activating Aurora-A gene expression. *Nucleic acids research* **36,** 4337–4351 (2008).

85. Jaganathan, S. *et al.* A functional nuclear epidermal growth factor receptor, SRC and Stat3 heteromeric complex in pancreatic cancer cells. *PloS one* **6,** e19605 (2011).

86. Lo, H.-W., Cao, X., Zhu, H. & Ali-Osman, F. Cyclooxygenase-2 is a novel transcriptional target of the nuclear EGFR-STAT3 and EGFRvIII-STAT3 signaling axes. *Molecular cancer research : MCR* **8,** 232–245 (2010).

87. Dittmann, K. *et al.* Nuclear EGFR renders cells radio-resistant by binding mRNA species and triggering a metabolic switch to increase lactate production. *Radiotherapy and oncology : journal of the European Society for Therapeutic Radiology and Oncology* **116,** 431–437 (2015).

88. Chang, Y.-S. *et al.* EGF Receptor Promotes Prostate Cancer Bone Metastasis by Downregulating miR-1 and Activating TWIST1. *Cancer research* **75,** 3077–3086 (2015).

89. Huang, W.-C. *et al.* Nuclear translocation of epidermal growth factor receptor by Akt-dependent phosphorylation enhances breast cancer-resistant protein expression in gefitinib-resistant cells. *The Journal of biological chemistry* **286,** 20558–20568 (2011).

90. Lo, H.-W. *et al.* Novel prognostic value of nuclear epidermal growth factor receptor in breast cancer. *Cancer research* **65,** 338–348 (2005).

91. Huo, L. *et al.* RNA helicase A is a DNA-binding partner for EGFR-mediated transcriptional activation in the nucleus. *Proceedings of the National Academy of Sciences of the United States of America* **107,** 16125–16130 (2010).

92. Bitler, B. G., Goverdhan, A. & Schroeder, J. A. MUC1 regulates nuclear localization and function of the epidermal growth factor receptor. *Journal of cell science* **123,** 1716–1723 (2010).

93. Dittmann, K. *et al.* Radiation-induced epidermal growth factor receptor nuclear import is linked to activation of DNA-dependent protein kinase. *The Journal of biological chemistry* **280,** 31182–31189 (2005).

94. Dittmann, K., Mayer, C. & Rodemann, H.-P. Inhibition of radiation-induced EGFR nuclear import by C225 (Cetuximab) suppresses DNA-PK activity. *Radiotherapy and oncology : journal of the European Society for Therapeutic Radiology and Oncology* **76,** 157–161.

95. Dittmann, K., Mayer, C., Kehlbach, R. & Rodemann, H. P. The radioprotector Bowman–Birk proteinase inhibitor stimulates DNA repair via epidermal growth factor receptor phosphorylation and nuclear transport. *Radiotherapy and oncology : journal of the European Society for Therapeutic Radiology and Oncology* **86,** 375–382.

96. Yu, Y.-L. *et al.* Nuclear EGFR Suppresses Ribonuclease Activity of Polynucleotide Phosphorylase through DNAPK-mediated Phosphorylation at Serine 776. *Journal of Biological Chemistry* **287,** 31015–31026 (2012).

97. Yu, Y.-L. *et al.* Nuclear EGFR suppresses ribonuclease activity of polynucleotide phosphorylase through DNAPK-mediated phosphorylation at serine 776. *The Journal of biological chemistry* **287,** 31015–31026 (2012).

98. Kuo, H.-Y. *et al.* The PML isoform IV is a negative regulator of nuclear EGFR's transcriptional activity in lung cancer. *Carcinogenesis* **34,** 1708–1716 (2013).

99. Barrette-Ng, I. H., Wu, S. C., Tjia, W. M., Wong, S. L. & Ng, K. K. S. The structure of the SBP-Tag-streptavidin complex reveals a novel helical scaffold bridging binding pockets on separate subunits. *Acta crystallographica. Section D, Biological crystallography* **69,** 879–887 (2013).

100. Laemmli, U. K. Cleavage of structural proteins during the assembly of the head of bacteriophage T4. *Nature* **227,** 680–685 (1970).

101. Bradford, M. M. A rapid and sensitive method for the quantitation of microgram quantities of protein utilizing the principle of protein-dye binding. *Analytical biochemistry* **72,** 248–254 (1976).

102. Macia, E., Paris, S. & Chabre, M. Binding of the PH and Polybasic C-Terminal Domains of ARNO to Phosphoinositides and to Acidic Lipids. *Biochemistry* **39,** 5893–5901 (2000).

103. Bilkova, E. *et al.* Calcium Directly Regulates Phosphatidylinositol 4,5-Bisphosphate Headgroup Conformation and Recognition. *Journal of the American Chemical Society* (2017).

104. Avery, J. *et al.* A cell-free system for regulated exocytosis in PC12 cells. *The Journal of cell biology* **148,** 317–324 (2000).

105. Wu, M. *et al.* Coupling between clathrin-dependent endocytic budding and F-BAR-dependent tubulation in a cell-free system. *Nature cell biology* **12,** 902–908 (2010).

106. Park, Y. *et al.* Synaptotagmin-1 binds to PIP(2)-containing membrane but not to SNAREs at physiological ionic strength. *Nature structural & molecular biology* **22,** 815–823 (2015).

107. Klarlund, J. K., Tsiaras, W., Holik, J. J., Chawla, A. & Czech, M. P. Distinct polyphosphoinositide binding selectivities for pleckstrin homology domains of GRP1-like proteins based on diglycine versus triglycine motifs. *The Journal of biological chemistry* **275,** 32816–32821 (2000).

108. Bettio, M. Membrane-model systems to study EGFR-ARNO interaction.

109. Benjamin Felix Crispin Weiche. Biochemical and structural studies of the interaction between ARNO and the Epidermal Growth Factor Receptor.

110. Baker, M. Reproducibility crisis. Blame it on the antibodies. *Nature* **521,** 274–276 (2015).

111. Weller, M. G. Quality Issues of Research Antibodies. *Analytical Chemistry Insights* **11,** ACI.S31614 (2016).

112. La Voskuil, J. The challenges with the validation of research antibodies. *F1000Research* **6,** 161 (2017).

113. Sieber, J. J., Willig, K. I., Heintzmann, R., Hell, S. W. & Lang, T. The SNARE Motif Is Essential for the Formation of Syntaxin Clusters in the Plasma Membrane. *Biophysical journal* **90,** 2843–2851 (2006).

114. Adler, J. & Parmryd, I. Quantifying colocalization by correlation: the Pearson correlation coefficient is superior to the Mander's overlap coefficient. *Cytometry. Part A : the journal of the International Society for Analytical Cytology* **77,** 733–742 (2010).

115. Dunn, K. W., Kamocka, M. M. & McDonald, J. H. A practical guide to evaluating colocalization in biological microscopy. *American journal of physiology. Cell physiology* **300,** C723-42 (2011).

116. McDonald, J. H. & Dunn, K. W. Statistical tests for measures of colocalization in biological microscopy. *Journal of microscopy* **252,** 295–302 (2013).

117. Willig, K. I. *et al.* Nanoscale resolution in GFP-based microscopy. *Nature methods* **3,** 721–723 (2006).

118. Abulrob, A. *et al.* Nanoscale imaging of epidermal growth factor receptor clustering: effects of inhibitors. *The Journal of biological chemistry* **285,** 3145–3156 (2010).

119. Honigmann, A. *et al.* Phosphatidylinositol 4,5-bisphosphate clusters act as molecular beacons for vesicle recruitment. *Nature structural & molecular biology* **20,** 679–686 (2013).

120. KOOPMANS, L. H., OWEN, D. B. & ROSENBLATT, J. I. Confidence intervals for the coefficient of variation for the normal and log normal distributions. *Biometrika* **51,** 25–32 (1964).

121. Zhu, W. *et al.* Interleukin receptor activates a MYD88-ARNO-ARF6 cascade to disrupt vascular stability. *Nature* **492,** 252–255 (2012).

122. Jayaram, B. & Kowluru, A. Phagocytic NADPH oxidase links ARNO-Arf6 signaling pathway in glucose-stimulated insulin secretion from the pancreatic beta-cell. *Cellular physiology and biochemistry : international journal of experimental cellular physiology, biochemistry, and pharmacology* **30,** 1351–1362 (2012).

123. Capuani, F. *et al.* Quantitative analysis reveals how EGFR activation and downregulation are coupled in normal but not in cancer cells. *Nature communications* **6,** 7999 (2015).

124. Kirisits, A., Pils, D. & Krainer, M. Epidermal growth factor receptor degradation: an alternative view of oncogenic pathways. *The international journal of biochemistry & cell biology* **39,** 2173–2182 (2007).

125. Han, W. & Lo, H.-W. Landscape of EGFR signaling network in human cancers: biology and therapeutic response in relation to receptor subcellular locations. *Cancer letters* **318,** 124–134 (2012).

126. Hsu, S.-C. & Hung, M.-C. Characterization of a novel tripartite nuclear localization sequence in the EGFR family. *The Journal of biological chemistry* **282,** 10432–10440 (2007).

127. Hanson, D. A. & Ziegler, S. F. Fusion of green fluorescent protein to the C-terminus of granulysin alters its intracellular localization in comparison to the native molecule. *Journal of negative results in biomedicine* **3,** 2 (2004).

128. Wang, Y.-N. *et al.* The translocon Sec61beta localized in the inner nuclear membrane transports membrane-embedded EGF receptor to the nucleus. *The Journal of biological chemistry* **285,** 38720–38729 (2010).

129. Lo, H.-W. *et al.* Nuclear-cytoplasmic transport of EGFR involves receptor endocytosis, importin beta1 and CRM1. *Journal of cellular biochemistry* **98,** 1570–1583 (2006).

130. Soderholm, J. F. *et al.* Importazole, a small molecule inhibitor of the transport receptor importin-beta. *ACS chemical biology* **6,** 700–708 (2011).

131. Kublun, I., Ehm, P., Brehm, M. A. & Nalaskowski, M. M. Efficacious inhibition of Importin alpha/beta-mediated nuclear import of human inositol phosphate multikinase. *Biochimie* **102,** 117–123 (2014).

132. Cherfils, J. Arf GTPases and their effectors. Assembling multivalent membrane-binding platforms. *Current opinion in structural biology* **29,** 67–76 (2014).

133. D'Souza-Schorey, C. & Chavrier, P. ARF proteins. Roles in membrane traffic and beyond. *Nature reviews. Molecular cell biology* **7,** 347–358 (2006).

134. Li, C.-C. *et al.* ARL4D recruits cytohesin-2/ARNO to modulate actin remodeling. *Molecular biology of the cell* **18,** 4420–4437 (2007).

135. Torii, T. *et al.* Arf6 guanine nucleotide exchange factor cytohesin-2 binds to CCDC120 and is transported along neurites to mediate neurite growth. *The Journal of biological chemistry* **289,** 33887–33903 (2014).

136. Lim, J., Zhou, M., Veenstra, T. D. & Morrison, D. K. The CNK1 scaffold binds cytohesins and promotes insulin pathway signaling. *Genes & development* **24,** 1496–1506 (2010).

137. Lee, S., Wurtzel, J. G. T. & Goldfinger, L. E. The RLIP76 N-terminus binds ARNO to regulate PI 3-kinase, Arf6 and Rac signaling, cell spreading and migration. *Biochemical and biophysical research communications* **454,** 560–565 (2014).

138. Mansour, M., Lee, S. Y. & Pohajdak, B. The N-terminal coiled coil domain of the cytohesin/ARNO family of guanine nucleotide exchange factors interacts with the scaffolding protein CASP. *The Journal of biological chemistry* **277,** 32302–32309 (2002).

139. DiNitto, J. P., Lee, M.-T., Malaby, A. W. & Lambright, D. G. Specificity and Membrane Partitioning of Grsp1 Signaling Complexes with Grp1 Family ARF Exchange Factors. *Biochemistry* **49,** 6083–6092 (2010).

140. Rizzuto, R. & Pozzan, T. Microdomains of intracellular Ca2+. Molecular determinants and functional consequences. *Physiological reviews* **86,** 369–408 (2006).

141. Choi, S., Thapa, N., Tan, X., Hedman, A. C. & Anderson, R. A. PIP kinases define PI4,5P(2) signaling specificity by association with effectors. *Biochimica et biophysica acta* **1851,** 711–723 (2015).

142. Suh, B.-C. & Hille, B. Electrostatic interaction of internal Mg2+ with membrane PIP2 Seen with KCNQ K+ channels. *The Journal of general physiology* **130,** 241–256 (2007).

143. Kang, J. K. *et al.* Increased intracellular Ca2+ concentrations prevent membrane localization of PH domains through the formation of Ca2+-phosphoinositides. *Proceedings of the National Academy of Sciences* **114,** 11926–11931 (2017).

144. Lee, S. Y. & Pohajdak, B. N-terminal targeting of guanine nucleotide exchange factors (GEF) for ADP ribosylation factors (ARF) to the Golgi. *Journal of cell science* **113 (Pt 11),** 1883–1889 (2000).

145. Katz, A. K., Glusker, J. P., Beebe, S. A. & Bock, C. W. Calcium Ion Coordination. A Comparison with That of Beryllium, Magnesium, and Zinc. *Journal of the American Chemical Society* **118,** 5752–5763 (1996).

146. Batoulis, H. *et al.* Concentration Dependent Ion-Protein Interaction Patterns Underlying Protein Oligomerization Behaviours. *Scientific reports* **6,** 24131 (2016).

147. Wang, J. *et al.* Lateral sequestration of phosphatidylinositol 4,5-bisphosphate by the basic effector domain of myristoylated alanine-rich C kinase substrate is due to nonspecific electrostatic interactions. *The Journal of biological chemistry* **277,** 34401–34412 (2002).

148. Rauch, M. E., Ferguson, C. G., Prestwich, G. D. & Cafiso, D. S. Myristoylated alanine-rich C kinase substrate (MARCKS) sequesters spin-labeled phosphatidylinositol 4,5-bisphosphate in lipid bilayers. *The Journal of biological chemistry* **277,** 14068–14076 (2002).

149. Alli, A. A. *et al.* Calmodulin and CaMKII modulate ENaC activity by regulating the association of MARCKS and the cytoskeleton with the apical membrane. *American journal of physiology. Renal physiology* **309,** F456-63 (2015).

150. Knudsen, S. L. J., Mac, A. S. W., Henriksen, L., van Deurs, B. & Grovdal, L. M. EGFR signaling patterns are regulated by its different ligands. *Growth factors (Chur, Switzerland)* **32,** 155–163 (2014).

151. Alberts, B., Wilson, J. & Hunt, T. *Molecular biology of the cell* (Garland Science, New York, 2008).

152. Sanchez-Gonzalez, P., Jellali, K. & Villalobo, A. Calmodulin-mediated regulation of the epidermal growth factor receptor. *The FEBS journal* **277,** 327–342 (2010).

153. Dagher, R. *et al.* A general strategy to characterize calmodulin-calcium complexes involved in CaM-target recognition. DAPK and EGFR calmodulin binding domains interact with different calmodulin-calcium complexes. *Biochimica et biophysica acta* **1813,** 1059–1067 (2011).

154. Gurevich, V. V. & Gurevich, E. V. Molecular Mechanisms of GPCR Signaling. A Structural Perspective. *International journal of molecular sciences* **18** (2017).

155. Manglik, A. & Kruse, A. C. Structural Basis for G Protein-Coupled Receptor Activation. *Biochemistry* **56,** 5628–5634 (2017).

156. Dong, C. *et al.* ADP-ribosylation factors modulate the cell surface transport of G protein-coupled receptors. *The Journal of pharmacology and experimental therapeutics* **333,** 174–183 (2010).

157. Anborgh, P. H., Seachrist, J. L., Dale, L. B. & Ferguson, S. S. Receptor/beta-arrestin complex formation and the differential trafficking and resensitization of beta2-adrenergic and angiotensin II type 1A receptors. *Molecular endocrinology (Baltimore, Md.)* **14,** 2040–2053 (2000).

158. Dong, C. & Wu, G. G-protein-coupled receptor interaction with small GTPases. *Methods in enzymology* **522,** 97–108 (2013).

159. Esseltine, J. L. & Ferguson, S. S. Regulation of G protein-coupled receptor trafficking and signaling by Rab GTPases. *Small GTPases* **4,** 132–135 (2013).

160. Mitchell, R. *et al.* Rhodopsin-family receptors associate with small G proteins to activate phospholipase D. *Nature* **392,** 411–414 (1998).

161. Shukla, A. K. *et al.* Visualization of arrestin recruitment by a G-protein-coupled receptor. *Nature* **512,** 218–222 (2014).

162. Claing, A. *et al.* beta-Arrestin-mediated ADP-ribosylation factor 6 activation and beta 2-adrenergic receptor endocytosis. *The Journal of biological chemistry* **276,** 42509–42513 (2001).

163. Mukherjee, S. *et al.* The ADP ribosylation factor nucleotide exchange factor ARNO promotes beta-arrestin release necessary for luteinizing hormone/choriogonadotropin receptor desensitization. *Proceedings of the National Academy of Sciences of the United States of America* **97,** 5901–5906 (2000).

164. Kahn, R. A. Is the model of signal amplification by GPCRs/GEFs activating multiple GTPases relevant to a broad spectrum of heterotrimeric and RAS superfamily GTPases? *Cellular logistics* **4,** e943602 (2014).

165. Liebmann, C. EGF receptor activation by GPCRs. An universal pathway reveals different versions. *Molecular and cellular endocrinology* **331,** 222–231 (2011).

166. Moody, T. W., Nuche-Berenguer, B., Nakamura, T. & Jensen, R. T. EGFR Transactivation by Peptide G Protein-Coupled Receptors in Cancer. *Current drug targets* **17,** 520–528 (2016).

167. Overland, A. C. & Insel, P. A. Heterotrimeric G proteins directly regulate MMP14/membrane type-1 matrix metalloprotease. A novel mechanism for GPCR-EGFR transactivation. *The Journal of biological chemistry* **290,** 9941–9947 (2015).

168. Wang, Z. Transactivation of Epidermal Growth Factor Receptor by G Protein-Coupled Receptors. Recent Progress, Challenges and Future Research. *International journal of molecular sciences* **17** (2016).

169. La Bernardino de Serna, J., Schutz, G. J., Eggeling, C. & Cebecauer, M. There Is No Simple Model of the Plasma Membrane Organization. *Frontiers in cell and developmental biology* **4,** 106 (2016).

170. Singer, S. J. & Nicolson, G. L. The fluid mosaic model of the structure of cell membranes. *Science (New York, N.Y.)* **175,** 720–731 (1972).

171. Sheetz, M. P., Schindler, M. & Koppel, D. E. Lateral mobility of integral membrane proteins is increased in spherocytic erythrocytes. *Nature* **285,** 510–511 (1980).

172. Sako, Y. & Kusumi, A. Compartmentalized structure of the plasma membrane for receptor movements as revealed by a nanometer-level motion analysis. *The Journal of cell biology* **125,** 1251–1264 (1994).

173. Kusumi, A., Ike, H., Nakada, C., Murase, K. & Fujiwara, T. Single-molecule tracking of membrane molecules. Plasma membrane compartmentalization and dynamic assembly of raft-philic signaling molecules. *Seminars in immunology* **17,** 3–21 (2005).

174. van Meer, G. & Simons, K. Viruses budding from either the apical or the basolateral plasma membrane domain of MDCK cells have unique phospholipid compositions. *The EMBO journal* **1,** 847–852 (1982).

175. Skwarek, M. Recent controversy surrounding lipid rafts. *Archivum immunologiae et therapiae experimentalis* **52,** 427–431 (2004).

176. Ilangumaran, S. & Hoessli, D. C. Effects of cholesterol depletion by cyclodextrin on the sphingolipid microdomains of the plasma membrane. *The Biochemical journal* **335 (Pt 2),** 433–440 (1998).

177. Destainville, N. Cluster phases of membrane proteins. *Physical review. E, Statistical, nonlinear, and soft matter physics* **77,** 11905 (2008).

178. Temburni, M. K., Rosenberg, M. M., Pathak, N., McConnell, R. & Jacob, M. H. Neuronal nicotinic synapse assembly requires the adenomatous polyposis coli tumor suppressor protein. *The Journal of neuroscience : the official journal of the Society for Neuroscience* **24,** 6776–6784 (2004).

179. MacDonald, L., Baldini, G. & Storrie, B. Does Super Resolution Fluorescence Microscopy Obsolete Previous Microscopic Approaches to Protein Co-localization? *Methods in molecular biology (Clifton, N.J.)* **1270,** 255–275 (2015).

180. van den Bogaart, G. *et al.* Membrane protein sequestering by ionic protein-lipid interactions. *Nature* **479,** 552–555 (2011).

181. Burkhard, P., Stetefeld, J. & Strelkov, S. V. Coiled coils. A highly versatile protein folding motif. *Trends in cell biology* **11,** 82–88 (2001).

182. Merklinger, E. *et al.* The packing density of a supramolecular membrane protein cluster is controlled by cytoplasmic interactions. *eLife* **6** (2017).

183. Costa, M. N., Radhakrishnan, K. & Edwards, J. S. Monte Carlo simulations of plasma membrane corral-induced EGFR clustering. *Journal of biotechnology* **151,** 10.1016/j.jbiotec.2010.12.009 (2010).

184. Lang, T. & Rizzoli, S. O. Membrane protein clusters at nanoscale resolution. More than pretty pictures. *Physiology (Bethesda, Md.)* **25,** 116–124 (2010).

185. Abe, N., Inoue, T., Galvez, T., Klein, L. & Meyer, T. Dissecting the role of PtdIns(4,5)P2 in endocytosis and recycling of the transferrin receptor. *Journal of cell science* **121,** 1488–1494 (2008).

186. Boulakirba, S. *et al.* Arf6 exchange factor EFA6 and endophilin directly interact at the plasma membrane to control clathrin-mediated endocytosis. *Proceedings of the National Academy of Sciences of the United States of America* **111,** 9473–9478 (2014).

187. Padron, D., Tall, R. D. & Roth, M. G. Phospholipase D2 is required for efficient endocytic recycling of transferrin receptors. *Molecular biology of the cell* **17,** 598–606 (2006).

188. Termini, C. M. *et al.* The membrane scaffold CD82 regulates cell adhesion by altering alpha4 integrin stability and molecular density. *Molecular biology of the cell* **25,** 1560–1573 (2014).

189. Clayton, A. H. A. *et al.* Ligand-induced dimer-tetramer transition during the activation of the cell surface epidermal growth factor receptor-A multidimensional microscopy analysis. *The Journal of biological chemistry* **280,** 30392–30399 (2005).

190. Saffarian, S., Li, Y., Elson, E. L. & Pike, L. J. Oligomerization of the EGF receptor investigated by live cell fluorescence intensity distribution analysis. *Biophysical journal* **93,** 1021–1031 (2007).

191. Jia, C., Zhou, Z., Liu, R., Chen, S. & Xia, R. EGF receptor clustering is induced by a 0.4 mT power frequency magnetic field and blocked by the EGF receptor tyrosine kinase inhibitor PD153035. *Bioelectromagnetics* **28,** 197–207 (2007).

192. Batzer, A. G., Rotin, D., Ureña, J. M., Skolnik, E. Y. & Schlessinger, J. Hierarchy of binding sites for Grb2 and Shc on the epidermal growth factor receptor. *Molecular and Cellular Biology* **14,** 5192–5201 (1994).

193. Bi, X., Schmitz, A., Hayallah, A. M., Song, J.-N. & Famulok, M. Affinity-based labeling of cytohesins with a bifunctional SecinH3 photoaffinity probe. *Angewandte Chemie (International ed. in English)* **47,** 9565–9568 (2008).

194. Hahn, I. *et al.* The Drosophila Arf GEF Steppke controls MAPK activation in EGFR signaling. *Journal of cell science* **126,** 2470–2479 (2013).

195. Kitano, J. *et al.* Tamalin, a PDZ domain-containing protein, links a protein complex formation of group 1 metabotropic glutamate receptors and the guanine nucleotide exchange factor cytohesins. *The Journal of neuroscience : the official journal of the Society for Neuroscience* **22,** 1280–1289 (2002).

196. Li, J. *et al.* Grp1 plays a key role in linking insulin signaling to glut4 recycling. *Developmental cell* **22,** 1286–1298 (2012).

197. Tehrani, N. *et al.* The Insulin/IGF Signaling Regulators Cytohesin/GRP-1 and PIP5K/PPK-1 Modulate Susceptibility to Excitotoxicity in C. elegans. *PloS one* **9,** e113060 (2014).

7 Appendix

7.1 Protein Sequences

7.1.1 ARNO-GFP

MGSHHHHHHENLYFQGSMEDGVYEPPDLTPEERMELENIRRRKQELLVEIQRL
REELSEAMSEVEGLEANEGSKTLQRNRKMAMGRKKFNMDPKKGIQFLVENEL
LQNTPEEIARFLYKGEGLNKTAIGDYLGEREELNLAVLHAFVDLHEFTDLNLVQ
ALRQFLWSFRLPGEAQKIDRMMEAFAQRYCLCNPGVFQSTDTCYVLSFAVIML
NTSLHNPNVRDKPGLERFVAMNRGINEGGDLPEELLRNLYDSIRNEPFKIPEDD
GNDLTHTFFNPDREGWLLKLGGGRVKTWKRRWFILTDNCLYYFEYTTDKEPR
GIIPLENLSIREVDDPRKPNCFELYIPNNKGQLIKACKTEADGRVVEGNHMVYRI
SAPTQEEKDEWIKSIQAAVSVDPFYEMLAARKKRISVKKKQEQPMVSKGEELFT
GVVPILVELDGDVNGHKFSVSGEGEGDATYGKLTLKFICTTGKLPVPWPTLVTT
LTYGVQCFSRYPDHMKQHDFFKSAMPEGYVQERTIFFKDDGNYKTRAEVKFE
GDTLVNRIELKGIDFKEDGNILGHKLEYNYNSHNVYIMADKQKNGIKVNFKIRH
NIEDGSVQLADHYQQNTPIGDGPVLLPDNHYLSTQSKLSKDPNEKRDHMVLLE
FVTAAGITLGMDELYK*

7.1.2 PH-GFP

MGSHHHHHHENLYFQGSGSDREGWLLKLGGGRVKTWKRRWFILTDNCLYYF
EYTTDKEPRGIIPLENLSIREVDDPRKPNCFELYIPNNKGQLIKACKTEADGRVV
EGNHMVYRISAPTQEEKDEWIKSIQAAVSVDPFYEMVSKGEELFTGVVPILVEL
DGDVNGHKFSVSGEGEGDATYGKLTLKFICTTGKLPVPWPTLVTTLTYGVQCF
SRYPDHMKQHDFFKSAMPEGYVQERTIFFKDDGNYKTRAEVKFEGDTLVNRIE
LKGIDFKEDGNILGHKLEYNYNSHNVYIMADKQKNGIKVNFKIRHNIEDGSVQL
ADHYQQNTPIGDGPVLLPDNHYLSTQSKLSKDPNEKRDHMVLLEFVTAAGITL
GMDELYK*

7.1.3 Sec7-PH-GFP

MGSHHHHHHENLYFQGSRNRKMAMGRKKFNMDPKKGIQFLVENELLQNTPEE
IARFLYKGEGLNKTAIGDYLGEREELNLAVLHAFVDLHEFTDLNLVQALRQFL
WSFRLPGEAQKIDRMMEAFAQRYCLCNPGVFQSTDTCYVLSFAVIMLNTSLHN
PNVRDKPGLERFVAMNRGINEGGDLPEELLRNLYDSIRNEPFKIPEDDGNDLTH
TFFNPDREGWLLKLGGGRVKTWKRRWFILTDNCLYYFEYTTDKEPRGIIPLENL
SIREVDDPRKPNCFELYIPNNKGQLIKACKTEADGRVVEGNHMVYRISAPTQEE
KDEWIKSIQAAVSVDPFYEMVSKGEELFTGVVPILVELDGDVNGHKFSVSGEGE
GDATYGKLTLKFICTTGKLPVPWPTLVTTLTYGVQCFSRYPDHMKQHDFFKSA
MPEGYVQERTIFFKDDGNYKTRAEVKFEGDTLVNRIELKGIDFKEDGNILGHKL
EYNYNSHNVYIMADKQKNGIKVNFKIRHNIEDGSVQLADHYQQNTPIGDGPVL
LPDNHYLSTQSKLSKDPNEKRDHMVLLEFVTAAGITLGMDELYK*

7.1.4 ΔCC-GFP

MGSHHHHHHENLYFQGSRNRKMAMGRKKFNMDPKKGIQFLVENELLQNTPEE
IARFLYKGEGLNKTAIGDYLGEREELNLAVLHAFVDLHEFTDLNLVQALRQFL
WSFRLPGEAQKIDRMMEAFAQRYCLCNPGVFQSTDTCYVLSFAVIMLNTSLHN

PNVRDKPGLERFVAMNRGINEGGDLPEELLRNLYDSIRNEPFKIPEDDGNDLTH
TFFNPDREGWLLKLGGGRVKTWKRRWFILTDNCLYYFEYTTDKEPRGIIPLENL
SIREVDDPRKPNCFELYIPNNKGQLIKACKTEADGRVVEGNHMVYRISAPTQEE
KDEWIKSIQAAVSVDPFYEMLAARKKRISVKKKQEQPMVSKGEELFTGVVPILV
ELDGDVNGHKFSVSGEGEGDATYGKLTLKFICTTGKLPVPWPTLVTTLTYGVQ
CFSRYPDHMKQHDFFKSAMPEGYVQERTIFFKDDGNYKTRAEVKFEGDTLVNR
IELKGIDFKEDGNILGHKLEYNYNSHNVYIMADKQKNGIKVNFKIRHNIEDGSV
QLADHYQQNTPIGDGPVLLPDNHYLSTQSKLSKDPNEKRDHMVLLEFVTAAGI
TLGMDELYK*

7.1.5 ΔPBR-GFP

MGSHHHHHHENLYFQGSMEDGVYEPPDLTPEERMELENIRRRKQELLVEIQRL
REELSEAMSEVEGLEANEGSKTLQRNRKMAMGRKKFNMDPKKGIQFLVENEL
LQNTPEEIARFLYKGEGLNKTAIGDYLGEREELNLAVLHAFVDLHEFTDLNLVQ
ALRQFLWSFRLPGEAQKIDRMMEAFAQRYCLCNPGVFQSTDTCYVLSFAVIML
NTSLHNPNVRDKPGLERFVAMNRGINEGGDLPEELLRNLYDSIRNEPFKIPEDD
GNDLTHTFFNPDREGWLLKLGGGRVKTWKRRWFILTDNCLYYFEYTTDKEPR
GIIPLENLSIREVDDPRKPNCFELYIPNNKGQLIKACKTEADGRVVEGNHMVYRI
SAPTQEEKDEWIKSIQAAVSVDPFYEMVSKGEELFTGVVPILVELDGDVNGHKF
SVSGEGEGDATYGKLTLKFICTTGKLPVPWPTLVTTLTYGVQCFSRYPDHMKQ
HDFFKSAMPEGYVQERTIFFKDDGNYKTRAEVKFEGDTLVNRIELKGIDFKEDG
NILGHKLEYNYNSHNVYIMADKQKNGIKVNFKIRHNIEDGSVQLADHYQQNTP
IGDGPVLLPDNHYLSTQSKLSKDPNEKRDHMVLLEFVTAAGITLGMDELYK*

7.1.6 Gn4Lz-Sec7-PH-GFP

MGSHHHHHHENLYFQGSRVKQLEDKVEELLSKNAHLENEVARLKKLRNRKM
AMGRKKFNMDPKKGIQFLVENELLQNTPEEIARFLYKGEGLNKTAIGDYLGER
EELNLAVLHAFVDLHEFTDLNLVQALRQFLWSFRLPGEAQKIDRMMEAFAQRY
CLCNPGVFQSTDTCYVLSFAVIMLNTSLHNPNVRDKPGLERFVAMNRGINEGG
DLPEELLRNLYDSIRNEPFKIPEDDGNDLTHTFFNPDREGWLLKLGGGRVKTWK
RRWFILTDNCLYYFEYTTDKEPRGIIPLENLSIREVDDPRKPNCFELYIPNNKGQL
IKACKTEADGRVVEGNHMVYRISAPTQEEKDEWIKSIQAAVSVDPFYEMVSKG
EELFTGVVPILVELDGDVNGHKFSVSGEGEGDATYGKLTLKFICTTGKLPVPWP
TLVTTLTYGVQCFSRYPDHMKQHDFFKSAMPEGYVQERTIFFKDDGNYKTRAE
VKFEGDTLVNRIELKGIDFKEDGNILGHKLEYNYNSHNVYIMADKQKNGIKVN
FKIRHNIEDGSVQLADHYQQNTPIGDGPVLLPDNHYLSTQSKLSKDPNEKRDHM
VLLEFVTAAGITLGMDELYK*

7.1.7 GST-PH-PBR-GFP

MGSHHHHHHENLYFQGSMSPILGYWKIKGLVQPTRLLLEYLEEKYEEHLYERD
EGDKWRNKKFELGLEFPNLPYYIDGDVKLTQSMAIIRYIADKHNMLGGCPKER
AEISMLEGAVLDIRYGVSRIAYSKDFETLKVDFLSKLPEMLKMFEDRLCHKTYL
NGDHVTHPDFMLYDALDVVLYMDPMCLDAFPKLVCFKKRIEAIPQIDKYLKSS
KYIAWPLQGWQATFGGGDHPPKSDEDDGNDLTHTFFNPDREGWLLKLGGGRV
KTWKRRWFILTDNCLYYFEYTTDKEPRGIIPLENLSIREVDDPRKPNCFELYIPN
NKGQLIKACKTEADGRVVEGNHMVYRISAPTQEEKDEWIKSIQAAVSVDPFYE
MLAARKKRISVKKKQEQPMVSKGEELFTGVVPILVELDGDVNGHKFSVSGEGE
GDATYGKLTLKFICTTGKLPVPWPTLVTTLTYGVQCFSRYPDHMKQHDFFKSA
MPEGYVQERTIFFKDDGNYKTRAEVKFEGDTLVNRIELKGIDFKEDGNILGHKL

EYNYNSHNVYIMADKQKNGIKVNFKIRHNIEDGSVQLADHYQQNTPIGDGPVL
LPDNHYLSTQSKLSKDPNEKRDHMVLLEFVTAAGITLGMDELYK*

7.1.8 SBP-PH

MDEKTTGWRGGHVVEGLAGELEQLRARLEHHPQGQREPSGENLYFQGSEFDR
EGWLLKLGGGRVKTWKRRWFILTDNCLYYFEYTTDKEPRGIIPLENLSIREVDD
PRKPNCFELYIPNNKGQLIKACKTEADGRVVEGNHMVYRISAPTQEEKDEWIKS
IQAAVSVDPFYEMLAA

7.1.9 SBP-ARNO

MDEKTTGWRGGHVVEGLAGELEQLRARLEHHPQGQREPSGENLYFQGSMEDG
VYEPPDLTPEERMELENIRRRKQELLVEIQRLREELSEAMSEVEGLEANEGSKTL
QRNRKMAMGRKKFNMDPKKGIQFLVENELLQNTPEEIARFLYKGEGLNKTAIG
DYLGEREELNLAVLHAFVDLHEFTDLNLVQALRQFLWSFRLPGEAQKIDRMME
AFAQRYCLCNPGVFQSTDTCYVLSFAVIMLNTSLHNPNVRDKPGLERFVAMNR
GINEGGDLPEELLRNLYDSIRNEPFKIPEDDGNDLTHTFFNPDREGWLLKLGGG
RVKTWKRRWFILTDNCLYYFEYTTDKEPRGIIPLENLSIREVDDPRKPNCFELYI
PNNKGQLIKACKTEADGRVVEGNHMVYRISAPTQEEKDEWIKSIQAAVSVDPF
YEMLAARKKRISVKKKQEQP

7.1.10 SBP-E156K

MDEKTTGWRGGHVVEGLAGELEQLRARLEHHPQGQREPSGENLYFQGSMEDG
VYEPPDLTPEERMELENIRRRKQELLVEIQRLREELSEAMSEVEGLEANEGSKTL
QRNRKMAMGRKKFNMDPKKGIQFLVENELLQNTPEEIARFLYKGEGLNKTAIG
DYLGEREELNLAVLHAFVDLHEFTDLNLVQALRQFLWSFRLPGKAQKIDRMM
EAFAQRYCLCNPGVFQSTDTCYVLSFAVIMLNTSLHNPNVRDKPGLERFVAMN
RGINEGGDLPEELLRNLYDSIRNEPFKIPEDDGNDLTHTFFNPDREGWLLKLGG
GRVKTWKRRWFILTDNCLYYFEYTTDKEPRGIIPLENLSIREVDDPRKPNCFELY
IPNNKGQLIKACKTEADGRVVEGNHMVYRISAPTQEEKDEWIKSIQAAVSVDPF
YEMLAARKKRISVKKKQEQP

7.1.11 SBP-R280C

MDEKTTGWRGGHVVEGLAGELEQLRARLEHHPQGQREPSGENLYFQGSMEDG
VYEPPDLTPEERMELENIRRRKQELLVEIQRLREELSEAMSEVEGLEANEGSKTL
QRNRKMAMGRKKFNMDPKKGIQFLVENELLQNTPEEIARFLYKGEGLNKTAIG
DYLGEREELNLAVLHAFVDLHEFTDLNLVQALRQFLWSFRLPGEAQKIDRMME
AFAQRYCLCNPGVFQSTDTCYVLSFAVIMLNTSLHNPNVRDKPGLERFVAMNR
GINEGGDLPEELLRNLYDSIRNEPFKIPEDDGNDLTHTFFNPDREGWLLKLGGG
RVKTWKRCWFILTDNCLYYFEYTTDKEPRGIIPLENLSIREVDDPRKPNCFELYI
PNNKGQLIKACKTEADGRVVEGNHMVYRISAPTQEEKDEWIKSIQAAVSVDPF
YEMLAARKKRISVKKKQEQP

7.1.12 SBP-Sec7

MDEKTTGWRGGHVVEGLAGELEQLRARLEHHPQGQREPSGENLYFQGSRNRK
MAMGRKKFNMDPKKGIQFLVENELLQNTPEEIARFLYKGEGLNKTAIGDYLGE
REELNLAVLHAFVDLHEFTDLNLVQALRQFLWSFRLPGEAQKIDRMMEAFAQR

YCLCNPGVFQSTDTCYVLSFAVIMLNTSLHNPNVRDKPGLERFVAMNRGINEG
GDLPEELLRNLYDSIRNEPFKIPED

7.2 Protein purification

7.2.1 SBP-tagged proteins

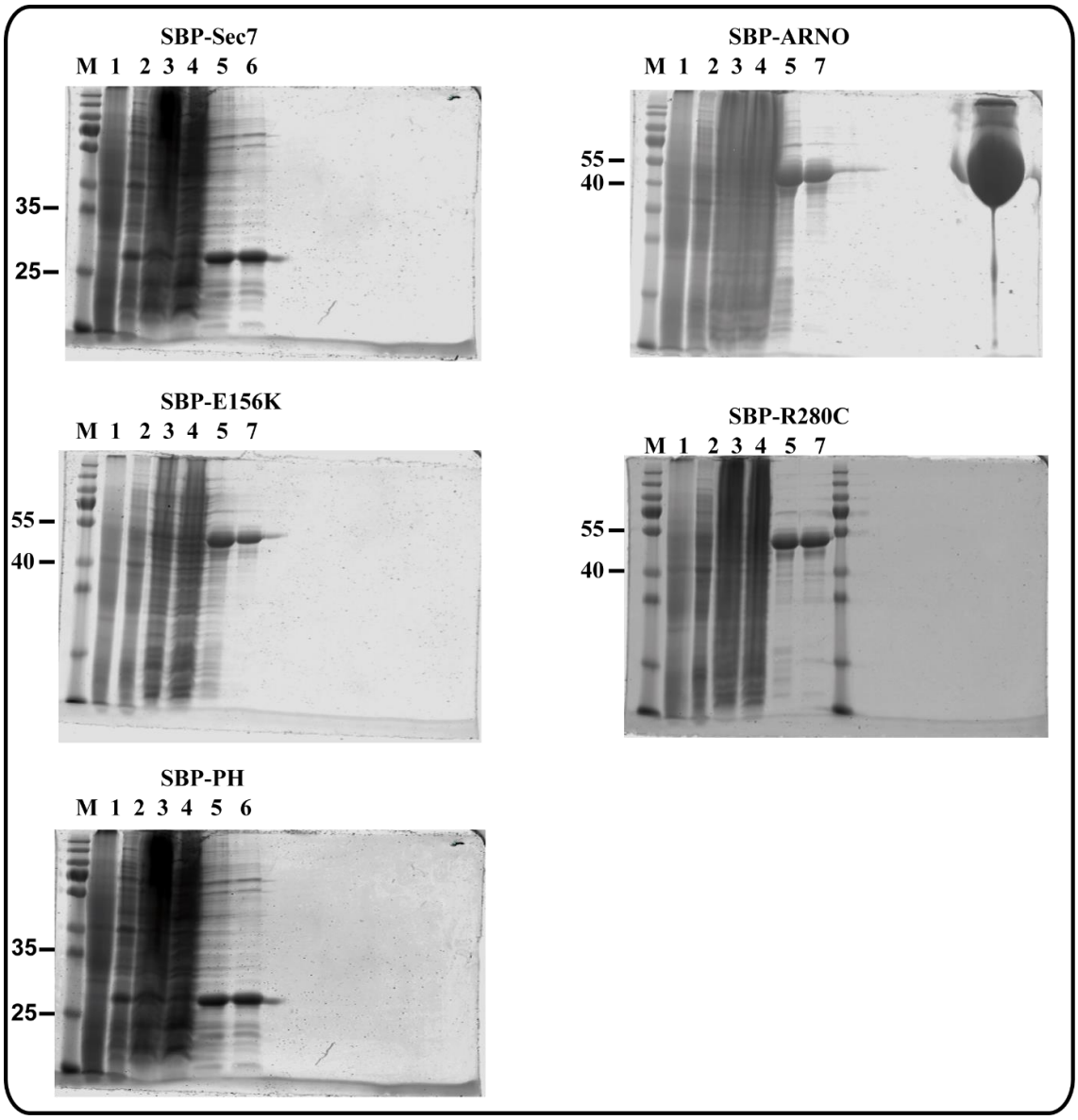

SI Figure 1: Coomassie gels of the purification process of the SBP-tagged proteins. *1: Before induction, 2: After induction, 3: Supernatant after lysis, 4: Supernatant after incubation with affinity beads, 5: Eluate, 6: Final sample, 7: Product after Gelfiltration. Expected MW: SBP-ARNO: 52 kDa, SBP-Sec7: 27 kDa, SBP-E156K: 52 kDa, SBP-R280C: 52 kDa, SBP-PH: 20,3 kDa.*

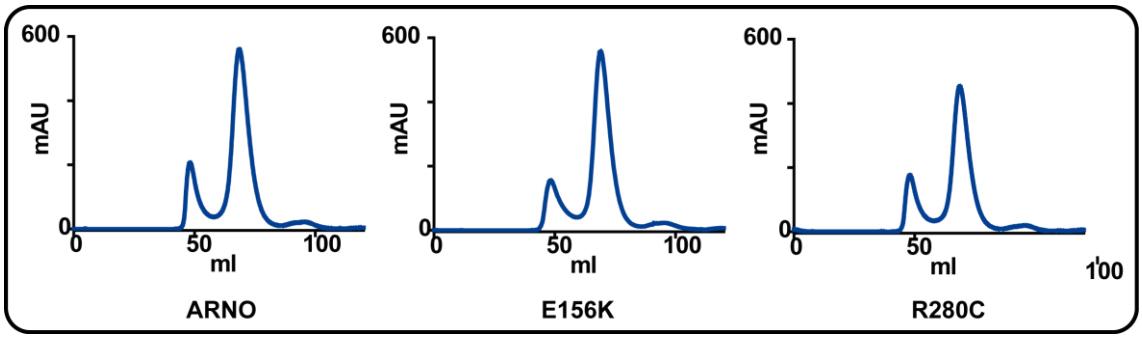

SI Figure 2: Gel filtration curves of SBP-tagged proteins.

7.2.2 GFP-tagged proteins

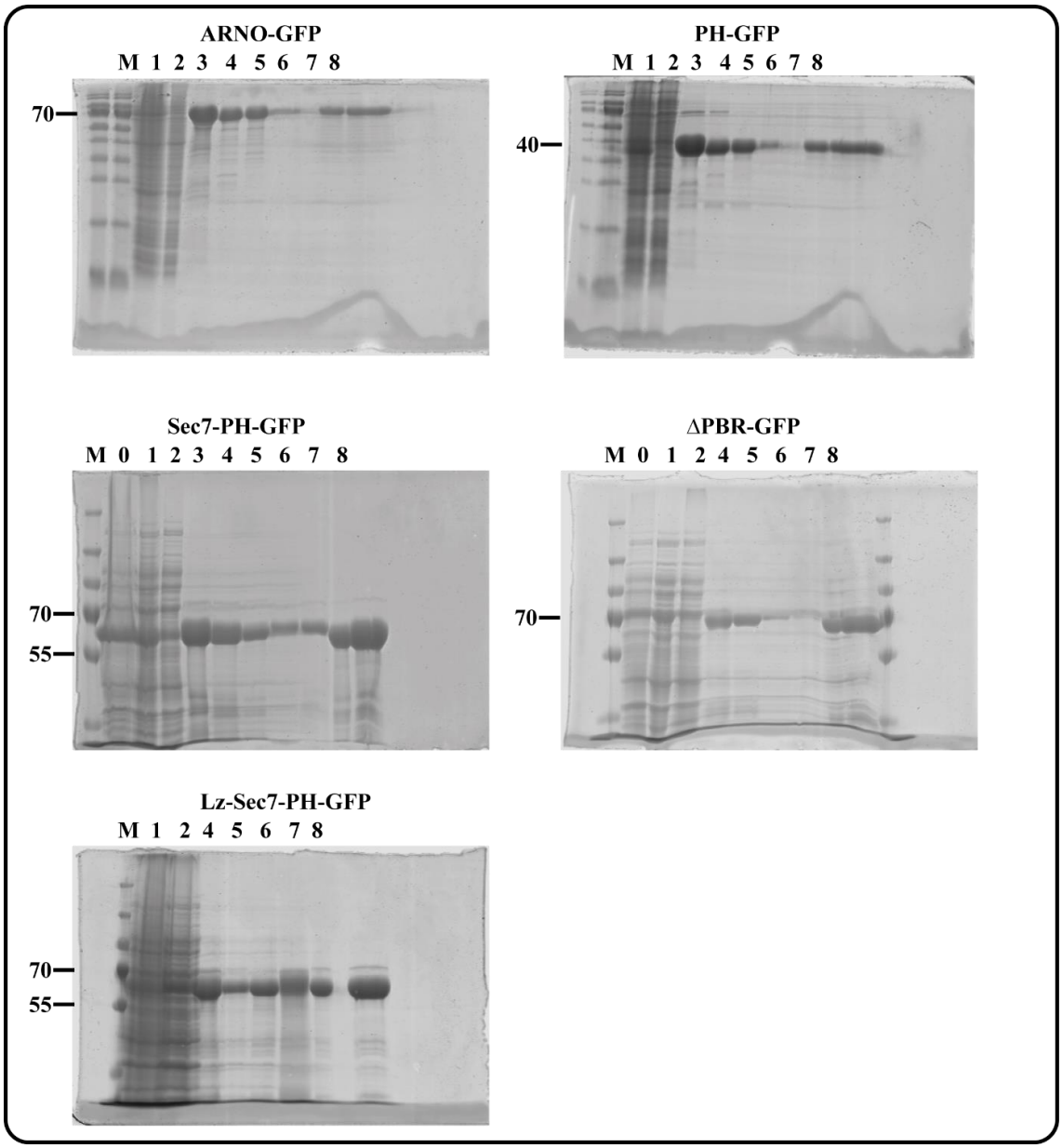

SI Figure 3: Coomassie gels for control of the purification of the GFP-tagged protein constructs. *: 0: After induction, 1: Supernatant after lysis, 2: Supernatant after incubation with affinity beads, 3: Eluate, 4: After TEV digest, 5: Flowthrough of rebinding column, 6: Wash fraction, 7: Eluate, 8: Final product after gelfiltration*

.Expected MW: ARNO-GFP: 75.5 kDa, PH-GFP: 43.4 kDa, Sec7-PH-GFP: 66.4 kDa, ΔPBR-GFP: 73.4 kDa, Lz-Sec7-PH-GFP: 69.8 kDa

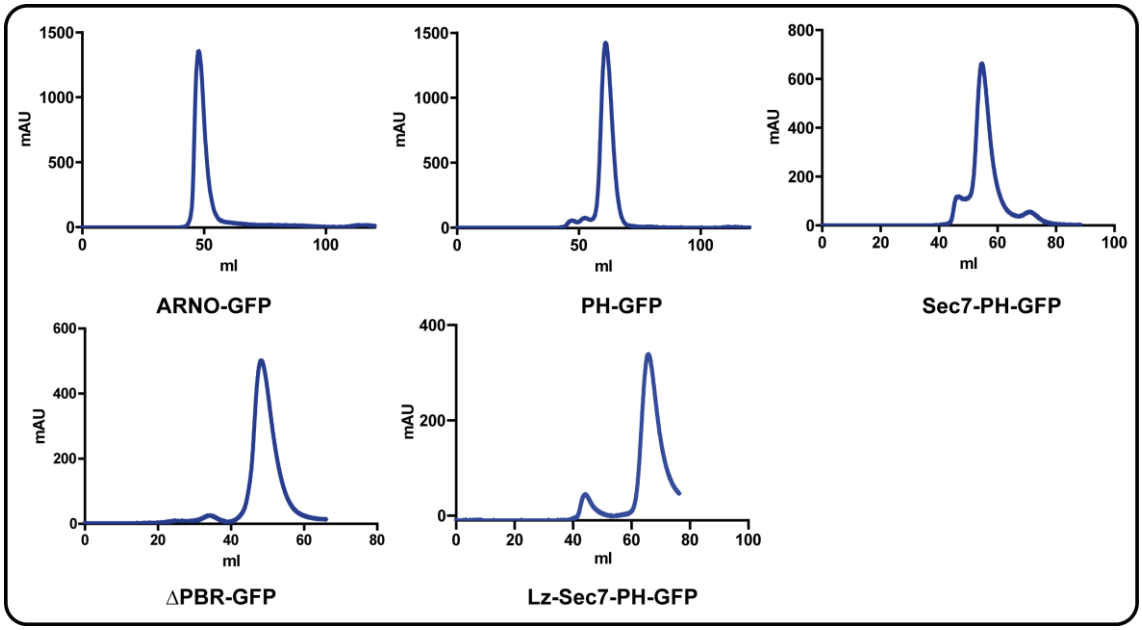

SI Figure 4: Gel filtration curves of GFP-tagged proteins.

7.3 Plasmid sequences

7.3.1 pGFP-PK

GCGGCCGCGATCTCTCGGCTGGACGAGCTGTACAGTACTCAGATCTCGAGC
TCAAGCTTCGAATTAATTCCCACGCTGCCATGGCAGACACCTTTCTGGAGCA
CATGTGCCGCCTGGACATCGACTCCGAGCCAACCATTGCCAGAAACACCGG
CATCATCTGCACCATCGGCCCAGCCTCCCGCTCTGTGGACAAGCTGAAGGA
AATGATTAAATCTGGAATGAATGTTGCCCGCCTCAACTTCTCGCACGGCACC
CACGAGTATCATGAGGGCACAATTAAGAACGTGCGAGAGGCCACAGAGAG
CTTTGCCTCTGACCCGATCACCTACAGACCTGTGGCTATTGCACTGGACACC
AAGGGACCTGAAATCCGAACTGGACTCATCAAGGGAAGTGGCACAGCAGA
GGTGGAGCTCAAGAAGGGCGCAGCTCTCAAAGTGACGCTGGACAATGCCTT
CATGGAGAACTGCGATGAGAATGTGCTGTGGGTGGACTACAAGAACCTCAT
CAAAGTTATAGATGTGGGCAGCAAAATCTATGTGGATGACGGTCTCATTTCC
TTGCTGGTTAAGGAGAAAGGCAAGGACTTTGTCATGACTGAGGTTGAGAAC
GGTGGCATGCTTGGTAGTAAGAAGGGAGTGAACCTCCCAGGTGCTGCGGTC
GACCTGCCTGCAGTCTCAGAGAAGGACATTCAGGACCTGAAATTTGGCGTG
GAGCAGAATGTGGACATGGTGTTCGCTTCCTTCATCCGCAAAGCTGCTGATG
TCCATGCTGTCAGGAAGGTGCTAGGGGAAAAGGGAAAGCACATCAAGATTA
TCAGCAAGATTGAGAATCACGAGGGTGTGCGCAGGTTTGATGAGATCATGG
AGGCCAGCGATGGCATTATGGTGGCCCGTGGTGACCTGGGTATTGAGATCC
CTGCTGAAAAAGTCTTCCTCGCACAGAAGATGATGATTGGGCGCTGCAACA
GGGCTGGCAAACCCATCATTTGTGCCACTCAGATGTTGGAAAGCATGATCA
AGAAACCTCGCCCGACCCGCGCTGAGGGCAGTGATGTTGCCAATGCAGTTC
TGGATGGAGCAGACTGCATCATGCTGTCTGGGGAGACCGCCAAGGGAGACT
ACCCACTGGAGGCTGTGCGCATGCAGCACGCTATTGCTCGTGAGGCTGAGG

CCGCAATGTTCCATCGTCAGCAGTTTGAAGAAATCTTACGCCACAGTGTACA
CCACAGGGAGCCTGCTGATGCCATGGCAGCAGGCGCGGTGGAGGCCTCCTT
TAAGTGCTTAGCAGCAGCTCTGATAGTTATGACCGAGTCTGGCAGGTCTGCA
CGCCTGGTGTCCCGGTACCGCGGGCCCGGGATCCACCGGATCTAGATAAAC
TGATCATATCAGCCTACCACTC

7.3.2 pGFP-EGFRJM-PK

ATGGTGAGCAAGGGCGAGGAGCTGTTCACCGGGGTGGTGCCCATCCTGGTC
GAGCTGGACGGCGACGTAAACGGCCACAAGTTCAGCGTGTCCGGCGAGGGC
GAGGGCGATGCCACCTACGGCAAGCTGACCCTGAAGTTCATCTGCACCACC
GGCAAGCTGCCCGTGCCCTGGCCCACCCTCGTGACCACCCTGACCTACGGC
GTGCAGTGCTTCAGCCGCTACCCCGACCACATGAAGCAGCACGACTTCTTCA
AGTCCGCCATGCCCGAAGGCTACGTCCAGGAGCGCACCATCTTCTTCAAGG
ACGACGGCAACTACAAGACCCGCGCCGAGGTGAAGTTCGAGGGCGACACC
CTGGTGAACCGCATCGAGCTGAAGGGCATCGACTTCAAGGAGGACGGCAAC
ATCCTGGGGCACAAGCTGGAGTACAACTACAACAGCCACAACGTCTATATC
ATGGCCGACAAGCAGAAGAACGGCATCAAGGTGAACTTCAAGATCCGCCAC
AACATCGAGGACGGCAGCGTGCAGCTCGCCGACCACTACCAGCAGAACACC
CCCATCGGCGACGGCCCCGTGCTGCTGCCCGACAACCACTACCTGAGCACC
CAGTCCGCCCTGAGCAAAGACCCCAACGAGAAGCGCGATCACATGGTCCTG
CTGGAGTTCGTGACCGCCGCCGGGATCACTCTCGGCATGGACGAGCTGTAC
AAGTACTCAGATCTCGAGCTCAAGCTTCGAATTAATTCCCACGCTGCCATGG
CAGACACCTTTCTGGAGCACATGTGCCGCCTGGACATCGACTCCGAGCCAA
CCATTGCCAGAAACACCGGCATCATCTGCACCATCGGCCCAGCCTCCCGCTC
TGTGGACAAGCTGAAGGAAATGATTAAATCTGGAATGAATGTTGCCCGCCT
CAACTTCTCGCACGGCACCCACGAGTATCATGAGGGCACAATTAAGAACGT
GCGAGAGGCCACAGAGAGCTTTGCCTCTGACCCGATCACCTACAGACCTGT
GGCTATTGCACTGGACACCAAGGGACCTGAAATCCGAACTGGACTCATCAA
GGGAAGTGGCACAGCAGAGGTGGAGCTCAAGAAGGGCGCAGCTCTCAAAG
TGACGCTGGACAATGCCTTCATGGAGAACTGCGATGAGAATGTGCTGTGGG
TGGACTACAAGAACCTCATCAAAGTTATAGATGTGGGCAGCAAAATCTATG
TGGATGACGGTCTCATTTCCTTGCTGGTTAAGGAGAAAGGCAAGGACTTTGT
CATGACTGAGGTTGAGAACGGTGGCATGCTTGGTAGTAAGAAGGGAGTGAA
CCTCCCAGGTGCTGCGGTCGACCTGCCTGCAGTCTCAGAGAAGGACATTCA
GGACCTGAAATTTGGCGTGGAGCAGAATGTGGACATGGTGTTCGCTTCCTTC
ATCCGCAAAGCTGCTGATGTCCATGCTGTCAGGAAGGTGCTAGGGGAAAAG
GGAAAGCACATCAAGATTATCAGCAAGATTGAGAATCACGAGGGTGTGCGC
AGGTTTGATGAGATCATGGAGGCCAGCGATGGCATTATGGTGGCCCGTGGT
GACCTGGGTATTGAGATCCCTGCTGAAAAAGTCTTCCTCGCACAGAAGATG
ATGATTGGGCGCTGCAACAGGGCTGGCAAACCCATCATTTGTGCCACTCAG
ATGTTGGAAAGCATGATCAAGAAACCTCGCCCGACCCGCGCTGAGGGCAGT
GATGTTGCCAATGCAGTTCTGGATGGAGCAGACTGCATCATGCTGTCTGGG
GAGACCGCCAAGGGAGACTACCCACTGGAGGCTGTGCGCATGCAGCACGCT
ATTGCTCGTGAGGCTGAGGCCGCAATGTTCCATCGTCAGCAGTTTGAAGAA
ATCTTACGCCACAGTGTACACCACAGGGAGCCTGCTGATGCCATGGCAGCA
GGCGCGGTGGAGGCCTCCTTTAAGTGCTTAGCAGCAGCTCTGATAGTTATGA
CCGAGTCTGGCAGGTCTGCACGCCTGGTGTCCCGGTACCGAAGACGCCACA
TCGTTCGGAAGCGCACGCTGCGGAGGCTGCTGCAGGAGAGGGAGCTTGTGG
AGCCTCTTACACCCAGTGGAGAAGCTCCCAACCAAGCTCTCTTGAGGATC

7.3.3 pCMVTag2-ARNO

ATGGAGGATGGCGTCTATGAACCCCCAGACCTGACTCCGGAGGAGCGGATG
GAGCTGGAGAACATCCGGCGGCGGAAGCAGGAGCTGCTGGTGGAGATTCA
GCGCCTGCGGGAGGAGCTCAGTGAAGCCATGAGCGAGGTGGAGGGGCTGG
AGGCCAATGAGGGCAGTAAGACCTTGCAACGGAACCGGAAGATGGCAATG
GGCAGGAAGAAGTTCAACATGGACCCCAAGAAGGGGATCCAGTTCTTGGTG
GAGAATGAACTGCTGCAGAACACACCCGAGGAGATCGCCCGCTTCCTGTAC
AAGGGCGAGGGGCTGAACAAGACAGCCATCGGGGACTACCTGGGGGAGAG
GGAAGAACTGAACCTGGCAGTGCTCCATGCTTTTGTGGATCTGCATGAGTTC
ACCGACCTCAATCTGGTGCAGGCCCTCAGGCAGTTTCTATGGAGCTTTCGCC
TACCCGGAGAGGCCCAGAAAATTGACCGGATGATGGAGGCCTTCGCCCAGC
GATACTGCCTGTGCAACCCTGGGGTTTTCCAGTCCACAGACACGTGCTATGT
GCTGTCCTTCGCCGTCATCATGCTCAACACCAGTCTCCACAATCCCAATGTC
CGGGACAAGCCGGGCCTGGAGCGCTTTGTGGCCATGAACCGGGGCATCAAC
GAGGGCGGGGACCTGCCTGAGGAGCTGCTCAGGAACCTGTACGACAGCATC
CGAAATGAGCCCTTCAAGATTCCTGAGGATGACGGGAATGACCTGACCCAC
ACCTTCTTCAACCCGGACCGGGAGGGCTGGCTCCTGAAGCTGGGAGGGGGC
CGGGTGAAGACGTGGAAGCGGCGCTGGTTTATCCTCACAGACAACTGCCTC
TACTACTTTGAGTACACCACGGACAAGGAGCCCCGAGGAATCATCCCCCTG
GAGAATCTGAGCATCCGAGAGGTGGACGACCCCCGGAAACCGAACTGCTTT
GAACTTTACATCCCCAACAACAAGGGGCAGCTCATCAAAGCCTGCAAAACT
GAGGCGGACGGCCGAGTGGTGGAGGGAAACCACATGGTGTACCGGATCTC
GGCCCCCACGCAGGAGGAGAAGGACGAGTGGATCAAGTCCATCCAGGCGG
CTGTGAGTGTGGACCCCTTCTATGAGATGCTGGCAGCGAGAAAGAAGCGGA
TTTCAGTCAAGAAGAAGCAGGAGCAGCCC

7.4 Complete original westernblots

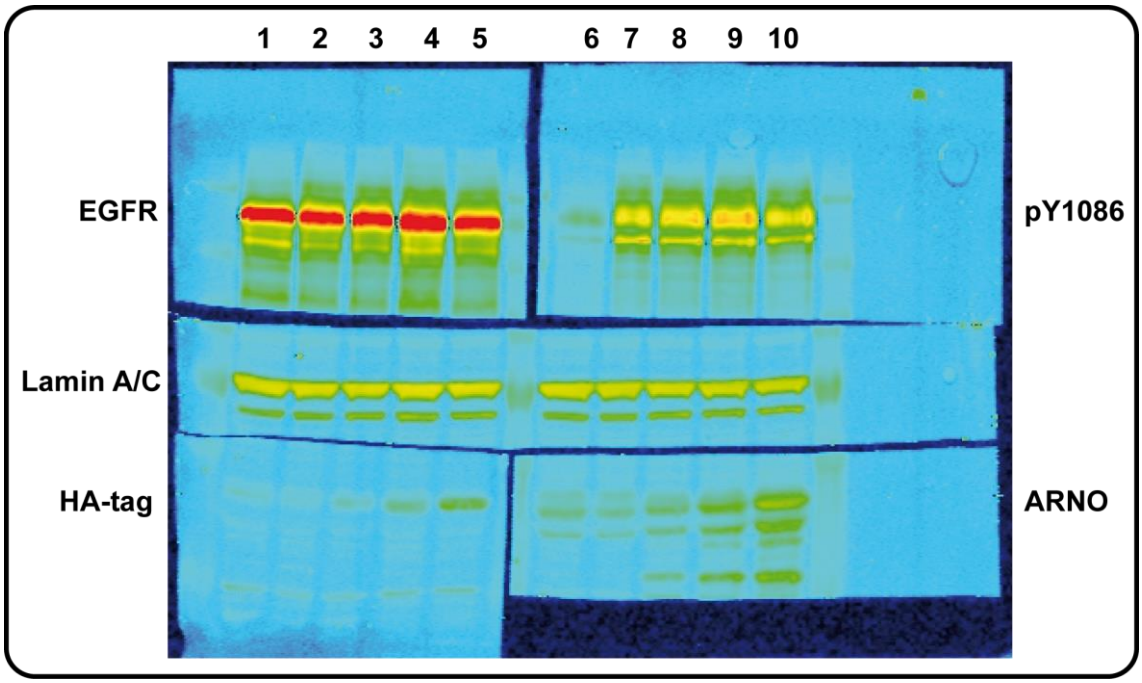

SI Figure 5: Full Westernblot corresponding to Figure 23. *The part stained for the HA-tag is not shown in the Figure.*

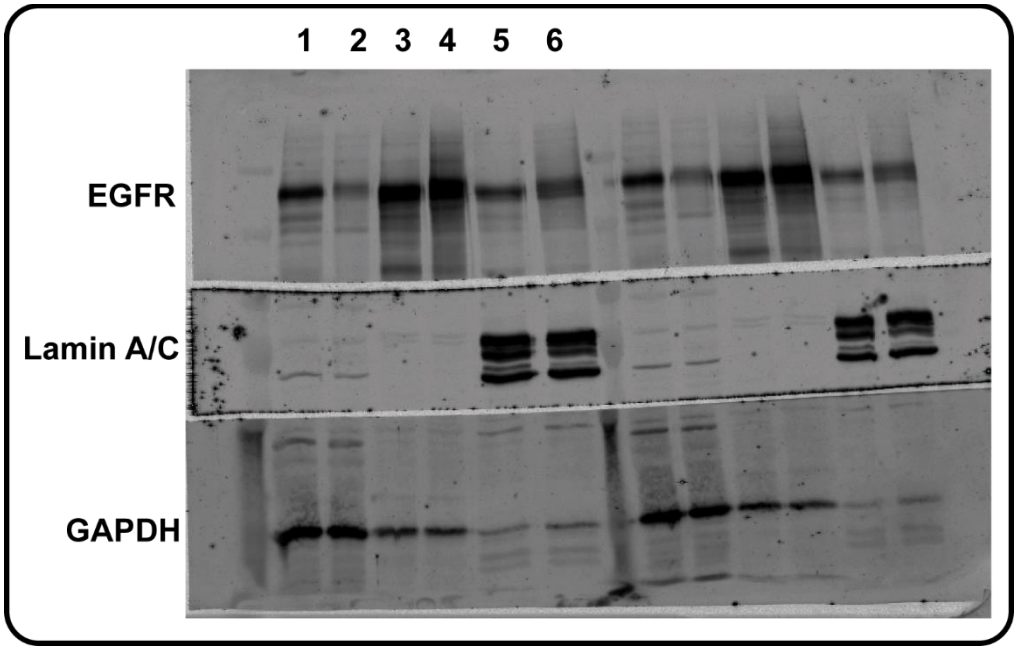

SI Figure 6: Full Westernblot corresponding to Figure 25. *Lanes 1-6 are shown in the Figure, on the right part of the blot, a repetition of the experiment is shown.*

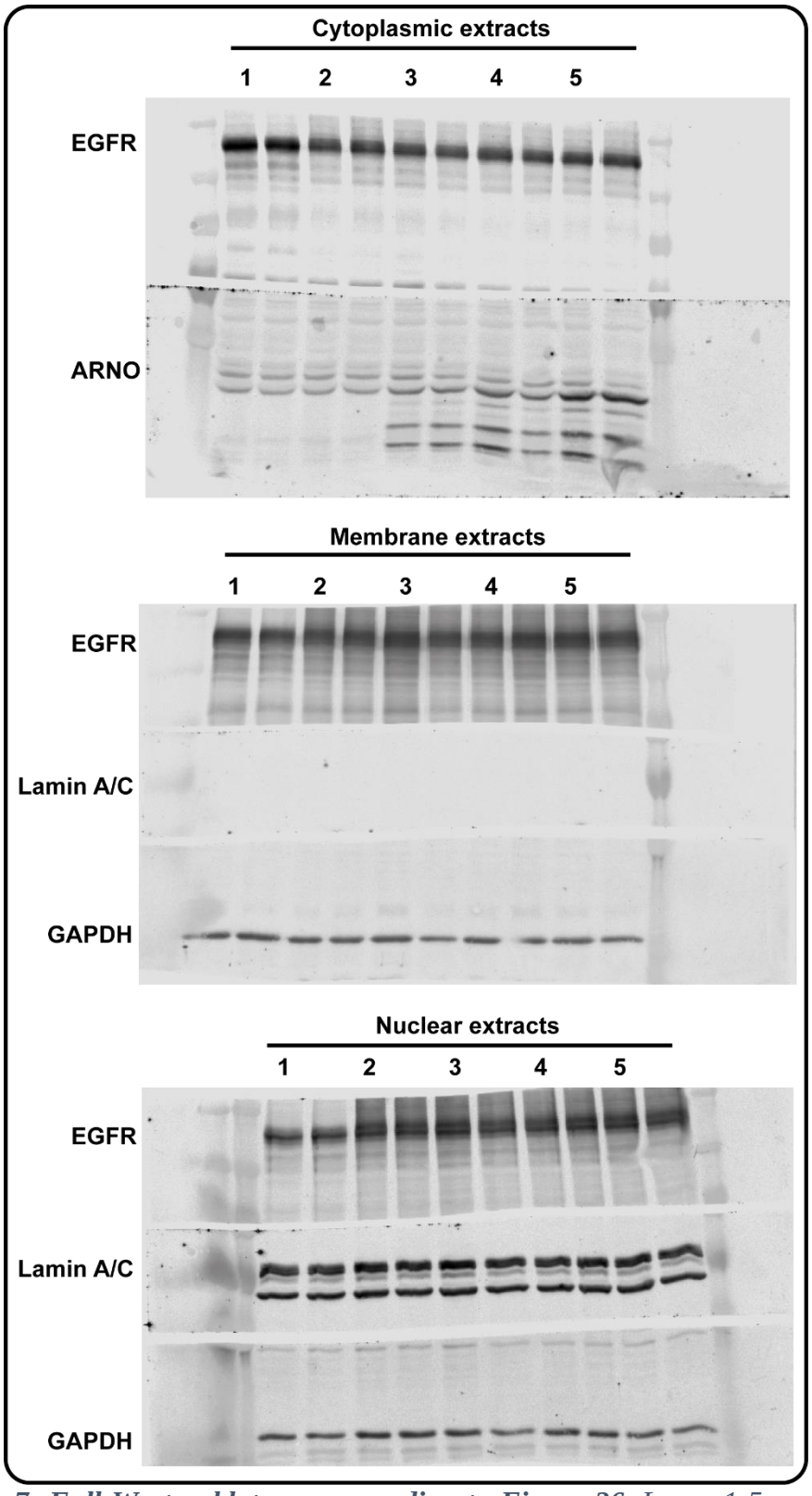

SI Figure 7: Full Westernblots corresponding to Figure 26. *Lanes 1-5 are shown in the Figure, the neighbouring lanes are a repetition of the experiment. The Lamin and GAPDH stainings are not shown in the Figure.*

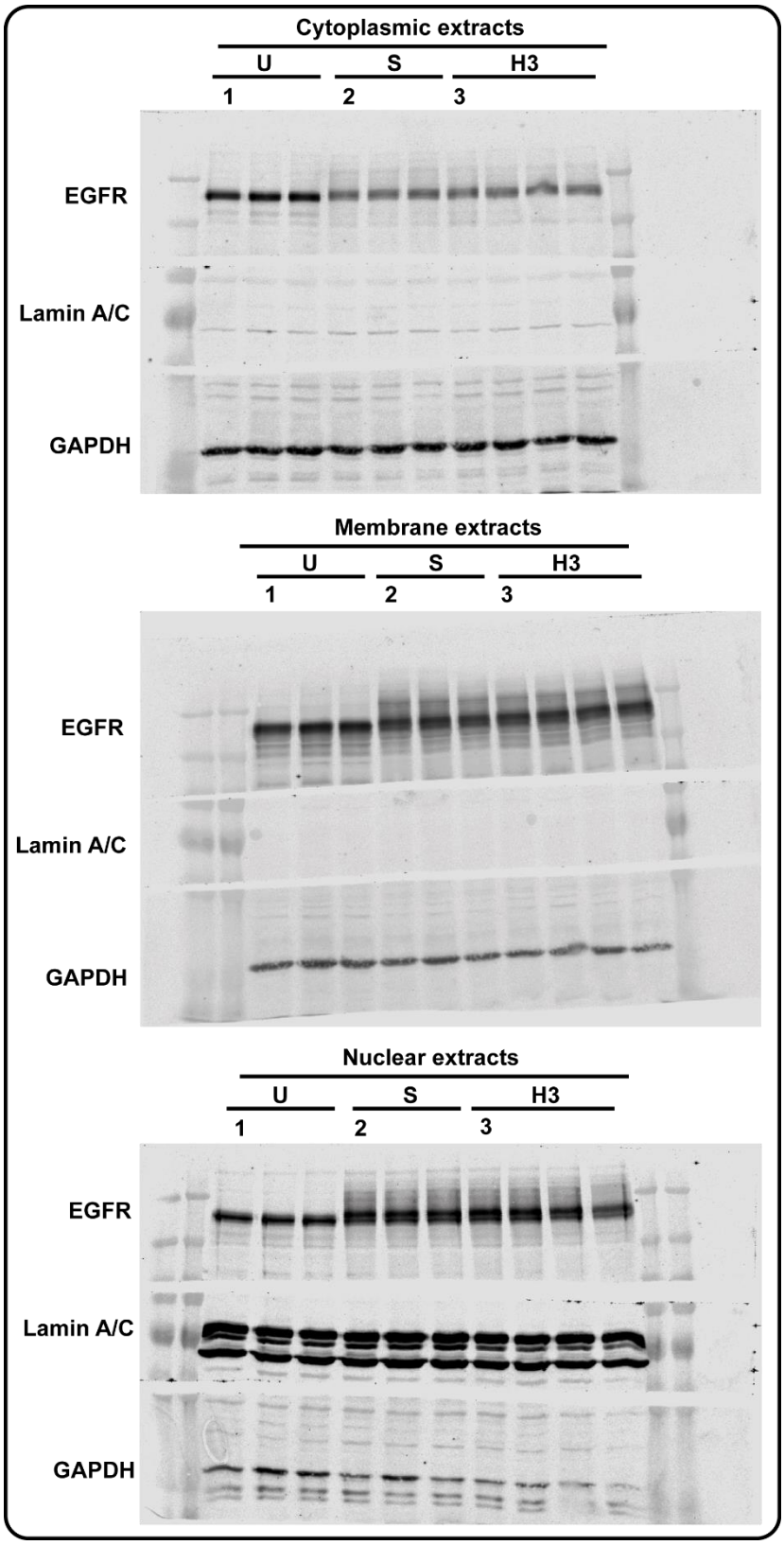

SI Figure 8: Full Westernblots corresponding to Figure 30. *Lanes 1-3 are shown in the Figure; the others are repetitions of the experiment.*

7.5 Characterization of Alexa594-PD168393

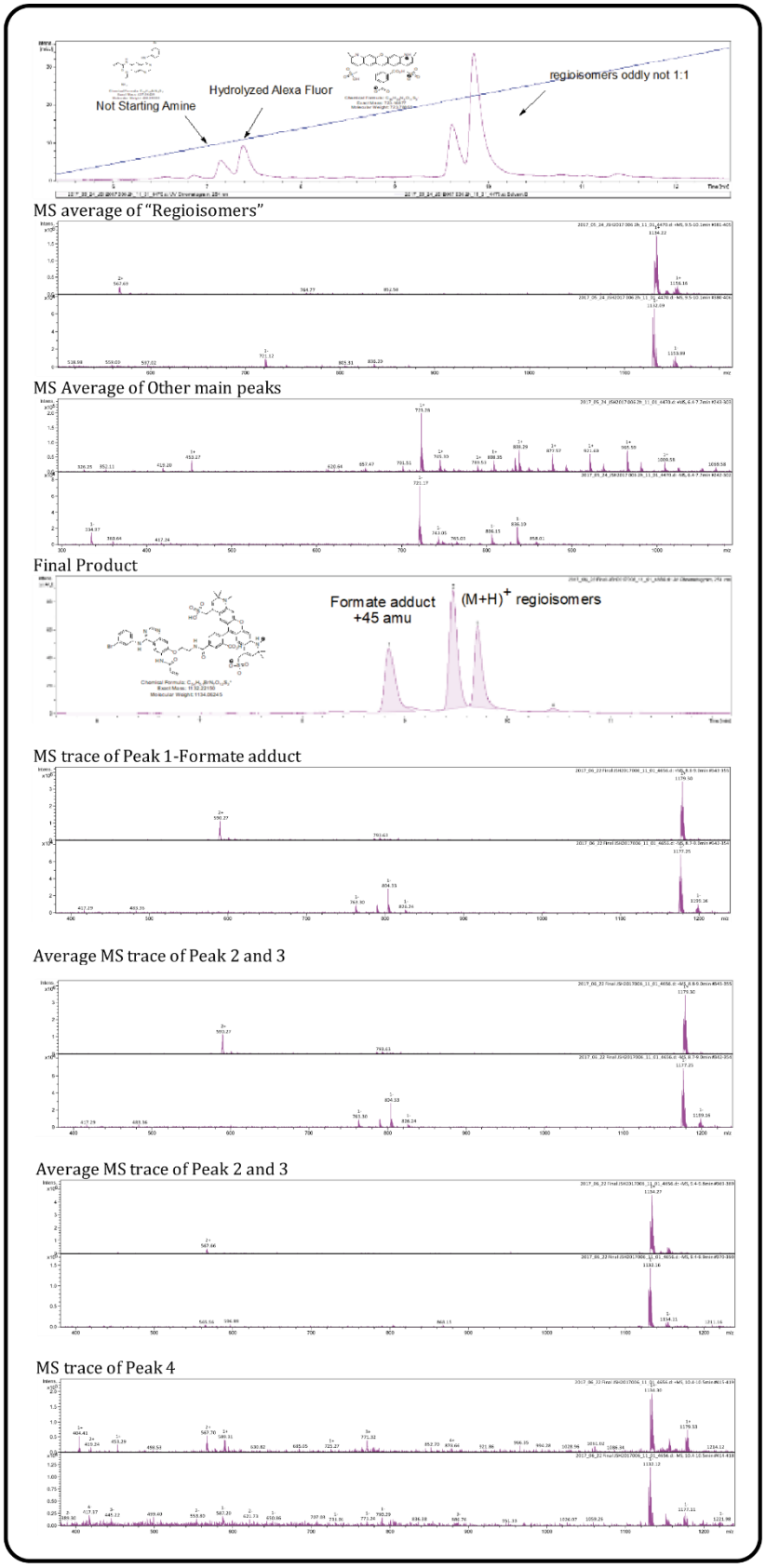

SI Figure 9: LCMS analysis of Alexa594-PD168393. *Compound and LCMS data kindly provided by Dr. Jeff Hannam*

8 Acknowledgements

First of all, I would like to thank Prof. Michael Famulok who has given me the opportunity to work in his lab for many years now and provided me with this interesting project. I really appreciate the amount of trust it must have taken to allow me to work this independently, while always being open to critical discussion.

I am deeply grateful for being part of the awesome cooperation between the Famulok lab and the lab of Prof. Thorsten Lang, who thankfully also agreed on being my second examiner. Prof. Thorsten Lang allowed me to work in his lab for about 18 months and I am stupefied by how much time he took and the effort he made to support me working out the reorientation of my project.

Furthermore, I want to thank Dr. Anton Schmitz for always being there to help and having the dedication to sit together brooding over my project for hours on end. The sharp criticism really made me push myself.

I am obliged to Dr. Jan-Gero Schloetel who helped greatly with image analysis as well as STED imaging.

I thank Dr. Philip Denner from the DZNE Laboratory Automation Core Facility for the amazing chance to work together with the Cell Voyager system and his advice as well as Dr. Christoph Moehl from the DZNE Image & Data Analysis Core Facility for helping with the analysis of the numerous resulting images.

Moreover, I am grateful for the opportunity to use the confocal microscope in the group of Dr. Annett Halle and would like to thank Hannes Beckert for helping with the operation of the microscope and teaching me the basics about microscopy and immunostaining.

A big thank you to Volker Fieberg for the tremendously helpful supervision of the protein expression and purification as well as for providing me with the proteins I didn´t have the time to purify myself.

In the Famulok as well as the Lang group, the team spirit among the lab members was exceptional. To work in an environment full of positive, caring and clever coworkers was a great pleasure and being able to discuss data freely in a non-formal environment really fueled the motivation even during the otherwise exhausting times. Specifically, I have to name Helena Batoulis, Elisa Merklinger, Dennis de Coninck, Pascal Weber, Jan-Gero Schloetel, Christian Sieg, Maren Hamann and Martina Bettio. Thank you, guys, for making this so much more enjoyable and productive!

Last, but not least I need to thank my family and friends for the constant support and encouragement, in complete disregard of not having any idea what exactly I was doing.

9 Zusammenfassung

Die Kompartimentalisierung von eukaryotischen Zellen durch Lipidmembranen dient der Trennung von biologischen Prozessen und Signalwegen. Der kontrollierte Transport von Proteinen zwischen Zellkompartimenten sowie die Rekrutierung der Proteine an die jeweiligen Membranen ist entscheidend für die einwandfreie Funktion der Zelle.

Verschiedene Möglichkeiten der Interaktion zwischen Proteinen und Membranen sind Gegenstand der Forschung. Beispielsweise interagieren Phosphoinositide spezifisch mit bestimmten Proteindomänen, wobei die anionischen Lipide eine elektrostatische Anziehung auf positiv geladene Proteindomänen ausüben.

Hauptfokus dieser Arbeit ist der Guanine-Nukleotid-Austauschfaktor ARNO, ein aus mehreren Domänen bestehendes Protein, welches die kleine GTPase Arf6 aktiviert und somit ein Teil der Vesikeltransport-Maschinerie der Zelle ist.

In seiner autoinhibierten Form liegt ARNO zytoplasmatisch vor, seine Rekrutierung zur Plasmamembran ist Grundvoraussetzung für die Aktivierung von Arf.

In diesem Zusammenhang haben sich vorangegangene Forschungsarbeiten auf die Interaktion zwischen der PH-Domäne und der PBR-Domäne mit artifiziellen Membransystemen konzentriert. Um die daraus gewonnenen Erkenntnisse in einem System zu erweitern, welches der enormen Komplexität der zellulären Plasmamembran Rechnung zu trägt, wurden in dieser Studie native Plasmamembranen für Bindungsstudien verwendet. Systematisch wurde die Rolle der verschiedenen ARNO-Domänen in der Bindung an zellfreie Plasmamembranen untersucht.

Es hat sich gezeigt, dass verschiedene ARNO-Domänen zur Interaktion mit der Membran auf kooperative Art und Weise beitragen. Während die PH-Domäne für die Assoziation des Proteins an die Membran absolut notwendig ist, ist sie jedoch nicht ausreichend um das Protein in der Membran zu verankern. Weiterhin wurde beobachtet, dass die Interaktion zwischen der PH-Domäne und den Phosphoinositiden durch den second messenger Ca^{2+} stark beeinflusst wird. Die Bindungsstudien dieser Arbeit zeigten weiterhin, dass die PBR-Domäne, die Sec7-Domäne sowie die Coiled-coil-Domäne zur Bindung an die Plasmamembran beitragen. Darüber hinaus verstärkt die Dimerisierung von ARNO die Bindung an die Plasmamembran, vermutlich aufgrund der Vergrößerung der lokalen Avidität.

Die mikroskopischen Analysen haben gezeigt, dass membrangebundenes ARNO in Clustern organisiert ist, die zum Teil eng mit EGFR Clustern assoziiert sind.

Die Überexpression von ARNO in HeLa Zellen führt zu einer Tendenz zur vermehrten Aktivierung des EGFR nach Stimulation mit EGF.
Beides deutet auf eine mögliche funktionelle Verbindung des EGFR-trafficking bzw. dessen Phosphorylierung und ARNO hin, die durch den second messenger Kalzium reguliert werden könnte.
Aktivierter EGFR kann mittels retrogradem endosomalen Transport in den Zellkern befördert werden. In Bezug auf diesen speziellen Transportweg wurde in dieser Studie kein Einfluss einer Überexpression oder Inhibition von ARNO gefund